Titre: Title:	New efficient methods for airfoil parameterization and iterative inverse aerodynamic design
Auteur: Author:	Jianzhong Yu
Date:	2002
Type:	Mémoire ou thèse / Dissertation or Thesis
Référence: Citation:	Yu, J. (2002). New efficient methods for airfoil parameterization and iterative inverse aerodynamic design [Mémoire de maîtrise, École Polytechnique de Montréal]. PolyPublie. https://publications.polymtl.ca/26177/

UNIVERSITÉ DE MONTRÉAL

NEW EFFICIENT METHODS FOR AIRFOIL PARAMETERIZATION AND ITERATIVE INVERSE AERODYNAMIC DESIGN

JIANZHONG YU
DÉPARTEMENT DE GÉNIE MÉCANIQUE
ÉCOLE POLYTECHNIQUE DE MONTRÉAL

MÉMOIRE PRÉSENTÉ EN VUE DE L'OBTENTION
DU DIPLÔME DE MAÎTRISE ÈS SCIENCES APPLIQUÉES
(GÉNIE MÉCANIQUE)
JUIN 2002

UNIVERSITÉ DE MONTRÉAL

ÉCOLE POLYTECHNIQUE DE MONTRÉAL

Ce mémoire intitulé:

NEW EFFICIENT METHODS FOR AIRFOIL PARAMETERIZATION AND ITERATIVE INVERSE AERODYNAMIC DESIGN

présenté par : YU Jianzhong

en vue de l'obtention du diplôme de : Maîtrise ès sciences appliquées

a été dûment par le jury d'examen constitué de :

M. ROBILLARD Luc, D.Sc., président

M. PARASCHIVOIU Ion, Ph.D., membre et directeur de recherche

M. TRÉPANIER Jean-Yves, Ph.D., membre

ACKNOWLEDGEMENTS

First I would like to express my gratitude to my advisor, Professor Ion Paraschivoiu for his financial support during the past two years and his permission to pursue my personal research interests.

I am also very grateful to Dr Farooq Saeed for his numerous helps such as the installation of Linux, especially for the useful programs that he offered to me. At the same time I'd like to thank Dr Stéphane Hallé for his assistance in treating miscellaneous affairs like ordering technical papers and preparing transparencies. And special thanks also go to my colleague, Vincent Desobry and Madam Manon Rioux for the verification of some part of this thesis written in French.

My gratitude is also expressed to Dr Mark Drela for using his exceptional code MSES and to Dr. David L. Carroll for his GA optimization code which really saved me a lot of time for programming.

Finally, I would like to acknowledge my wife and my son. Without their supports and understandings, I could not spend most of my spare times working at this research.

RÉSUMÉ

Deux nouvelles méthodes efficaces sont proposées dans ce mémoire. La première concerne la représentation paramétrique du profil aérodynamique et la seconde, la conception aérodynamique inversée.

La représentation paramétrique du profil aérodynamique est une façon bien adaptée pour améliorer l'efficacité de conception d'un profil ou d'une aile, ce qui permet de réduire le nombre des paramètres de conception ou du bruit de la fonction objective en l'optimisant d'une manière significative. Les méthodes existantes ont l'un des deux défauts suivants : difficile à obtenir des paramètres de contrôle ou besoin de plus de points de contrôle pour satisfaire la précision donnée. Si on prend plus de points, il est plus difficile de contrôler l'égalité et la monotonie du profil. Donc une nouvelle méthode optimisée a été inventée pour régler ce problème. La représentation du profil de cette méthode est basée sur la spline paramétrique de 5^e degré, mais avec des traitements spécifiques pour ajouter automatiquement des nœuds additionnels de spline afin d'améliorer la précision. Quatre paramètres de contrôle, la pente, la courbure et les deux abscisses des points de contrôle, sont nécessaires pour chaque point qui peuvent en général être sélectionnés directement à partir des points originaux du profil d'après leur distribution de l'abscisse x. Donc dans ce cas là, la pente et la courbure ont seulement besoin d'être optimisées par une méthode de gradient conjugué, et la convergence rapide de l'optimisation peut être assurée en prenant les valeurs initiales de l'interpolation de la spline de 5^e degré issues des points originaux du profil. Par conséquent, les paramètres de contrôle peuvent être obtenus en 10 secondes. Dans les quelques cas où cette méthode des localisations de x ne peut pas satisfaire l'exigence de précision, la méthode d'algorithme génétique (GA) est adaptée pour optimiser ces localisations en combinaison avec la méthode de gradient conjugué pour les autres paramètres. Puisque le micro GA est employé et que cette optimisation n'est faite que pour peu de points discrets du profil original, la méthode est encore efficace. D'ailleurs, les résultats de calcul confirment que cette nouvelle méthode permet de représenter presque tous les profils précisément par 7 à 13 points de contrôle. Bien

que la pente et la courbure soient exigées pour chaque point de contrôle, elles sont néanmoins beaucoup plus faciles à utiliser pour contrôler la géométrie du profil que les positions des points. De plus, il est plus aisé d'ajouter des contraintes, de calculer des caractéristiques géométriques et de faire des modifications locales du profil. Par conséquent, cette méthode possède un grand potentiel pour améliorer l'efficacité de la conception du profil, de l'aile ou d'autres applications multidisciplinaires.

Les caractéristiques aérodynamiques sont très sensibles à la forme géométrique du bord d'attaque du profil. En conséquence, la deuxième partie de ces recherches est consacrée à développer une nouvelle méthode itérative de conception aérodynamique inversée qui est non seulement efficace, mais permet aussi de calculer la région de bord d'attaque assez précisément. Ceci demeure impossible pour beaucoup d'autres méthodes. Au lieu de l'hypothèse des variations des courbures des lignes de courant normales à la paroi du profil, une équation géométrique de petite perturbation est déduite à partir de l'équation de moment de ligne de courant, de l'équation de continuité et des relations isentropiques avec l'hypothèse de la similitude de la ligne de courant proche à la paroi du profil. En plus, la correction transsonique pour cette équation est prise en compte avec l'hypothèse sur les effets des ondes reflétées de la frontière libre (la ligne sonique), car cette méthode n'est basée que sur les valeurs aérodynamiques de surface. Alors, elle ne peut pas refléter les caractéristiques transsoniques telles que les interférences des ondes. Les perturbations géométriques normales à la paroi du profil sont calculées en résolvant cette équation différentielle ordinaire de deuxième ordre avec des valeurs initiales. Les techniques comme lisser le profil, la relaxation non uniforme et le "strained coordinate transfer" qui était utilisé pour supprimer les non-uniformités des solutions de perturbation des problèmes non linéaires, sont employées pour accélérer la convergence. Les résultats démontrent l'efficacité et l'exactitude de cette méthode non seulement pour les conceptions d'écoulement compressible, mais aussi pour celles de basse vitesse surtout que le bord d'attaque peut être désigné précisément. Ceci demeure inaccessible presque pour toutes les autres méthodes.

ABSTRACT

Two new efficient methods for airfoil design are proposed in this thesis. One concerns the optimized airfoil parameterization and another for iterative inverse aerodynamic design.

The airfoil parameterization is a commonly accepted way to improve airfoil design efficiency, which can greatly reduce design parameters and noises of objective function in optimization. The existed methods have one of the two drawbacks: hard to get control points or needing more control points at the given representation precision. The more control points, the more difficult to control the smoothness and the monotony of airfoils. Thus a new optimized approach is put forward to solve the above problems. The airfoil representation of this method is based on the general 5th degree parametric spline but with special treatments for automatically adding additional spline nodes in order to improve the precision. Four control parameters, the slope, the curvature and the two coordinates of control points, are needed for each control point which can be selected directly from the original airfoil ones according to their x location distribution. Thus in this case, only the slop and the curvature need to be optimized by a conjugate-gradient method and the rapid optimization convergence can be guaranteed by taking initial parameters from the 5th degree spline interpolation of the original airfoil points. Therefore, the control parameters can be obtained within 10 seconds. For fewer cases that this way to localize control points cannot meet the precision requirements, a genetic algorithm (GA) method is adapted for optimization of the x locations combined with the gradient method for other parameters. As the micro GA is used and the x location optimization is only carried out for fewer discrete original airfoil points, the method is still relatively efficient in this case. Moreover, the calculation results confirm that this new method can accurately represent nearly any airfoil by 7 to 13 control points. Furthermore, it is simpler to add constrains, to calculate geometric characteristics and to make local airfoil modifications than the other methods. Thus the method possesses a

great potential to improve airfoil and wing design efficiency, especially for multi-point and multi-discipline optimization design.

Aerodynamic characteristics are very sensitive to airfoil leading edge geometry. Therefore, the second part of this research is concentrated on developing an iterative inverse design method which is not only efficient but also can work well in the leading edge region, which is impossible for many other methods. Instead of assumptions of streamline curvature variations normal to airfoil surface as in the streamline curvature methods, a small geometric perturbation equation is deduced from the streamline momentum equations, the continuity equation and the isentropic relations with the geometry similarity assumption of near streamlines to the airfoil surface. Moreover, the transonic correction is considered in this equation with the assumption for the effects of waves reflected from the free surface (sonic line) because the method based on the surface flow values cannot take into account the transonic characteristics such as wave interference. The geometric perturbation normal to the airfoil surface is then calculated by solving this second order initial-value ordinary differential equation and the airfoil is designed in iteration. The techniques like airfoil smoothing, non-uniform relaxation and the strained coordinate transfer which was used to remove non-uniformity from perturbation solutions of non-linear problems, are applied for accelerating the convergence. The design cases demonstrate the high efficiency and accuracy of this method not only for compressible flows but also for low speed flows, especially the leading edge can be precisely calculated, which compensates for the deficiencies of the other methods.

CONDENSÉ EN FRANÇAIS

Deux méthodes efficaces pour la conception du profil aérodynamique sont proposées dans ce mémoire.

1. Représentation paramétrique optimisée du profil aérodynamique

1.1 Introduction

La représentation paramétrique du profil est une méthode qui est employée pour représenter un profil avec beaucoup moins de points que l'original. Donc elle est bien adaptée pour améliorer l'efficacité de conception d'un profil ou d'une aile, ce qui permet de réduire le nombre des paramètres de conception ou du bruit de la fonction objective en l'optimisant d'une façon significative.

Les méthodes pour représentation paramétrique du profil peuvent se diviser en deux genres : le classique et le moderne. Le premier basé sur quelques fonctions de forme de base n'est pas flexible à cause de sa capacité limitée et le second révélé avec le développement de la conception assistée par l'ordinateur est beaucoup plus pratique, parmi lequel la spline de Bézier, B-spline et B-spline non uniforme rationnelle (NURBS). Des résultats satisfaisants ont été obtenus avec toutes ces méthodes modernes dans ces applications. Mais les premières ne sont pas assez précises ou requièrent plus de points de contrôle pour satisfaire la précision donnée. Si on prend plus de points, alors il est plus difficile de contrôler l'égalité et la monotonie du profil. Le NURBS est très puissante, mais les paramètres de contrôle sont calculés avec une méthode d'optimisation basée sur le gradient qui dépend des valeurs initiales données. Puisque le problème d'optimisation contient de nombreuses minima locales et qu'il n'est pas possible d'assurer des valeurs initiales appropriées, la solution ne peut pas être garantie et, de ce fait, il est difficile d'obtenir des paramètres de contrôle avec cette méthode. Par conséquent, une nouvelle méthode optimisée a été inventée pour régler ce problème.

1.2 Méthodes de représentation et d'optimisation

La représentation du profil avec cette méthode repose sur la spline paramétrique de 5^{e} degré car il est raisonnable de garder les courbures du profil non seulement continues mais aussi lisses. Cependant, la spline générale ne peut pas être employée directement pour la représentation paramétrique du profil parce que les distances ou les variations entre deux nœuds proches peuvent être trop grandes en raison du faible nombre de points de contrôle. Donc il faut régler les trois problèmes principaux ci-après : 1) Approximation des longueurs des segments de courbe qui sont contenues dans les fonctions de spline. La longueur de corde, qui est bien adaptée pour des applications générales, est trop imprécise pour être utilisée. Mais le calcul de la longueur exacte de courbe qui est obtenue en résolvant un système d'équations non linéaires n'est pas garanti (le calcul diverge parfois). Donc la longueur de courbe est l'approximation de l'arc circulaire moyen. Mais ce traitement conduit à un autre problème. 2) Réduction des paramètres de contrôle. Il y a trois vecteurs de contrôle à chaque nœud de spline de 5^{e} degré, le vecteur de position, le vecteur tangent et son gradient qui correspondent à six paramètres de contrôle dans le cas bidimensionnel. Si on prend les longueurs exactes des segments de courbe, quatre de ces six paramètres sont indépendants, car la norme du vecteur tangent est unitaire et les derniers vecteurs sont normaux entre eux. Donc il existe quatre paramètres de contrôle pour chaque nœud. Mais si les longueurs des segments de courbe sont approximatives, ces six paramètres sont tout indépendants. Alors il faut effectuer la normalisation pour réduire le nombre des paramètres de six à quatre, qui sont deux abscisses de position, la pente et la courbure. 3) Ajouter des nœuds de spline additionnels. La spline générale ne peut pas satisfaire l'exigence de précision spéciale du profil à cause du faible nombre des nœuds de spline qui sont des points de contrôle pour un profil paramétrique. Mais ça n'a pas de sens physique d'ajouter plus de points dans ce cas là. Donc les nœuds additionnels sont ajoutés automatiquement pour améliorer la précision, en maintenant continues les dérivées curvilignes de troisième degré et de

quatrième degré à chaque nœud ajouté. Pour cela, il est nécessaire de résoudre un système d'équations non linéaires qui ne prennent en compte que les voisins de nœud.

Puisque les nœuds de contrôle de spline adaptée se situent exactement sur les courbes de la spline, les points de contrôle peuvent être sélectionnés directement à partir des points originaux du profil. Alors deux stratégies peuvent être employées : 1) Les points de contrôle peuvent être simplement fixés d'après leur distribution de l'abscisse x déterminé par une fonction polynomiale donnée et la distribution de courbure du profil. Ainsi dans ce cas là, la pente et la courbure ont seulement besoin d'être optimisées par une méthode de gradient conjugué. Mais il faut que les valeurs initiales soient proches du minimum global, car cette méthode d'optimisation ne permet de trouver qu'un minimum local sans contraintes. Ceci peut être assuré en prenant les valeurs initiales de l'interpolation de la spline de 5^e degré à partir des points originaux du profil. Donc la convergence rapide de l'optimisation peut être garantie et les paramètres de contrôle peuvent être obtenus en 10 secondes avec un ordinateur de 800 M Hz. Bien que les résultats calculés de cette manière soient exceptionnels, ils ne correspondent probablement qu'à un minimum local puisqu'on ne peut pas trouver de différences entre un minimum local et le minimum global même mathématiquement. Si cette méthode des localisations de x ne peut pas satisfaire l'exigence de précision, la deuxième stratégie sera adaptée : 2) Les points de contrôle sont aussi déterminés par optimisation. Dans ce cas là, la méthode d'algorithme génétique (GA) est adaptée pour optimiser les localisations de x en combinaison avec la méthode de gradient conjugué pour les autres paramètres. Puisque le micro GA est employé et que cette optimisation n'est faite que pour peu de points discrets du profil original, la méthode est encore efficace.

1.3 Résultats et discussions

Pour confirmer la capacité de cette méthode, divers types de profils paramétriques sont présentés dans ce mémoire, y compris les profils NACA, les profils supercritiques de

RAE et de NASA, le profil naturellement laminaire et celui pour le "rotor-craft". Le nombre des points de contrôle et l'erreur maximum entre les profils paramétriques et les originaux figurent dans le tableau 2.1. Les résultats démontrent que la plupart des profils les plus employés pour les avions, peuvent être présentés précisément en déterminant les points de contrôle d'après leur distribution de l'abscisse x : les profils de NACA avec 7 à 9 points de contrôle avec des erreurs maximums entre 5.1×10^{-5} à 7.7×10^{-5}, les profils supercritiques avec 11 points de contrôle et des erreurs maximums entre 2.5×10^{-5} à 6.5×10^{-5}. On peut visualiser les résultats presque tout de suite. Pour les autres profils dont les points de contrôle ont besoin d'être optimisés, les précisions sont encore excellentes, mais ne sont pas aussi bonnes que celles obtenues dans les premiers cas. La raison principale est la suivante : il est très difficile de spécifier avec une bonne adéquation les régions de variations pour chaque point de contrôle parce que le GA utilisé adapte un code binaire et qu'il faut que ces régions satisfassent la relation 2^n-1, où n est entier. En conséquence, la solution obtenue par ce biais est seulement une correspondante à un des minima locaux. Ceci est très manifeste dans l'observation des distributions des erreurs non uniformes.

En plus, les effets de la fonction objective sur les solutions d'optimisation sont aussi étudiés dans cette recherche. Cette étude confirme que: 1) le choix de la fonction objective a une forte influence sur les résultats d'optimisation, 2) l'approximation des moindres carrés est appropriée pour le profil paramétrique et 3) la fonction objective, qui contient l'erreur moyenne et les erreurs maximums de tous les segments de courbe, est bien meilleure pour la représentation paramétrique du profil que celle qui inclut l'erreur moyenne et la seule erreur maximum, quoique cette dernière forme de fonction soit néanmoins généralement acceptable. Les raisons en sont les suivantes : la première forme de fonction peut relativement garder sa valeur monotone et pour la dernière fonction plusieurs minima locaux seraient formés par un mouvement aléatoire de la position de l'erreur maximum d'un segment de courbe à l'autre, ce qui est néfaste pour l'optimisation, surtout pour celle basée sur le gradient.

1.4 Conclusion

Les résultats de calcul démontrent que cette nouvelle méthode permet de représenter presque tous les profils non seulement précisément mais aussi efficacement par 7 à 13 points de contrôle, surtout les profils plus employés pour l'avion avec 11 points ou moins, ce qui compense les insuffisances des autres méthodes. Bien que la pente et la courbure soient exigées pour chaque point de contrôle, elles sont néanmoins beaucoup plus faciles à utiliser pour contrôler la géométrie du profil que les positions des points. De plus, il est plus aisé d'ajouter des contraintes telles que les épaisseurs du profil, de calculer des caractéristiques géométriques comme les courbures et de procéder à des modifications locales du profil avec cette méthode qu'avec les autres. Par conséquent, cette méthode possède un grand potentiel pour améliorer l'efficacité de la conception du profil, de l'aile ou d'autres applications multidisciplinaires.

2. Méthode itérative de conception aérodynamique inversée

2.1 Introduction

La conception aérodynamique inversée permet de fournir la forme géométrique pour les valeurs objectives spécifiées comme la distribution de pression ou celle de vitesse. Avec le développement de l'informatique et des méthodes de dynamique numérique de fluide, la conception aérodynamique inversée devient un outil privilégié pour désigner des profils, les ailes d'avion, les pales pour l'éolienne, l'hélicoptère et le compresseur.

De nombreuses méthodes de conception aérodynamique inversée existent et, en particulier les méthodes itératives comme la méthode de Takanashi et celle de courbure de ligne de courant de la NASA qui sont plus puissantes pour des applications d'ingénierie car 1) Le programme pour résoudre les écoulements peut rester inchangé.

Alors elles permettent d'être couplées directement avec les logiciels aérodynamiques récents. 2) Les méthodes sont basées sur les corrections itératives des différences de pression ou de vitesse entre les profils objectif et calculé. Elles ne sont requises que pour prédire la correcte tendance au lieu des valeurs exactes, car la solution sera améliorée pendant le processus d'itération. Donc elles peuvent être plus facilement utilisées pour les configurations compliquées à cause de ses flexibilités.

Cependant, ces méthodes comme les nombreuses autres méthodes ne peuvent pas calculer la forme du bord d'attaque du profil précisément à cause des grandes variations de l'écoulement et de la distribution de haute courbure dans cette région. Cela limite leurs applications pratiques parce que les caractéristiques aérodynamiques sont très sensibles à la forme géométrique du bord d'attaque. Alors plusieurs approches sont proposées pour régler ce problème. La nouvelle méthode de courbure de ligne de courant a donné de bons résultats, mais elle est développée principalement pour l'écoulement de basse vitesse et se révèle moins efficace dans les autres cas. La représentation du profil par des fonctions analytiques est satisfaisante dans certains cas, mais les résultats de conception sont restreints. Par conséquent, une nouvelle méthode est proposée, qui est requis d'être non seulement efficace mais aussi précise.

2.2 Méthode de conception

Au lieu de l'hypothèse des variations des courbures des lignes de courant normales à la paroi du profil comme ce qui est fait dans les méthodes de courbure de ligne de courant, une équation géométrique de petite perturbation est déduite à partir de l'équation de moment de ligne de courant, de l'équation de continuité et des relations isentropiques avec l'hypothèse de la similitude de la ligne de courant proche à la paroi du profil. Les perturbations géométriques normales à la paroi du profil sont calculées en résolvant cette équation différentielle ordinaire de deuxième ordre avec des valeurs initiales. Mais cette équation est très ''stiff'', car le coefficient de dérivée seconde a le même ordre que les

autres seulement dans la région du bord d'attaque. Bien que ce problème puisse être solutionné mathématiquement, il n'est pas physique de garder ce coefficient dans les autres régions, car les termes ignorés auraient le même ordre voire seraient plus grands que lui. Ainsi cette équation ne s'applique que dans la région de bord d'attaque. Du point où un saut de perturbation géométrique apparaît ou où le taux du coefficient de dérivée seconde aux autres est inférieur à une valeur donnée (environ 1%), une équation algorithmique, obtenue à partir de l'équation ci-dessus en ignorant le terme de dérivée seconde, est utilisée à la place. Mais pour la zone supersonique dans l'écoulement transsonique, il est plus approprié d'employer cette équation en forme différentielle puisque la zone d'influence d'un point se limite seulement à sa zone de Mach. Par ailleurs, cette équation n'est basée que sur les valeurs aérodynamiques de surface au lieu du champ de l'écoulement. Alors, elle ne peut pas refléter les caractéristiques transsoniques telles que les interférences des. Donc la correction transsonique est prise en compte dans la réalisation de l'hypothèse de la similitude de la ligne de courant proche à la paroi du profil mais avec l'autre hypothèse sur les effets des ondes reflétées de la frontière libre (la ligne sonique).

Pour la conception subsonique, les équations peuvent être résolues directement mais la convergence n'est pas rapide. Pour la conception transsonique, on ne peut pas trouver de solution par ce biais. Donc il faut mettre en oeuvre des traitements spécifiques pour assurer l'efficacité et la précision. Les trois mesures principales et les raisons d'utilisation sont explicitées ci-après. (1) Transfert déformé des coordonnées (the strained coordinate transfer) : Les différences entre la pression objective et celle calculée près du bord d'attaque et de l'onde de choc, peuvent être si grandes (surtout pendant les premières itérations) que les perturbations géométriques calculées soient fortement déformées à cause des grandes différences entre les positions des points d'arrêt, des sommets de pression négative et des chocs. Ceci peut être réglé en lissant le profil, mais le transfert déformé des coordonnées pourrait accroître l'efficacité. Cette technique était employée pour supprimer les non-uniformités des solutions de perturbation des problèmes non

linéaires en transférant les points critiques d'un profil tels que le point d'arrêt, la position du sommet de pression négative et du choc aux points correspondants de l'autre profil. (2) Lisser le profil : C'est une technique bien adaptée pour les autres méthodes itératives et elle est essentielle pour l'écoulement transsonique en raison des discontinuités des perturbations géométrique causées par l'onde de choc. En général, le profil est lissé une fois par une itération de conception. Pour cette méthode de conception, trois méthodes sont employées pour lisser le profil : (a) La méthode de la représentation paramétrique du profil décrite dans la première partie de ce mémoire. Cette méthode peut garder les dérivées d'ordre trois continues mais elle a tendance à trop peu lisser le profil car elle est développée pour présenter le profil précisément. Donc les deux autres méthodes sont utilisées pour lisser le profil localement. (b) Lisser les dérivées secondes des perturbations géométriques et ensuite, les abscisses du profil sont obtenues par intégration. Cette méthode est employée principalement pour lisser la région supersonique. (c) La fonction de Bézier est utilisée pour lisser la région de bord d'attaque car elle permet de garder la tendance d'origine d'une courbe et d'amortir les valeurs de sommet. 3) Relaxation non uniforme : la convergence est aussi accélérée avec la technique de relaxation, mais les facteurs de relaxation sont différents sur les endroits différents du profil en considérant les caractéristiques de la solution de perturbation.

2.3 Résultats de conception

Pour vérifier cette méthode de conception, les calculs sont effectués pour plusieurs cas. Les coefficients de pression sont issus du code MSES qui est basé sur la méthode d'Euler couplée avec celle de la couche limite. Pour les résultats de haute vitesse subsonique (M_∞ = 0.60 à 0.725) illustré dans les figures 4.1 et 4.2, le profil objectif et celui initial sont respectivement RAE2822 et NACA0012. Les grandes différences entre les deux profils sont adéquates pour tester la capacité de la méthode. Pour le premier cas de conception (M_∞ = 0.60, α = 1.50 d et Re = 1.00×10^7) où le transfert déformé des coordonnées est appliqué, les résultats montrent que : en 5 itérations, les différences des distributions de

pression et celles géométriques entre le profil objectif et celui de conception sont si petites que les résultats de conception seraient employés pour des applications pratiques. En 15 itérations, la différence maximum de coefficient de pression est 0.006 et les erreurs géométriques sont plus petites que 5.0×10^{-5} près du bord d'attaque. Pour le deuxième cas ($M_\infty = 0.725$, $\alpha = 0.00$ d et $Re = 1.00\times10^{7}$), la solution de la même précision est obtenue en 20 itérations. La convergence est un peu plus lente, car le transfert déformé des coordonnées ne peut pas être utilisé en raison des grandes différences des positions de sommet de pression négative entre les profils objectif et initial. Pour les deux cas de basse vitesse ($M_\infty = 0.3$, $\alpha = 4.00$ à 5.00 d et $Re = 1.00\times10^{7}$) illustrés dans les figures 4.4 et 4.5 avec le profil initial NACA0012 et les profils objectifs RAE 5212 et NACA2412, les résultats précis sont atteints en 15 à 20 itérations mais ils ne sont pas aussi bons que dans les premiers cas. Pour le cas transsonique (figure 4.6), la solution obtenue en 25 itérations est excellente du point de vue pratique et en comparaison avec les résultats des autres méthodes itératives, bien qu'il y ait des différences visibles autour des chocs.

2.4 Conclusion

Tous les résultats de conception ci-dessus démontrent l'efficacité et l'exactitude de cette méthode non seulement pour les conceptions d'écoulement compressible, mais aussi pour celles de basse vitesse, surtout que le bord d'attaque peut être désigné précisément. Ceci demeure inaccessible presque pour toutes les autres méthodes. Ils confirment aussi que l'efficacité et la précision de conception dépendent des techniques pour lisser le profil et accélérer la convergence et d'autres telles que le transfert déformé des coordonnées, mais toutes ces techniques nécessitent d'être amélioré. Ainsi, elle pourrait remplacer les anciennes méthodes et se répandre aux applications pratiques.

TABLE OF CONTENTS

ACKNOWLEDGEMENTS iv
RÉSUMÉ v
ABSTRACT vii
CONDENSÉ EN FRANÇAIS ix
LIST OF APPENDICES xxi
LIST OF TABLES xxii
LIST OF FIGURES xxiii
NOMENCLATURE xxvi

INTRODUCTION 1
0.1 Airfoil Parameterization 1
0.2 Iterative Inverse Aerodynamic Design 3

CHAPTER 1 : METHOD FOR OPTIMIZED AIRFOIL PARAMETERIZATION 7
1.1 Airfoil representation 7
1.1.1 Basic formulations 7
1.1.2 Special problems to be solved 10
1.1.2.1 Curve length approximation 10
1.1.2.2 Parameter Reduction 11
1.1.2.3 Adding spline nodes 12
1.2 Airfoil approximation optimization 13
1.2.1 Approximation errors and tolerance 13
1.2.2 Selection of objective function 15
1.2.3 Determining control points 17
1.2.4 Optimization 17
1.2.4.1 Conjoint-gradient method 18

1.2.4.2 Genetic algorithm 20

CHAPTER 2 : CALCULATION RESULTS FOR AIRFOIL PARAMETERIZATION
.....22

2.1 Study of objective functions 22

2.2 Scaling effects to the solutions of the conjugate-grading method 29

2.3 Parametric airfoil representation results 29

2.3.1 Optimized airfoil parameterization with control points fixed 31

2.3.2 Airfoil parameterization with x locations optimized 39

2.3.3 Comparisons with some other results 45

CHAPTER 3 : ITERATIVE INVERSE AERODYNAMIC DESIGN METHOD 46

3.1 Governing equations 46

3.2 Perturbation calculation, design process and flow solver 55

3.2.1 Initial conditions 55

3.2.1.1 Selection of initial points 55

3.2.1.2 Initial values 56

3.2.2 Geometric perturbation calculation 57

3.2.3 Design process and convergence criteria 58

3.2.4 Flow solver 59

3.3 Some special treatments 60

3.3.1 Strained coordinate transfer 60

3.3.2 Airfoil smoothing 62

3.3.3 Non-uniform relaxation 63

CHAPTER 4 : AIRFOIL INVERSE DESIGN RESULTS 65

4.1 Airfoil design for high subsonic flows 65

4.2 Airfoil design for low speed flows 72

4.3 Transonic airfoil design 78

CONCLUSION 83
5.1 Optimized airfoil parameterization 83
5.2 Iterative inverse aerodynamic design 84

REFERENCES 86

APPENDICES 89

LIST OF APPENDICES

APPENDIX 1 : SIXTH ORDER HERMITE INTERPOLATION FUNCTION 89

APPENDIX 2 : INTRODUCTION TO PROGRAM AIRY 90

APPENDIX 3 : FLOW CHART OF MAIN PROGRAM AIRY 92

APPENDIX 4 : FLOW CHART IN SUBROUTINE SPLINE
FOR SPLINE INTERPOLATION 93

APPENDIX 5 : SIMPLIFIED FLOW CHART OF SUBROUTINE CONFOIL
FOR PARAMETRIC AIRFOIL OPTIMIZATION 94

APPENDIX 6 : SIMPLIFIED FLOW CHART OF SUBROUTINE REVERSE
FOR ITERATIVE INVERSE AERODYNAMIC DESIGN 95

APPENDIX 7 : INPUT DATA DISCRIPTIONS
FOR PROGRAM AIRY 96

APPENDIX 8 : INPUT CONTROL FILE FORMAT EXAMPLE 99

APPENDIX 9 : OUTPUT FILES DISCRIPTIONS 100

LIST OF TABLES

Table 2.1 : Control Numbers and Maximum Errors
for Calculated Parametric Airfoils 31

Table 2.2 : Control Point Number and Maximum Error Comparisons 45

LIST OF FIGURES

Figure 1.1 A Ferguson curve segment 7
Figure 1.2 General error definition demonstration 13
Figure 1.3 Error definition used in this thesis 14
Figure 2.1 Error distribution Comparisons
for Different Objective Functions (9 control points for NACA65-215) 23
Figure 2.2 Error Distribution Comparisons for the First Form
of Objective Functions with Different Power Indies 24
Figure 2.3 Error Distribution Comparisons for the Second Form
of Objective Functions with Different Power Indies 25
Figure 2.4 Error Distribution Comparisons for the Third Form
of Objective Functions with Different Power Indies 26
Figure 2.5 Maximum Error Variations with Different Power Indies
for Three Forms of Objective Functions 28
Figure 2.6 Scaling Effects to Maximum Errors 30
Figure 2.7 Parametric Airfoil Optimization Results
(11 control points for RAE2822) 33
Figure 2.8 Parametric Airfoil Optimization Results
(11 control points for RAE5215) 34
Figure 2.9 Parametric Airfoil Optimization Results
(9 control points for NACA65-215) 35
Figure 2.10 Parametric Airfoil Optimization Results
(9 control points for NACA64a-010) 36
Figure 2.11 Parametric Airfoil Optimization Results for NACA2412 37
Figure 2.12 Parametric Airfoil Optimization Results
(7 control points for NACA0012) 38
Figure 2.13 Parametric Airfoil Optimization Results
(for NASA NLF(2)-0415) 41

Figure 2.14 Parametric Airfoil Optimization Results
(11 control points for NASA SC(2)-0714) 42
Figure 2.15 Parametric Airfoil Optimization Results
(11 control points for VR-12) 43
Figure 2.16 Parametric Airfoil Optimization Results
(13 control points for S1210) 44
Figure 3.1 Streamline Tube and Its Coordinates near Airfoil 47
Figure 3.2 Geometric relations among a airfoil surface, a near streamline
and a left characteristic line from the airfoil 54
Figure 4.1 Inverse Airfoil Design Results--- Airfoils and Pressure Distribution
Comparisons (M_∞ = 0.6, Re = 1×10^7 and α = 1.50 d.) (a) 66
Figure 4.1 Inverse Airfoil Design Results--- Airfoils and Pressure Distribution
Comparisons (M_∞ = 0.6, Re = 1×10^7 and α = 1.50 d.) (b) 67
Figure 4.2 Convergence Curves
Maximum Error Variations via Iterations 68
Figure 4.3 Inverse Airfoil Design Results--- Airfoils and Pressure Distribution
Comparisons(M_∞ = 0.725, Re = 1×10^7 and α = 0.00 d.) (a) 70
Figure 4.3 Inverse Airfoil Design Results--- Airfoils and Pressure Distribution
Comparisons(M_∞ = 0.725, Re = 1×10^7 and α = 0.00 d.) (b) 71
Figure 4.4 Inverse Airfoil Design Results--- Airfoils and Pressure Distribution
Comparisons(M_∞ = 0.30, Re = 1×10^7 and α = 4.00 d.) (a) 73
Figure 4.4 Inverse Airfoil Design Results--- Airfoils and Pressure Distribution
Comparisons(M_∞ = 0.30, Re = 1×10^7 and α = 4.00 d.) (b) 74
Figure 4.5 Inverse Airfoil Design Results--- Airfoils and Pressure Distribution
Comparisons(M_∞ = 0.30, Re = 1×10^7 and α = 5.00 d.) (a) 75
Figure 4.5 Inverse Airfoil Design Results--- Airfoils and Pressure Distribution
Comparisons(M_∞ = 0.30, Re = 1×10^7 and α = 5.00 d.) (b) 76
Figure 4.5 Inverse Airfoil Design Results--- Airfoils and Pressure Distribution
Comparisons(M_∞ = 0.30, Re = 1×10^7 and α = 5.00 d.) (c) 77

Figure 4.6 Inverse Airfoil Design Results--- Airfoils and Pressure Distribution Comparisons(M_∞ = 0.715, Re = 1×10^7 and α = 2.30 d.) (a) 79

Figure 4.6 Inverse Airfoil Design Results--- Airfoils and Pressure Distribution Comparisons(M_∞ = 0.715, Re = 1×10^7 and α = 2.30 d.) (b) 80

Figure 4.6 Inverse Airfoil Design Results--- Airfoils and Pressure Distribution Comparisons(M_∞ = 0.715, Re = 1×10^7 and α = 2.30 d.) c 81

NOMENCLATURE

Δ	Increment
α	Angle of attack or step size in conjugate-gradient optimization
β	Direction coefficient in conjugate-gradient optimization
δ	Increment
γ	Ratio of specific heat
η	Direction or coordinate normal to surface
κ	Curvature
μ	Angle between characteristic line and streamline line
ϑ	Streamline line angle relative to Cartesian coordinate x
ρ	Density
ω	Prandtl-Meyer function
ξ	Cartesian coordinate corresponding to x
Σ	Summation
a	Sound velocity
A	Equation coefficients or function
B	Equation coefficient
c_p, CP	Pressure coefficient
d	Derivative
d	Direction vector
C, D	Constants
f, F	Function of Mach number and pressure coefficient
fcm	Factor for maximum error
G	Gradient
H	Hermite function
M	Mach number
n	Unit normal vector
ofun	Objective function

p	Pressure or power index
P, P′, P′′	Position, tangent vectors and its gradient receptively
R	Gas constant
Re	Reynolds number
s	Streamline direction or curve coordinate
t	Curve parameter
T	Temperature
V	Velocity
w	Weighted factor
x, y	Cartesian coordinates
x	Position parameter vector

Subscripts

0	Initial value
∞	Free-stream value
i, j, k, n	Number or node or curve segment index
max	Maximum value
o	Objective or target value
s	Surface value
t, tt, ttt	First, second and third order derivatives to t respectively

INTRODUCTION

This thesis is divided into two parts: (1) Optimized Airfoil Parameterization and (2) Iterative Inverse Aerodynamic Design. Each part can be used independently and all the research belongs to the project of "Laminar Flow Control" which is financially supported by Bombardier Aerospace. Although the developed methods intend to be employed in laminar flow control design, they can be applied for general purposes such as aircraft, turbine or other concerned design applications.

0.1 Airfoil Parameterization

With the developments of the computer and the computational fluid dynamics methods, multi-point and multi-discipline optimization design attracts more and more interests. But there are still a lot of engineers who hesitate to use optimization methods. This may be due to the following reasons. 1) There is still a long way to use this kind of methods as a "black box". The results of optimization depend on appropriate selection of many parameters determined by user's concerned knowledge and calculation experiences. 2) In many cases, optimization methods are still not efficient enough to meet practical needs. Although it is rapid for gradient-based methods to find a local minimum, solutions depend too much on the given initial value and the calculation convergence cannot be guaranteed in practical applications that often contain too much noise, that is to say, too many local minima. Evolution computation methods, such as the genetic algorithm, can ensure to find a better solution, but much more computation time has to be spent in complicated cases. Therefore, it is very practical to develop methods that can reduce design parameters and noises of the objective function in optimization and with which it is easy to add constrains and to coordinate with different disciplines. What is more, the methods must be able to precisely represent airfoils with special smoothness requirements. Furthermore, it should be convenient to take into account airfoil characteristics, for example, curvatures and slops are larger only near the leading edge,

airfoil curves are monotonous for most part of the airfoil and inflection points may occur only at some special places.

Airfoil parameterization is a kind of method by which an airfoil can be represented by its parametric one with much fewer points than the original. It is a commonly accepted way to improve the airfoil or wing design efficiency, especially for multi-point and multi-discipline optimization design and it is in practice use for a long time. However, it did not find wide applications because the early methods that are generally based on some basic shape functions are not flexible enough and their capabilities to accurately represent airfoils are limited. Though this kind of methods can be useful, it has tendencies to bias a design by making it fall into certain geometric families.

In recent years, achievements in computer aided geometric design also bring forward some new more powerful tools to airfoil parameterization, among which Bézier polygon by Venkataraman, B-spline (Burgreen et al) and most recently the non-uniform rational B-spline (NURBS) by Trépanier and al. All these methods have been successfully applied in airfoil or wing designs. But generally speaking, the formers are not accurate enough for fewer control points or need more control points for the given precision requirement. The more control points, the more local minima there are in objective functions and thus it is more difficult to control the smoothness or monotony of airfoils. NURBS is most powerful and very simple for geometry control. But it is difficult to obtain control parameters because their calculation depends on optimization methods and on the initial guess to the solution. As a result, an acceptable solution cannot be guaranteed. Thus the practical applications of this method may be limited unless some of its special treatments are improved.

In this research, a new optimized airfoil parameterization approach is proposed which use four control parameters, the slope, the curvature and the two coordinates of control points for each point. The airfoil representation is based on the general 5th degree spline in Hermite form but with additional spline nodes automatically added from the

information of the neighboring control points since the spline with very fewer nodes cannot meet the airfoil special precision requirements. The parametric airfoil points can be selected directly from the original ones according to their x locations, which generally determined by some distribution function. Thus in this case, only the slope and the curvature at each control point are unknown and they are obtained by a conjugate-gradient optimization method. The initial parameters taken from 5th degree spline interpolation of the original airfoil points and the relatively monotonous variations of the objective function with those of the curvature and the slope can ensure the rapid optimization convergence. For fewer cases that fixed x locations cannot satisfy the precision requirements, a genetic algorithm (GA) method is adapted for optimization of the x locations combined with the gradient method for other parameters.

The high accuracy and efficiency of this new method are confirmed by the representations of several types of airfoils including supercritical, natural laminar and low speed ones. Moreover, some concerned problems like influences of different objective functions to optimization solutions are also discussed in detail with calculation results.

0.2 Iterative Inverse Aerodynamic Design

Inverse problems are treated to obtain geometric properties for specified aerodynamic characteristics in contrast to direct problems for which aerodynamic performances are solved at given geometric conditions. Inverse aerodynamic design is used for designing or modifying airfoils at specified target airfoil surface pressure or velocity distributions to meet the special design requirements. As one of the design tools, inverse aerodynamic design methods have found wide applications in aircraft, turbine machine and wind energy equipment design with the development of the computer and the computational fluid dynamics (CFD) methods.

There are numerous inverse design methods among which iterative residual-correction methods such as Takanashi's and NASA's (Barger, Campbell, William H. and Yu N.) streamline curvature method are very powerful for engineering applications because of the following fact. The iterative methods are based on iterative correction of pressure or velocity differences between the target and designed airfoils and they are only required to predict the correct geometric variation tendencies rather than the exact values because the solution will be improved during the iteration process. In addition, the flow solver is retained in its original form and can be treated just like a "black box". Therefore they can be directly coupled with any newly developed, more efficient flow solver and can be easily applied to complicated configurations because of their flexibilities.

Generally speaking, there also exist the following problems for inverse design methods: it is only for a single design point, hard to add constraints and to coordinate with other disciplines, not accurate enough in most of practical cases and the specified target pressure distribution cannot guarantee the minimum drag. Therefore, it is generally used in the initial stage of industry designs and it seems that the efficiency has been the main object of this kind of methods about which there are rarely precision discussions such as maximum tolerances or maximum pressure coefficient difference. It is generally accepted that from the practical point of view, if the graphic differences between the target and design pressure distributions are small enough, the accuracy of the method is taken for granted because in this case the lift, drag and moment differences between the two airfoil are also so small that the design requirements can be met without any problem.

As a result of limitations of inverse design, efforts must be made for geometry smoothing and what's more, verification of aerodynamic performance at off-design conditions and other constrains, and modifications of target pressure distribution which is often obtained in engineering design by modifying the one of an existed airfoil of which some characteristics intend to be reserved and the others to be improved. As aerodynamic

characteristics are very sensitive to the leading edge geometry that plays a very important role in low speed maximum lift, transonic shock movement, etc., it is very hard to reserve the key aerodynamic performances of the original airfoil if the applied design method cannot work well in the leading edge region. Therefore, accurate calculation of airfoil shapes, especially leading edge shapes is essential for efficiency of inverse design methods.

The streamline curvature method invented by Barger is based on the following simple equation $d V/ V = -\kappa(\eta)\, d\eta$ where V is velocity, κ is streamline curvature and η is distance normal to the streamline. For given velocity differences dV between a target airfoil and an initial one, the geometric perturbations $d\eta$ can be calculated with the assumed variation relations of curvature normal to the streamline. The method is very flexible owing to its simple formulation but it is physically based on taking the two airfoils as streamlines of the same flow field. Thus its physical meaning is not very clear because (a) streamlines cross with each other only at singular points such as a stagnation point while these two airfoils can do at any point, (b) the mass continuity is satisfied between streamlines but not between the two airfoils and (c) the formula cannot tell the difference between subsonic and supersonic flows. Moreover, as the stagnation point is a singular point to this method, the leading edge region cannot be solved very well with this method.

Takanashi's method based on the inversely formulated transonic small-perturbation equation is the most popular in engineering, but the small perturbation assumption is not valid near the stagnation point. Thus the method cannot be expected to work quite well near the leading edge with so large flow variations and so high curvature distribution unless some corrections are made. Many other design methods have also demonstrated some deficiencies in this region. Thus several approaches have been tried to improve the situations. William H. successfully calculated some results for low speed flows with his new streamline curvature method but the method is less efficient and accurate in the

other cases. Representation of airfoil geometry by families of smooth analytic functions (Bernard, Hartwich and al) is an effective way but the design results are restrictive.

The objective of this research is to develop an iterative inverse method that is not only efficient but also accurate enough. Instead of assumptions to streamline curvature variations normal to airfoil surface as in the streamline curvature methods, a small perturbation geometric equation is obtained from the streamline momentum equations, the continuity equation and the isentropic relations with the geometry similarity assumption of near streamlines to the airfoil surface. Moreover, the transonic correction is also considered in this equation. The geometric perturbation normal to the airfoil surface can be calculated by solving this ordinary differential equation as initial-value problems and the airfoil is designed in iteration. The techniques like airfoil smoothing, non-uniform relaxation and the strained coordinate transfer are applied for accelerating the convergence. The high efficiency and accuracy of this method is demonstrated by several subsonic and transonic airfoil design cases. In addition, some concerned problems are also discussed in detail.

CHAPTER 1
METHOD FOR OPTIMIZED AIRFOIL PARAMETERIZATION

1.1 Airfoil representation

1.1.1 Basic formulations

As it is appropriate to keep airfoil curvatures not only continuous but also smooth, the sixth order parametric spline is selected for airfoil representation. A sixth order spline can keep fourth order derivatives continuous in globe use and third order derivatives continuous for local control. The formulation is different from general purposes and thus the explanations are needed.

A Ferguson curve for segment i-1 to i as shown in Figure 1.1 can be expressed as following:

$$\mathbf{P}(t)_i = H_{0,0}\mathbf{P}_{i-1} + H_{0,1}\mathbf{P}_i + H_{1,0}\mathbf{P}_{t\,i-1} + H_{1,1}\mathbf{P}_{t\,i} + H_{2,0}\mathbf{P}_{tt\,i-1} + H_{2,1}\mathbf{P}_{tt\,i} \qquad (1.1)$$

where $\mathbf{P}$ is a position vector, $\mathbf{P}_t = d\mathbf{P}/dt$, $P_{tt} = d^2\mathbf{P}/dt^2$, subscript i-1 and i are curve index or node index corresponding to t = 0 and t = 1 of curve segment i. $H_{0,0}$ to $H_{2,1}$ are Hermite interpolation functions defined as followings by Fujio and are given in Appendix 1.

Figure 1.1 A Ferguson curve segment

For the i-th curve segment $\mathbf{P}(t)_i$, $0 \le t \le 1$ corresponds to $s_{i-1} \le s \le s_i$. Suppose curve coordinate s and parameter t have the following relation:

$$s = s_{i-1} + (s_i - s_{i-1})\,t \tag{1.2}$$

Therefore, for the i-th curve segment

$$\begin{aligned}
\mathbf{P}_{t\,i-1} &= \mathbf{P}_t(0)_i = \left(\frac{d\mathbf{P}}{ds}\right)_{s=s_{i-1}}(s_i - s_{i-1}) = (s_i - s_{i-1})\,\mathbf{P}'(s_{i-1}) \\
\mathbf{P}_{t\,i} &= \mathbf{P}_t(1)_i = \left(\frac{d\mathbf{P}}{ds}\right)_{s=s_i}(s_i - s_{i-1}) = (s_i - s_{i-1})\,\mathbf{P}'(s_i) \\
\mathbf{P}_{tt\,i-1} &= \mathbf{P}_{tt}(0)_i = \left(\frac{d^2\mathbf{P}}{ds^2}\right)_{s=s_{i-1}}(s_i - s_{i-1})^2 = (s_i - s_{i-1})^2\,\mathbf{P}''(s_{i-1}) \\
\mathbf{P}_{tt\,i} &= \mathbf{P}_{tt}(1)_i = \left(\frac{d^2\mathbf{P}}{ds^2}\right)_{s=s_i}(s_i - s_{i-1})^2 = (s_i - s_{i-1})^2\,\mathbf{P}''(s_i)
\end{aligned} \tag{1.3}$$

From the i-th curve segment function given by formula (1.1), using relation (1.2), the third order curvilinear derivative at node i :

$$\mathbf{P}'''(s_i)_i = \left(\frac{d^3\mathbf{P}}{ds^3}\right)_{s=s_i} = \frac{1}{(s_i - s_{i-1})^3}\left(\frac{d^3\mathbf{P}}{dt^3}\right)_{t=1} = \frac{\mathbf{P}_{ttt}(1)}{(s_i - s_{i-1})^3} \tag{1.4}$$

In the same way, for node i but from the i+1-th curve segment function:

$$\mathbf{P}'''(s_i)_{i+1} = \left(\frac{d^3\mathbf{P}}{ds^3}\right)_{s=s_i} = \frac{1}{(s_{i+1} - s_i)^3}\left(\frac{d^3\mathbf{P}}{dt^3}\right)_{t=0} = \frac{\mathbf{P}_{ttt}(0)}{(s_{i+1} - s_i)^3} \tag{1.5}$$

For a spline curve of which each segment is represented by formula (1.1), third and fourth curvilinear derivatives should be continuous at each node. From formula (1.1), (1.3), (1.4), (1.5) and Hermite basis, the equation for the continuity of third derivatives at node i can be conducted as

$$20\,\delta s^3_{i+1}\,\mathbf{P}_{i-1} + 8\,\delta s_i\,\delta s^3_{i+1}\,\mathbf{P}'_{i-1} + \delta s^2_i\,\delta s^3_{i+1}\,\mathbf{P}''_{i-1} -$$
$$20\,(\delta s^3_i + \delta s^3_{i+1})\,\mathbf{P}_i - 12\,\delta s_i\,\delta s_{i+1}\,(\delta s^2_i - \delta s^2_{i+1})\,\mathbf{P}'_i - 3\,\delta^2 s_i\,\delta^2 s_{i+1}\,(\delta s_i +$$
$$\delta s_{i+1})\,\mathbf{P}''_i + 20\,\delta s^3_i\,\mathbf{P}_{i+1} - 8\,\delta s^3_i\,\delta s_{i+1}\,\mathbf{P}'_{i+1} + \delta s^3_i\,\delta s^2_{i+1}\,\mathbf{P}''_{i+1} = 0 \qquad (1.6)$$

where $\delta s_i = s_i - s_{i-1}$, $\delta s_{i+1} = s_{i+1} - s_i$ are corresponding curve segment lengths.

In the same way, the equation for the continuity of fourth derivatives at node i is as following:

$$30\,\delta s^4_{i+1}\,\mathbf{P}_{i-1} + 14\,\delta s_i\,\delta s^4_{i+1}\,\mathbf{P}'_{i-1} + 2\,\delta s^2_i\,\delta s^4_{i+1}\,\mathbf{P}''_{i-1} +$$
$$30\,(\delta s^4_i - \delta s^4_{i+1})\,\mathbf{P}_i + 16\,\delta s_i\,\delta s_{i+1}\,(\delta s^3_i + \delta s^3_{i+1})\,\mathbf{P}'_i + 3\,\delta^2 s_i\,\delta^2 s_{i+1}\,(\delta s^2_i -$$
$$\delta s^2_{i+1})\,\mathbf{P}''_i - 30\,\delta s^4_i\,\mathbf{P}_{i+1} + 14\,\delta s^4_i\,\delta s_{i+1}\,\mathbf{P}'_{i+1} + 2\,\delta s^4_i\,\delta s^2_{i+1}\,\mathbf{P}''_{i+1} = 0 \qquad (1.7)$$

For given n nodes, that is to say, n **P** vector given, equations (1.6) and (1.7) compose a system of 2(n-2) equations for 2n unknown. Another four equations can be obtained from free end conditions that the third and fourth derivatives are zero at the two ends:

$$20\,\mathbf{P}_1 - 20\,\mathbf{P}_2 + 12\,\delta s_1\,\mathbf{P}'_1 + 8\,\delta s_1\,\mathbf{P}'_2 + 3\,\delta s^2_1\,\mathbf{P}''_1 - \delta s^2_1\,\mathbf{P}''_2 = 0$$
$$30\,\mathbf{P}_1 - 30\,\mathbf{P}_2 + 16\,\delta s_1\,\mathbf{P}'_1 + 14\,\delta s_1\,\mathbf{P}'_2 + 3\,\delta s^2_1\,\mathbf{P}''_1 - 2\,\delta s^2_1\,\mathbf{P}''_2 = 0 \qquad (1.8)$$
$$20\,\mathbf{P}_{n-1} - 20\,\mathbf{P}_n + 8\,\delta s_{n-1}\,\mathbf{P}'_{n-1} + 12\,\delta s_{n-1}\,\mathbf{P}'_n + \delta s^2_{n-1}\,\mathbf{P}''_{n-1} - 3\,\delta s^2_{n-1}\,\mathbf{P}''_n = 0$$
$$30\,\mathbf{P}_{n-1} - 30\,\mathbf{P}_n + 14\,\delta s_{n-1}\,\mathbf{P}'_{n-1} + 16\,\delta s_{n-1}\,\mathbf{P}'_n + 2\,\delta s^2_{n-1}\,\mathbf{P}''_{n-1} - 3\,\delta s^2_{n-1}\,\mathbf{P}''_n = 0$$

Thus for n given **P**, equations (1.6), (1.7) and (1.8) compose a closed system of 2n equations with $\mathbf{P}'$ and $\mathbf{P}''$ as unknowns. For most cases that the curve length δs between two neighbouring nodes are not large and the curve variation is slow, the curve length can be approximated by the chord length, the distance between the two nodes, without causing larger errors. As a result, the coefficients of the above equations are constant and it is easy to solve this linear system of equations with its diagonal matrix. But for

parametric airfoil whose neighbouring nodes are not near, this treatment will cause unacceptably large errors.

In programming, another end condition of given $\mathbf{P}'$ and $\mathbf{P}''$ can also be used. In addition, there is an option that the problem can also be solved for the fixed slope $\mathbf{P}'$ at the leading edge because $\mathbf{P}'$ is normal to the chord line for numerous airfoils. In this case, only the third derivative is kept continuous at the leading edge.

1.1.2 Special problems to be solved

1.1.2.1 Curve length approximation

As the approximation of curve lengths by chord lengths is much less accurate for parametric airfoil, other methods must be tried instead. Thus, exact curve lengths may be used. In this case, the system of equations (1.6), (1.7) and (1.8) are nonlinear and it can be solved in iteration with the common methods such as fixed constant coefficients, Newton and etc. But the solution depends on the initial guess and the calculation will diverge if an inflection point occurs on the curve during the iteration process. Consequently another method given by Fujio (PP 354) is accepted. In this method, curve lengths are approximated by average circular arc lengths. Therefore, the system of equations becomes linear again and can be easily solved. What is more, the calculation results show that the differences between using exact curve lengths and these approximated can be too small to be ignored. That is why the circular arc length is the default option in programming. But considering different application purposes, there are four option for curve length approximations in the corresponding program Airy: 1) chord length, 2) circular arc length, 3) curve length approximated by a cubic spline and 4) curve length approximated by the sixth order spline.

As the curve length cannot be calculated accurately, its approximation will give rise to a serious problem that there are too many control parameters.

1.1.2.2 Parameter Reduction

For a spline curve segment represented by formula (1.1), there are three control vectors, $\mathbf{P}$, $\mathbf{P}'$ and $\mathbf{P}''$ at each node. For airfoils, one vector has two components and so there are six control parameters at each node. In fact, according to the following formula in Fujio's book (pp. 31), only two of four parameters for $\mathbf{P}'$ and $\mathbf{P}''$ are independent and thus there are total four control parameters at each node:

$$|\mathbf{P}'| = 1 ; \quad \mathbf{P}' \mathbf{P}'' = 0 ; \qquad \mathbf{P}'' = \kappa \mathbf{n} \tag{1.9}$$

where $\mathbf{n}$ is normal unit vector and κ is curvature

$$\kappa = \frac{|\mathbf{P}_t \times \mathbf{P}_{tt}|}{|\mathbf{P}_t|^3} \tag{1.10}$$

As the curve lengths are approximated, so are derivatives $\mathbf{P}'$ and $\mathbf{P}''$ calculated with formula (1.3). Consequently the approximated $\mathbf{P}'$ and $\mathbf{P}''$ do not satisfy relation (1.9), especially the normal relation. Thus all the six parameters at each node are independent. Therefore the normalization is necessary in order to reduce control parameters. The process of normalization is like: 1) make tangent vectors $\mathbf{P}'$ become unit vectors once more, 2) calculate the normal unit vectors $\mathbf{n}$ from their normal relation with $\mathbf{P}'$, 3) calculate curvatures κ according to formula (1.10) and 4) calculate new $\mathbf{P}'' = \kappa \mathbf{n}$.

1.1.2.3 Adding spline nodes

As parametric airfoils are represented with only several control points, generally speaking, the approximation precision of a spline curve cannot meet the special airfoil design requirements because the distance between two neighbouring nodes can be too large. Moreover, it is not practical to solve this problem by increasing control points. So some other effective ideas have to be used. In this research, adding more nodes for the spline curve is found to be much more effective. Of cause, these nodes must be determined only from their neighbouring control points, that means, the parameters at these nodes can be automatically calculated. The relations used for adding nodes are also formula (1.6) and (1.7), which is based on the same idea that third or (and) fourth order derivatives at each node should be continuous for each curve segment.

The process for adding nodes is as following: a) determine the x location of an adding node between its two neighbouring control points according to the geometric variation of the curve segment, b) formulate the two equation for the two x direction components of $\mathbf{P}'$ and $\mathbf{P}''$ at this x location with two third order derivative continuity equations respectively obtained at this node and its neighbouring node according to formula (1.6), c) formulate three equations for the y coordinate and the two y components of $\mathbf{P}'$ and $\mathbf{P}''$ at the given x in the same way as the last step but with one more equation added, which is the fourth order derivative continuity equation (1.7) for the added node and d) solve the system of equations non-linear because y is also unknown and so is the curve length. The equations must be solved iteratively. The numerical method used is just a fixed constant coefficient method.

In programming, there are three options for adding nodes between every two neighbouring control points: 1) adding one more node, 2) adding two more nodes and 3) no more nodes added. Adding more nodes is also possible, but the system of equations so obtained is generally ill conditioned and the solutions may not be accepted. As the added

nodes have no direct influences to control parameters, their normalization is not necessary.

1.2 Airfoil approximation optimization

As original airfoils are going to be represented by parametric ones, the problems like approximation errors, objective function selection, strategy for determining control parameters, approximation methods and etc, must be decided.

1.2.1 Approximation errors and tolerance

The approximation error to an original airfoil point is generally defined as the distance between this point and the approximated airfoil as shown in Figure 1.2. The calculation of the error defined in this way needs finding a minimum by solving non-linear equations that may be more complicated to the present case. So a different definition as shown in Figure 1.3 is applied for the final error estimation in this research, in which the error is defined as the distance between an original airfoil point and the parametric airfoil one with which the normal line to this original airfoil point crosses. As the tangent vector $\mathbf{P}'$

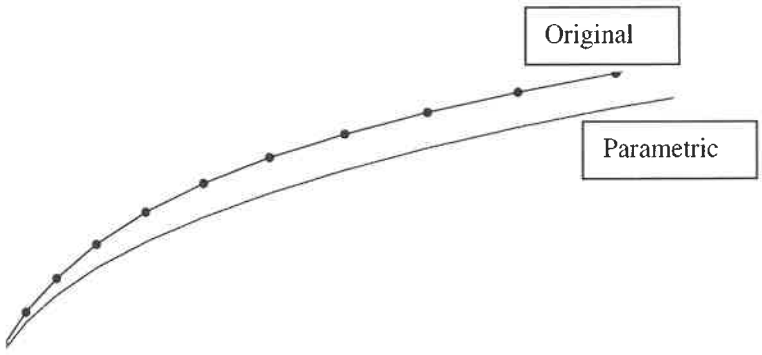

Figure 1.2 General error definition demonstration

at the original airfoil is calculated by the sixth order spline, it is convenient to determine the normal line. What is more, this definition takes already into account the global geometric tendencies of the original airfoil and thus it is more appropriate for airfoils than the general error definition which is only determined from discrete points. But the error defined in this way is generally larger than that commonly defined, which is a little conservative.

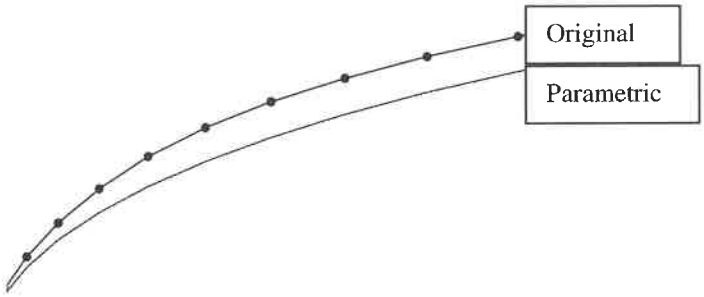

Figure 1.3 Error definition used in this thesis

The error calculation also needs solving non-linear equations, which are two equations for x, and y determined by formula (1.1) and one equation for the normal line. This equation system is solved by Newton iteration and the solution converges generally within 5 or 7 iterations. But it must be found which curve segment the normal line crosses with as the spline curve consists of several curve segments.

In objective functions, the error is just taken as the difference of two corresponding y coordinates between the original and parametric airfoils for calculation conveniences. As curves are parametric, the non-linear equation (1.1) for x needs to be solved to obtain parametric values t at given x locations and then y values are calculated at known t. The error like this is generally larger than that defined above. But the difference is small except near the leading edge where the curve slope is much larger than in the other parts. This has such an equivalent weighted effect on the objective function that the

approximated errors in this region tend to be reduced, which is aerodynamically favourable.

The manufacturing relative tolerance is about 10^{-4} in the key aerodynamic range which includes the leading edge area and the forepart of airfoil upper surface and is near 5×10^{-4} in other ranges, which is determined by aerodynamic sensitivity studies. For theoretic airfoils, the tolerance should be smaller. Thus in this research, the tolerance used is about 5×10^{-5} in the key aerodynamic range and 10^{-4} for the other part.

1.2.2 Selection of objective functions

Selection of objective function is crucial to approximation problems. But unluckily, there is no much mathematical basis about this problem because it concerns the problems like the error probability which belongs to the area of statistics (William H. Press and al, pp 650). Therefore, selection of objective functions depends on physical understanding of the concerned problems rather than mathematical reasoning. For airfoil approximations, it is necessary to control not only average errors but also the maximum because the maximum error must satisfy tolerance requirements. In this research, there are three forms of objective function applied among which one is as

$$\text{ofun}(\mathbf{P}, \mathbf{P}', \mathbf{P}'') = \sum_{i=1}^{n} w_i \left| y_{oi} - y_i \right|^p \qquad (1.11)$$

where n is the total number of original airfoil points or spline-interpolated points, i is the point number index, w is the weighted factor and p is the power index for which different values are used. The form with p =2 is most commonly used in this research.

If $p > 1$, larger errors will occupy more proportion in the objective function (1.11). Thus the maximum error can be better controlled even with all the $w_i = 1$ than the case of $p = 1$. If the error probability satisfies the normal distribution, the least-squires ($p = 2$)

correspond to the minimum error distribution. But this may not true and sometimes the maximum error control is more important. Therefore, larger p values are also tested in this research.

The second form of objective functions used is

$$\text{ofun}(\mathbf{P}, \mathbf{P}', \mathbf{P}'') = \frac{1}{n}\sum_{i=1}^{n}(y_{oi} - y_i)^p + \frac{fcm}{k-1}\sum_{j=1}^{k-1}\delta y_{max\,j}{}^p \qquad (1.12)$$

where k is the total number of control points, fcm is the factor between 0.3 and 1 for controlling the order of the second term, the subscript j is the curve segment index and $\delta y_{max\,j}$ is the maximum y difference on segment j.

In order to make comparisons, the third form of objective functions is also tried:

$$\text{ofun}(\mathbf{P}, \mathbf{P}', \mathbf{P}'') = \frac{1}{n}\sum_{i=1}^{n}(y_{oi} - y_i)^p + fcm\ \delta y_{max}{}^p \qquad (1.13)$$

where δy_{max} is the maximum y difference of the airfoil.

The second type (1.12) is specially tried to control the maximum error. The form of the second term is used to keep the objective function monotonous and is different from that used by some other authors. The form generally used contains only the maximum error as in the third type (1.13) with p = 1 and may not be appropriate for airfoil parameterization which is locally controlled by different parameters. The concerned discussions will be given in 3.1 with calculation results.

1.2.3 Determining control points

In this research, control points can be taken directly from the original airfoil and thus optimizations are not needed to get control points in this case. This is a great advantage over the other methods. The control points are selected according to their x locations which are nearest to the corresponding x values determined by the following simple distribution function:

$$x_i = A\,\xi_i^{\,2} - (A-1)\,\xi_i^{\,3} \tag{1.14}$$

where subscript i represents the control point number index, A is a constant (= 1.5 ~ 3), ξ_i corresponding to x_i is equally distributed over the airfoil chord and $0 \le \xi_i \le 1$.

The correction is generally needed for the two control points near the leading edge according to the leading edge curvature distribution. In addition, for airfoils of which the original points are not well distributed, the control points should be chosen from the interpolated spline points rather than the original ones.

1.2.4 Optimization

If approximation can be treated as a linear least-squires fit problem, it is more efficient to solve norm equations or to use the singular value decomposition (SVD). But for most of practical problems like airfoil designs that are generally strongly non-linear, the above methods may not be appropriate and thus optimization methods are often applied. Generally speaking, efficient gradient-based methods like steepest-descent and conjugate-gradient for finding one minimum cannot be used except that the initial guess is near a good solution, which is very difficult because the objective function generally contains a lot of minima. Consequently one of appropriate way is that the genetic algorithm is applied for the globe search and a gradient-based method used for the local

search if the objective function does not contain much noise. After all, it doesn't matter which kind of methods are used, the optimization is most likely to make the airfoil parameterization less efficient unless some special measures are taken.

In this research, as the control points can be determined without optimization and the initial values for the other two parameters (slope and curvature) are from calculation of the sixth order spline and can be supposed near the ones corresponding to a globe minimum. Moreover, the variations of the objective function are generally monotonous with those of slops and curvatures for fixed control points. As a result, an unconstrained conjugate-gradient method can be used, which can guarantee the efficiency of the airfoil parameterization. Of cause, it is possible that the obtained solution were only a local minimum rather than a globe one that cannot be confirmed even in mathematics theories.

1.2.4.1 Conjoint-gradient method

The conjugate-gradient method used in this research is based on Ashok and William H. Press. The new parameter vector position is equal to

$$\mathbf{x}_{k+1} = \mathbf{x}_k + \alpha_k \mathbf{d}_k \tag{1.15}$$

where the subscripts k +1 and k respectively mean the next iteration and the present iteration, $\mathbf{x}$: the vector position of optimization parameters, α: the step size and $\mathbf{d}$ is the conjugate direction vector.

In this research, the initial $\mathbf{x}_0$ is from the spline calculation as talked before, the initial direction $\mathbf{d}_0$ is taken equal to the steepest descent direction which is the opposite direction of the gradient of the objective function and the step size α_k is determined from the line search in which the minimum of the objective function at the given direction $\mathbf{d}_k$

is first bracketed by a three-point pattern and then calculated in iteration by Brent's quadratic fit. The next direction $\mathbf{d}_{k+1}$ is determined by

$$\mathbf{d}_{k+1} = -\mathbf{g}_{k+1} + \beta_k \mathbf{d}_k \tag{1.16}$$

where the vector $\mathbf{g}$ is the gradient of the objective function and β_k is calculated according to the following Polak-Rebiere formula:

$$\beta_k = \frac{\mathbf{g}_{k+1}^T (\mathbf{g}_{k+1} - \mathbf{g}_k)}{\mathbf{g}_k^T \mathbf{g}_k} \tag{1.17}$$

There is also another option in the program for calculating β_k:

$$\beta_k = \frac{\mathbf{g}_{k+1}^T \mathbf{g}_{k+1}}{\mathbf{g}_k^T \mathbf{g}_k} \tag{1.18}$$

Which is the Fletcher-Reeves version as results of considering $\mathbf{g}_{k+1}^T \mathbf{g}_k = 0$.

As generally objective functions are not quadratic and the search directions are not fully conjugated, the optimization is most likely not to converge within the iterations times equal to the total number n of control parameters. Thus a restart of optimization is needed every n iterations wherein a steepest descent step is taken. Moreover, uniformly scaling all parameters is essential for good behaviour of the conjugate-gradient method, especially in the cases of many parameters used.

In this research, it is relatively easy to scale the control parameters because the scaling is generally needed only between the slope and the curvature for which each parameter has its own local and relatively uniform control region and thus the difference among slope

derivatives is not large and so is that among curvature ones. In addition, it is found to be more effective that the factors multiplying slopes and curvatures are taken directly as the optimization parameters with their unitary initial values rather than slopes and curvatures themselves because these factors are more convenient for scaling and gradient calculations. However, the initial slopes and curvatures must be good enough in this case, for example, if any initial value is zero, it can never be improved during the optimization, though this kind of situations has never happened during the calculations.

How to calculate the gradient is also very crucial because it is impossible to obtain the gradient analytically in most practical applications. The precision of approximation methods is important but the numerical step is also one of the key factors. Too small step choice leads to a loss of significance error and too large step results in a large truncation error. A thumb rule given by Ashok and al, that the step is equal to the maximum of the minimum step and one percent of the initial parameter, is also proved working well in this research.

1.2.4.2 Genetic algorithm

Although the control points determined by the distribution function works well in most cases, they cannot meet the precision requirements sometimes. Consequently the optimization for control points is carried out. As it is difficult to use gradient-based methods to handle the problem, a genetic algorithm method is adapted.

The genetic algorithm is a powerful tool for difficult optimization problems. It is based on the evolution via survival of the fittest. The optimization is based on the code of David L. Carroll. The initial population is randomly selected which consists of the sample of individuals with different parameters. The tournament selection with a shuffling technique for choosing random pairs for mating is used as the selection scheme directing the genetic search. The binary encoding is used in the program to encode a

solution into a chromosome. The reproduction is made by jump mutation, creep mutation and the crossover operation with the option for single-point or uniform crossover. Niching (sharing) and an option for the number of children per pair of parents are also included. Moreover, the program has an option for the use of a micro-GA that accepts a very small population with only crossover operation for reproduction. Micro-GA can lead to more rapid convergence and its frequent re-generation of random population members can ensure the diversity during the search process.

The main modification to this code is that one of the individuals in the initial population is determined by the design experiences rather than randomly selected because all the members randomly selected are generally very far away from an acceptable solution and a reasonable initial guess is much better. This treatment can accelerate convergences but has the possibility to cause a premature optimization termination, which may depend on the globe search strategy.

As control points are only selected from airfoil points, a discrete optimization method like a GA with binary encoding is appropriate. Furthermore, it is more convenient to use the number index of control points as the optimization parameter instead of the x location. But besides the severe drawback due to the existence of Hamming cliffs, the binary encoding gives rise to some disadvantages to the application. It is very hard to determine properly variation ranges of optimization parameters which cannot be made continuous because it should satisfy the relation like 2^n-1 like 3, 7, 15, etc. while the overlap of control points is not allowed.

In this research, a micro-GA with a population of size 5 is confirmed to be very efficient but acceptable solutions depend too much on the appropriate division of the variation range for each parameter. Thus in the future research, it is practical to employ other GA methods such as ones with real number encoding and techniques for automatic adaptation of parameter variation ranges.

CHAPTER 2
CALCULATION RESULTS FOR AIRFOIL PARAMETERIZATION

2.1 Study of objective functions

The effects of the three forms of objective functions (defined in 1.2.2) to optimization solutions are studied first as their selections depend on particular problems.

Error distribution comparisons for different objective functions are shown in Figure 2.1 for NACA65-215 with 9 control points (one spline node automatically added between every two neighboring control points except the ones at the trailing edge). The result in Figure 2.1(a) is obtained by twice conjugate-gradient optimizations with a least-squires objective function (first form). The first time optimization from which the result is illustrated in Figure 2.1(b) is not weighted and the second is based on the first with the weighted factors for the points where errors surpass the given tolerance. The reduction of the maximum errors is about 4.5×10^{-5} in this case. This method is effective only if differences between surpassed errors and the tolerance are not large since error decreases in one area generally accompany increases in its neighboring area controlled by the same parameters because of the representation ability limit of a given spline function. The result in Figure 2.1(c) demonstrates that the second form can better control the maximum error than the first but the difference is not large.

Moreover, error distributions of NACA65-215 with 9 control points are presented in Figures 2.2, 2.3 and 2.4 respectively for the three forms of objective functions with different power Indices. Together with Figure 2.1(b), it is obvious: 1) the best results that the maximum error is smallest and the error distribution is more uniform always correspond to the power index $p = 2$ that is the least-squires form but for the third form

□ upper surface point △ lower surface point

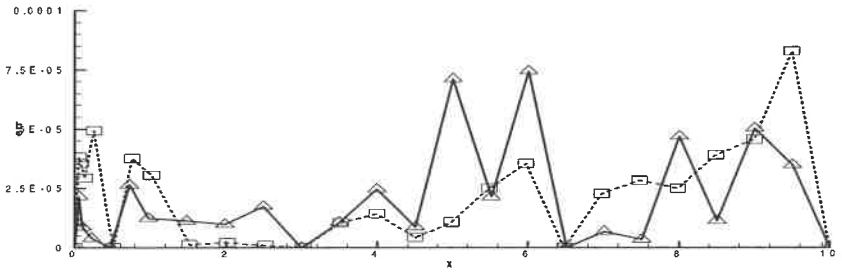

(a) Weighted least-squire : Max. error: $7.7*10^{-5}$

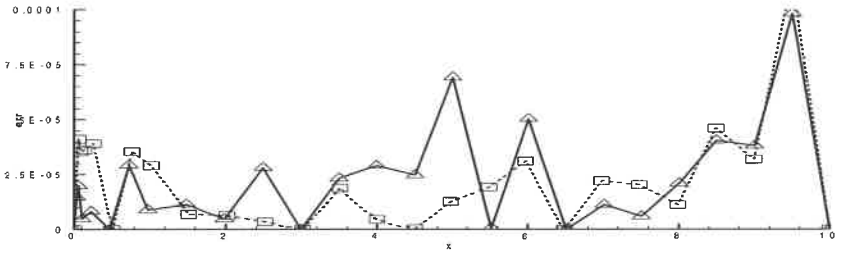

(b) Least-squire without weighted factors: Max. error: $1.15*10^{-4}$

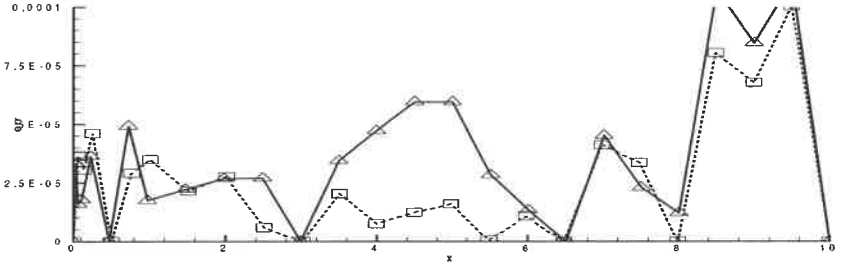

(c) Least-squire with the term added for max. error control without weighting: Max. error: $1.05*10^{-4}$

Figure 2.1 Error distribution Comparisons for Different Objective Functions

9 control points for NACA65-215

□ upper surface point △ lower surface point

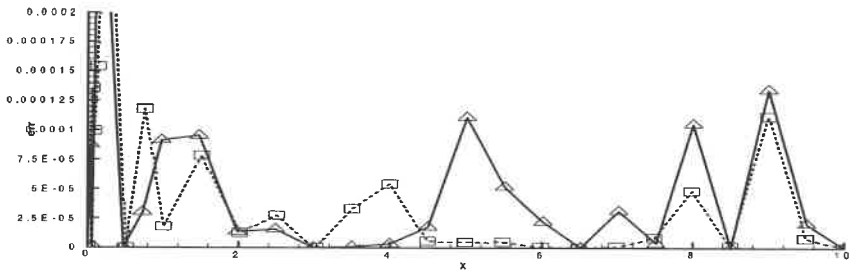

(a) Power index = 1 : Max. error: $3.63*10^{-4}$

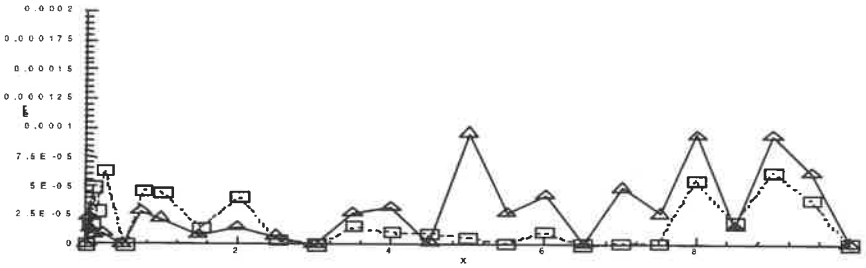

(b) Power index = 2 : Max. error: $9.56*10^{-5}$

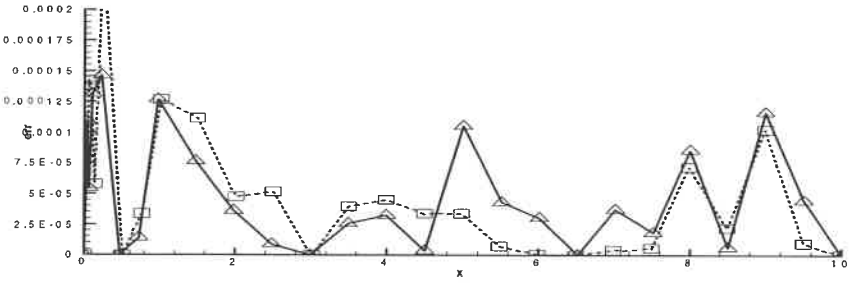

(c) Power index = 3 : Max. error: $2.41*10^{-4}$

Figure 2.2 Error Distribution Comparisons for the First Form of Objective Functions with Different Power Indices

9 control points for NACA65-215

□ upper surface point △ lower surface point

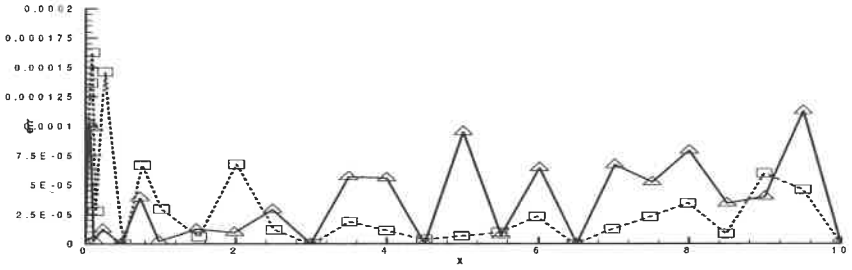

(a) Power index = 1 : Max. error: $1.63*10^{-4}$

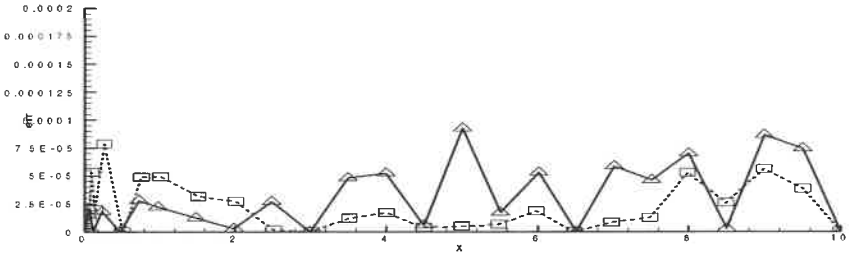

(b) Power index = 2 : Max. error: $9.24*10^{-5}$

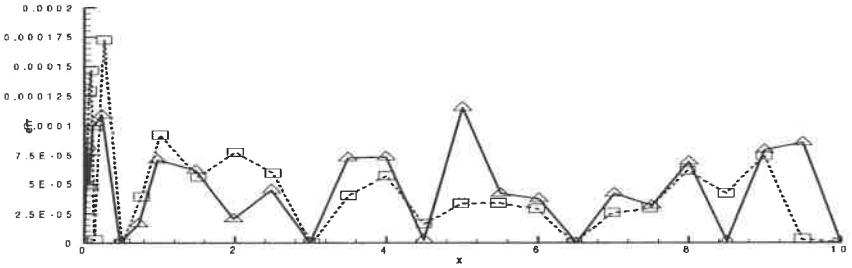

(c) Power index = 3 : Max. error: $1.73*10^{-4}$

Figure 2.3 Error Distribution Comparisons for the Second Form of Objective Functions with Different Power Indices

9 control points for NACA65-215

□ upper surface point △ lower surface point

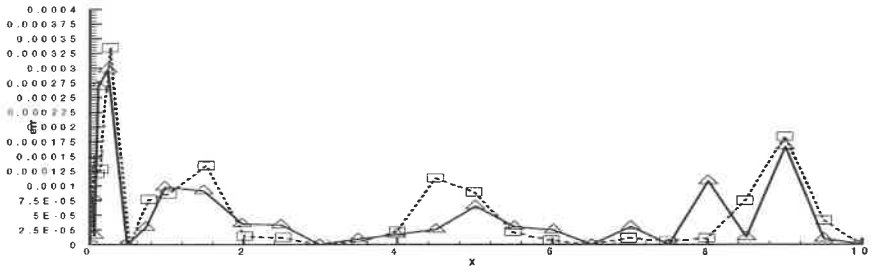

(a) Power index = 1 : Max. error: $3.32*10^{-4}$

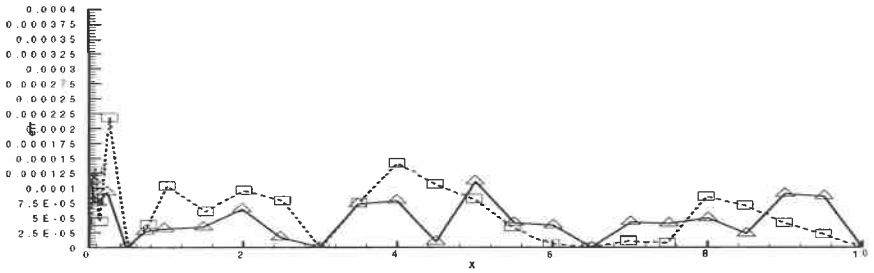

(b) Power index = 2 : Max. error: $2.25*10^{-4}$

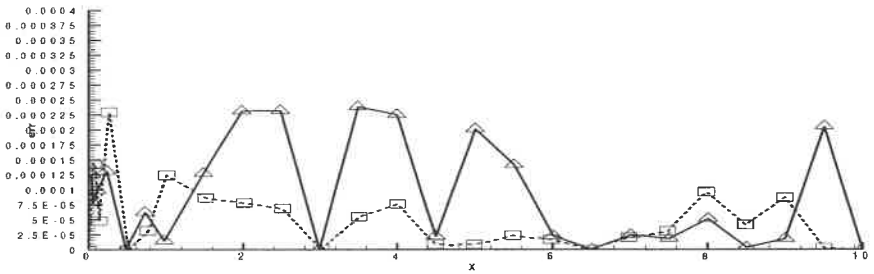

(c) Power index = 3 : Max. error: $2.41*10^{-4}$

Figure 2.4 Error Distribution Comparisons for the Third Form of Objective Functions with Different Power Indices

9 control points for NACA65-215

the variation differences are smaller among different power indices, 2) the error distributions for the second form are most uniform of the three forms for the entire power indices studied and the maximum errors are generally smallest. But the differences between the second and the first are small for the least-squires form and 3) for power index p = 2, the third form always corresponds to the worst situations of the three forms. The maximum errors are largest and the error distributions are less uniform.

Furthermore, maximum error variations of three airfoils (NACA65-215, NACA0012 and RAE2822) with different power indices are illustrated in Figure 2.5 for these three forms of objective functions. The similar conclusion can be obtained once more with a little exception that for NACA0012 the minimum maximum errors appear at p = 1 for the second and third forms, which also confirm that the two forms do have the control effects to the maximum error. Moreover, the variation relations of maximum errors with these of power indices are different among the three airfoils; for example, the maximum errors for third form are always about 4 times larger than the other ones for RAE2822 airfoil.

The least-squires formula can better control not only the average error but also the maximum error maybe because the error probability distribution approaches the normal distribution and larger errors make more contribution to the objective function with p >1 as discussed in 1.2. The second form of objective function is obviously superiors to the third one maybe owing to the following fact: the variations of the maximum error are not monotonous with these of the control parameters for the third form because the location of the maximum error can move randomly from one curve segment to another which is locally controlled by different parameters. As a result, more local minima are most likely to be formed artificially, which is unfavourable to optimization, especially to gradient-based methods. Thus the results may correspond only to ones of the many local minima formed in this way. The much more rapid convergence in these cases may also confirm the reasoning indirectly. The second form that contains the minima for all the curve segments can ensure relatively monotonous variations of objective functions. Of cause,

□ first form △ second form ○ third form

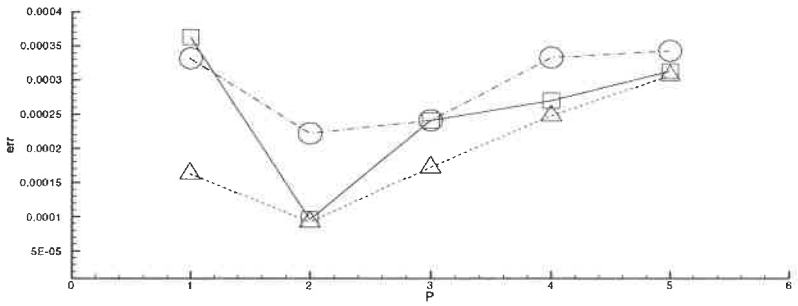

(a) 9 control points for NACA65-215

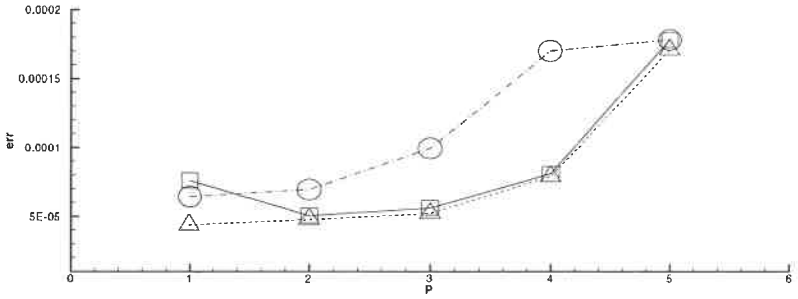

(b) 7 control points for NACA0012

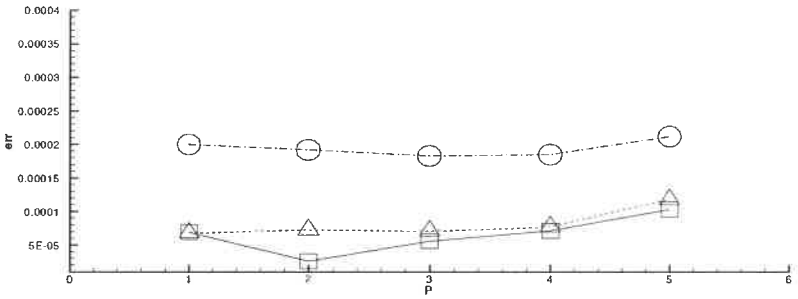

(c) 11 control points for RAE2822

Figure 2.5 Maximum Error Variations with Different Power Indices For Three Forms of Objective Functions

the behaviour of objective functions depends on particular problems and the above conclusion may not be general.

2.2 Scaling effects to the solutions of the conjugate-grading method

As the slope is not dimensional and the curvature has the dimension of length inverse, the scaling between the slope and the curvature can be made just by taking different airfoil chord lengths.

The scaling effects to the solutions of the conjugate-grading method are illustrated in Figure 2.6 by the maximum error variations with the changes of airfoil chord lengths for three airfoils. From the results, the calculations diverge for airfoil NACA65-215 and NACA0012 and don't converge well for RAE2822 if the chord lengths are smaller than one. For larger airfoil chord lengths, all the calculations converge but their differences are not large.

In theory, conjugate-gradient methods overcome the problems resulted from poor parameter scaling. In practice however, if the differences between the derivatives are too large, some direction may never be sufficiently explored because the search directions are generally not fully conjugated and the calculation will diverge or not converge to an optimized solution. Therefore, it is necessary to make all the derivatives the same order by uniformly scaling all parameters.

2.3 Parametric airfoil representation results

The results of the optimized airfoil parameterization for different types of airfoils including supercritical, natural laminar, low speed airfoils, ones for rotorcraft, etc. are shown in Figures 2.7 to 2.15 and Table 1.

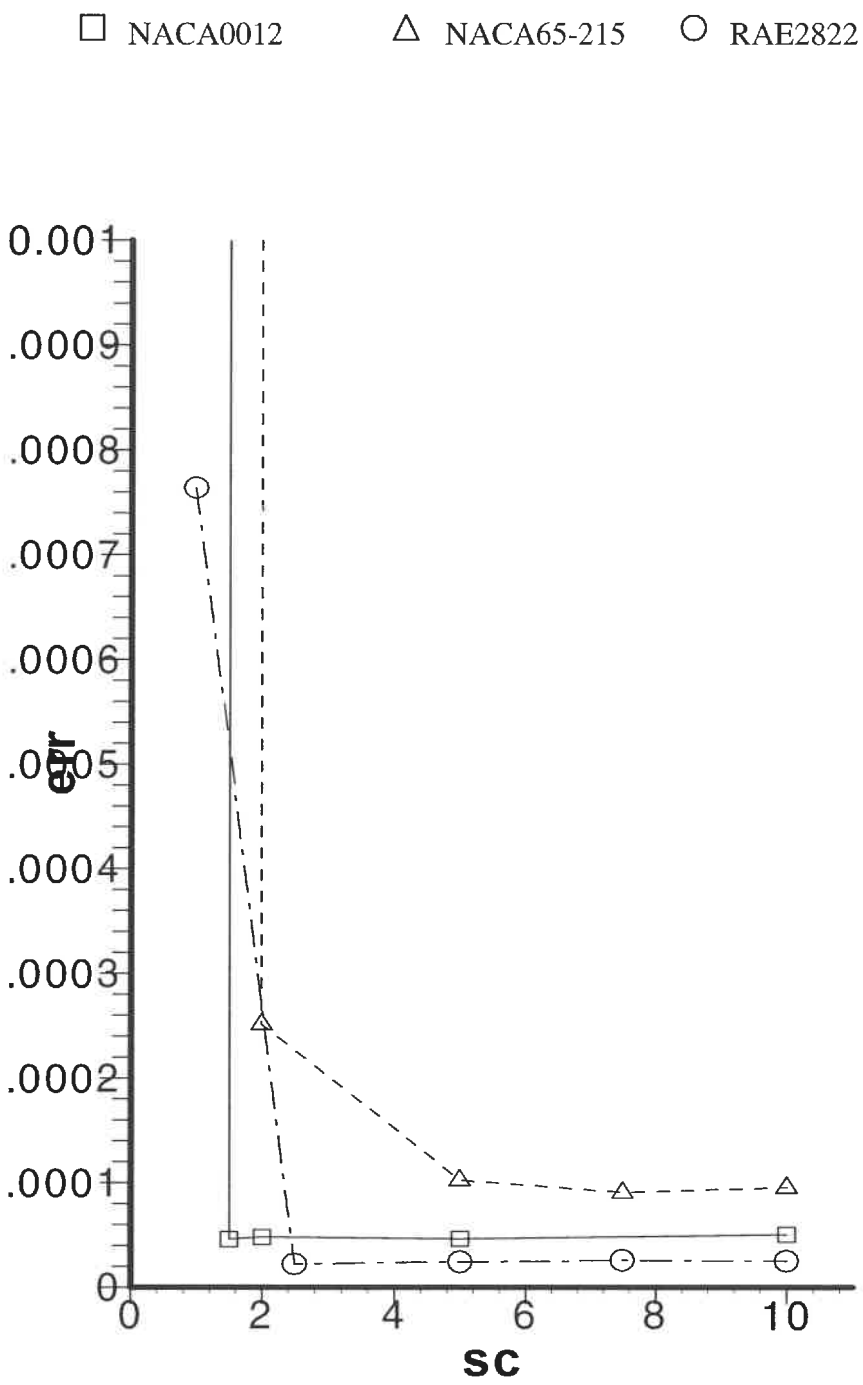

Figure 2.6 Scaling Effects to Maximum Errors

2.3.1 Optimized airfoil parameterization with control points fixed

The control points are fixed by the distribution function for the first six airfoils, RAE2822, RAE5215, NACA65-215, NACA64a-010, NACA2412 and NACA0012 in Table 2.1. The other control parameters are obtained by the conjugate-gradient optimization and all the calculations converge within 10 second (PC 800 MHz). These airfoils are represented with 7 to 11 control points and the maximum errors are between 2.5×10^{-5} to 7.7×10^{-5}. In all these cases, the airfoil representations are not only efficient

Table 2.1 Control Numbers and Maximum Errors for Calculated Parametric Airfoils

(KAR: key aerodynamic range; NKAR: non key aerodynamic range)

Airfoils	Number of Control Points	Maximum Errors	Location of Max. Errors
NACA0012	7	5.1×10^{-5}	KAR
NACA2412	9	5.7×10^{-5}	KAR
NASA64a010	9	6.4×10^{-5}	KAR
$NACA65_215$	9	7.7×10^{-5}	NKAR
RAE5215	11	6.5×10^{-5}	KAR
RAE2822	11	2.5×10^{-5}	NKAR
NASA SC(2)-0714	11	9.1×10^{-5}	NKAR
VR-12	11	1.0×10^{-4}	NKAR
NASA NLF(2)-0415	13	7.6×10^{-5}	NKAR
S1210	13	9.7×10^{-5}	NKAR

but also more accurate with fewer control points than the other methods, which is attributed not only to the techniques of airfoil representation but also to the treatments for optimization.

From the error distributions illustrated in Figures 2.7 to 2.12, some of solutions should be near the globe minima, e.g., for the supercritical airfoil RAE2822 with 11 control points and the maximum error of 2.5×10^{-5}, the error distribution is very uniform. But for the other cases, e.g., RAE5215, it is possible that the results correspond only to a near local minimum because of the limit of the optimization method that only searches one local minimum, although initial guesses from the spline calculation can generally guarantee better solutions. Moreover, the strategy used for selecting control points results from the efficiency consideration. The representation precision should be improved further if control points are also optimized.

Figure 2.7, 2.8 and 2.9 also show that adding spline nodes is essential to the representation precision, the maximum errors without adding nodes are three to five times higher than those with nodes added. In addition, the number and the position of added nodes have great influences to the precision of parametric airfoils. For RAE2822, RAE5215, NACA65-215, NACA64a-010 shown in Figure 2.7 to 2.10, one spline node is automatically added on each curve segment except the ones at the trailing edge. The similar is For NACA2412 and NACA0012 shown in Figure 2.11 and 2.12 but two nodes added at the two segments near the leading edges.

Some of above airfoils can be also represented with fewer control points and the results are also acceptable as shown in Figure 2.11 for NACA 2412 with 7 points and the maximum error 9.1×10^{-5}. Moreover, the effects of the weighted optimization are demonstrated again in Figure 2.9 to 2.10. All these two results are from twice optimizations. In this case, the method is still efficient (within 15 seconds) but it does not always function.

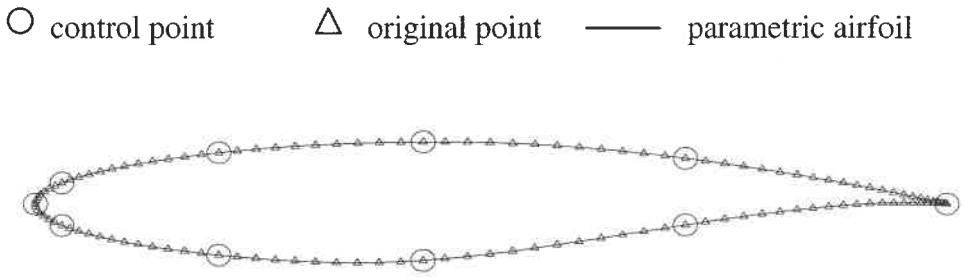

(a) Geometric form comparison between the parametric and original airfoils

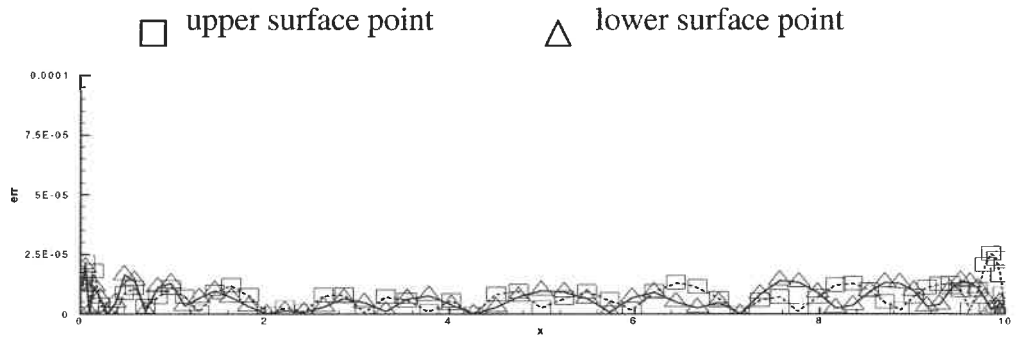

(b) Error distribution with additional nodes automatically added

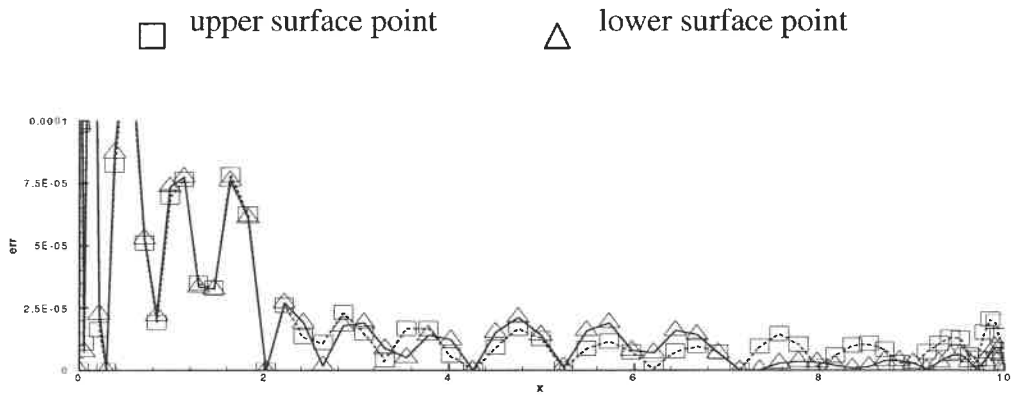

(c) Error distribution without additional nodes added

Figure 2.7 Parametric Airfoil Optimization Results

11 control points for RAE2822 Max. error: $2.5*10^{-5}$

○control point △original point ____parametric airfoil

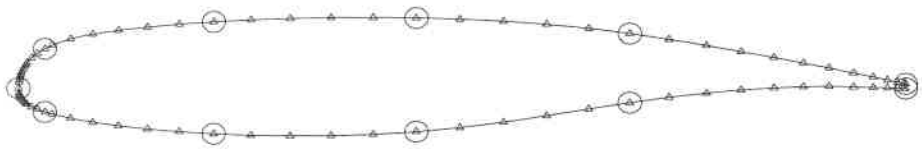

(a) Geometric form comparison between the parametric and original airfoils

□ upper surface point △ lower surface point

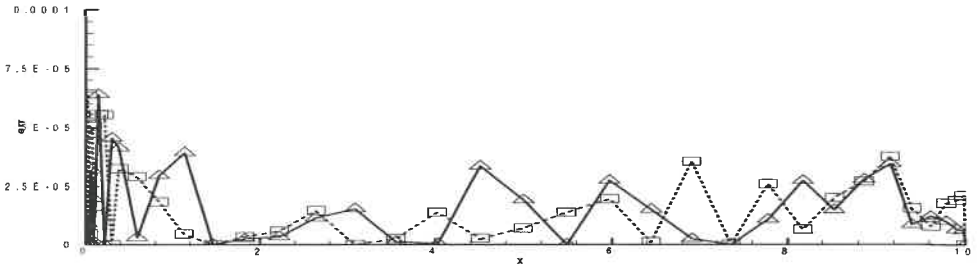

(b) Error distribution with additional nodes automatically added

□ upper surface point △ lower surface point

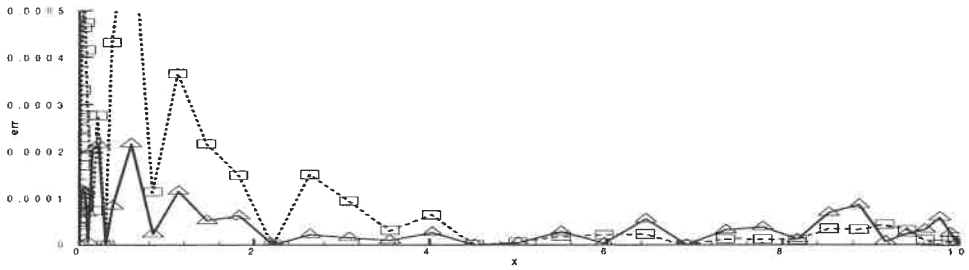

(c) Error distribution without additional nodes added

Figure 2.8 Parametric Airfoil Optimization Results

11 control points for RAE5215 Max. error: $6.5*10^{-5}$

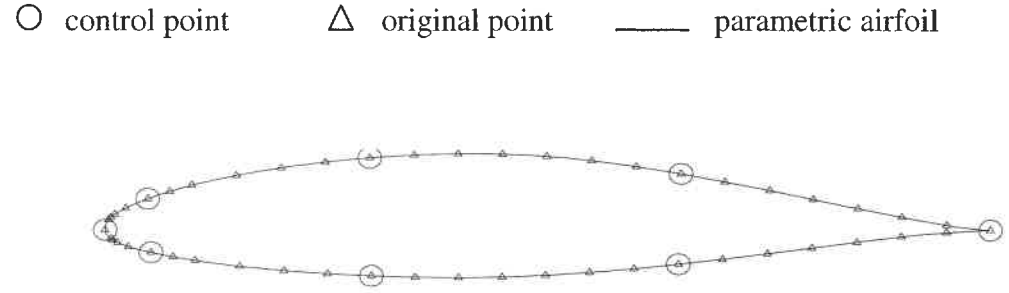

(a) Geometric form comparison between the parametric and original airfoils

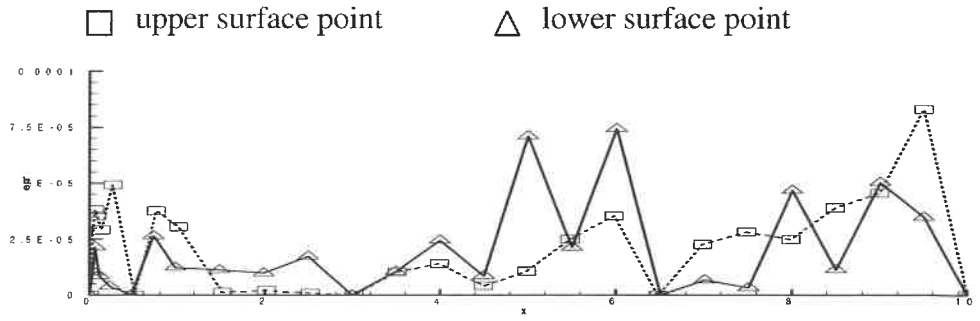

(b) Error distribution with weighted least-squire optimization

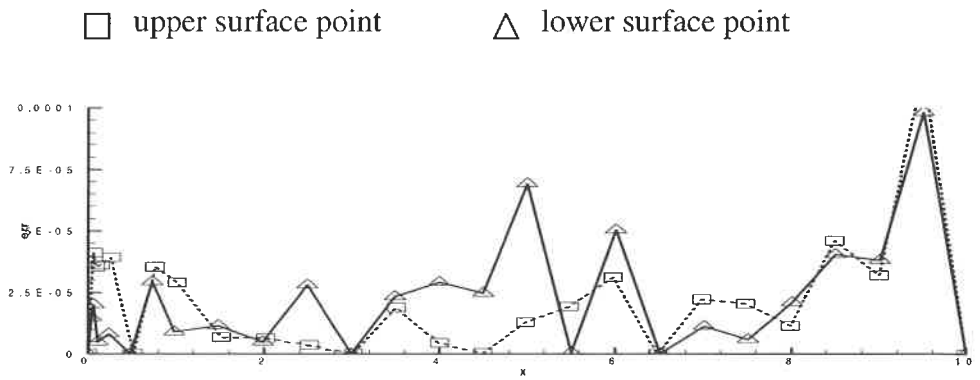

(c) Error distribution without weighted optimization

Figure 2.9 Parametric Airfoil Optimization Results

9 control points for NACA65-215 Max. error: $7.7*10^{-5}$

○ control point △ original point ____ parametric airfoil

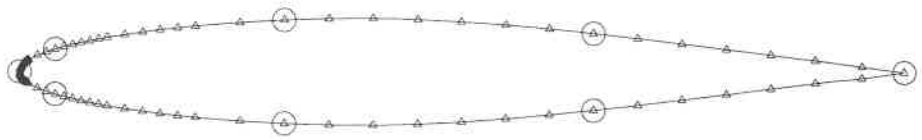

(a) Geometric form comparison between the parametric and original airfoils

□ upper surface point △ lower surface point

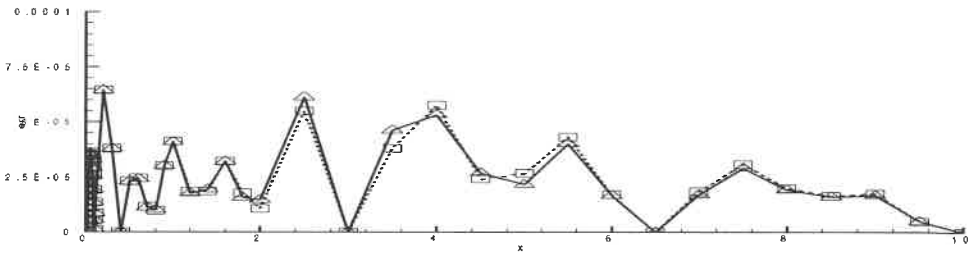

(b) Error distribution with weighted least-squire optimization

□ upper surface point △ lower surface point

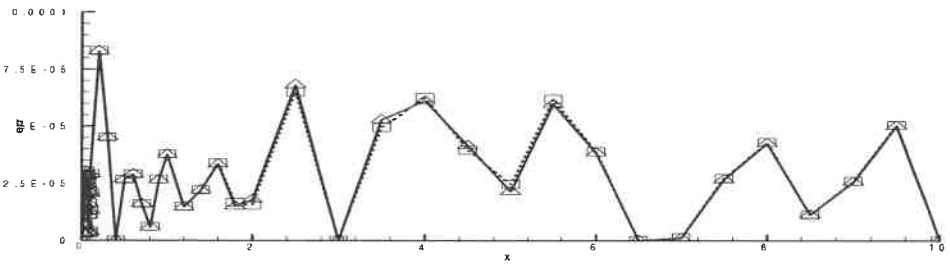

(c) Error distribution without weighted optimization

Figure 2.10 Parametric Airfoil Optimization Results

9 control points for NACA64a-010 Max. error: $6.4*10^{-5}$

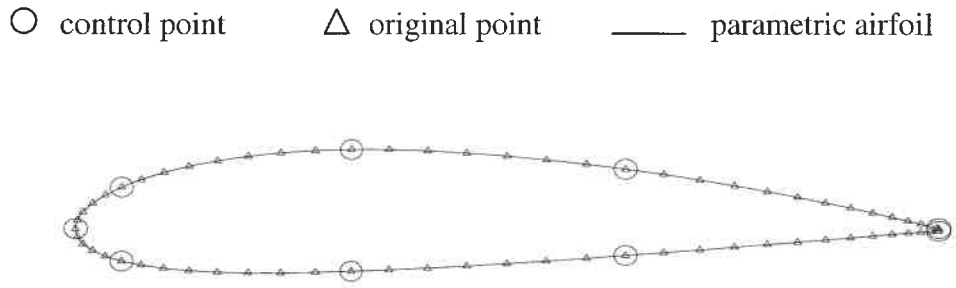

(a) Geometric form comparison with 9 control points between the parametric and original airfoils

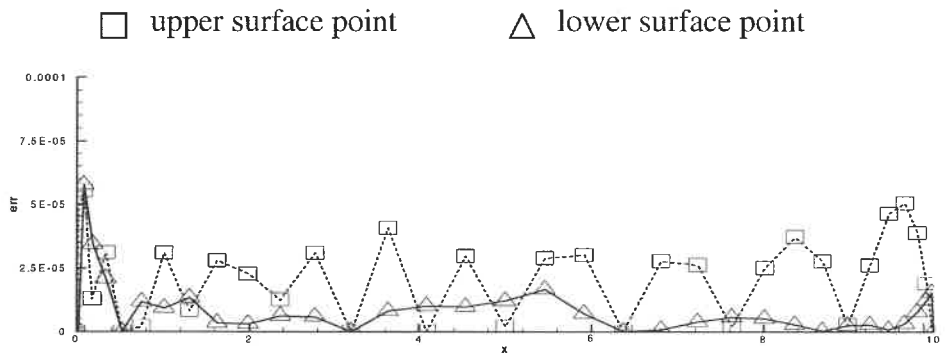

(b) Error distribution with 9 control points; Max. error: $5.7*10^{-5}$

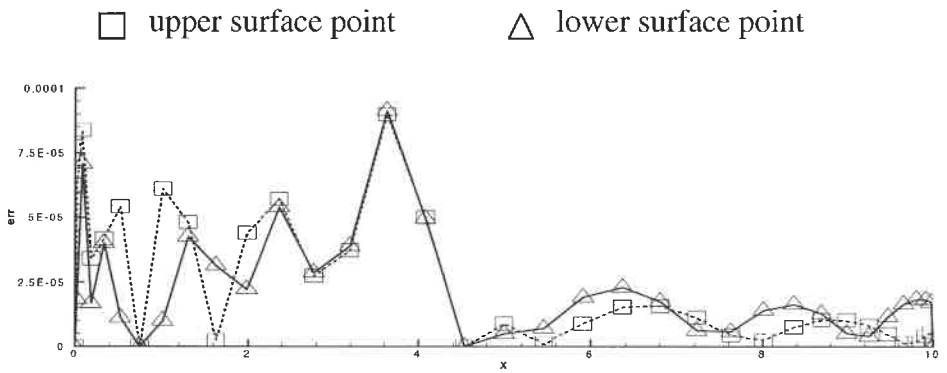

(c) Error distribution with 7 control points; Max. error: $9.1*10^{-5}$

Figure 2.11 Parametric Airfoil Optimization Results

for NACA2412

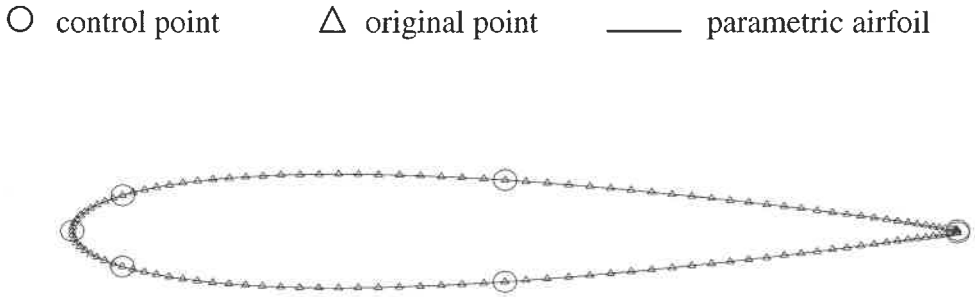

(a) Geometric form comparison between the parametric and original airfoils

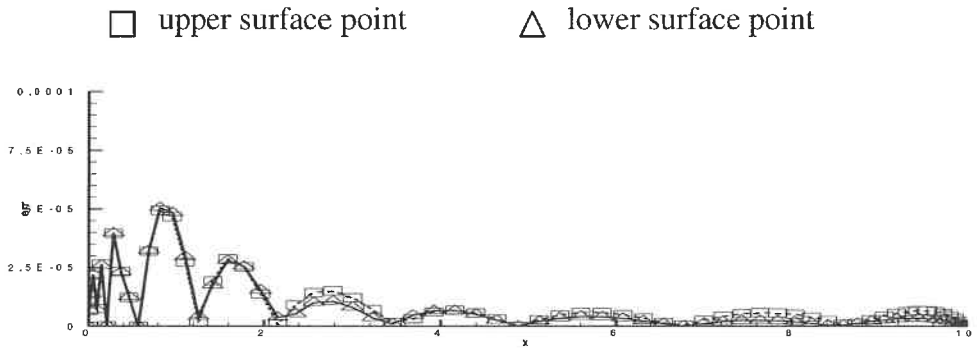

(b) Error distribution with additional nodes automatically added

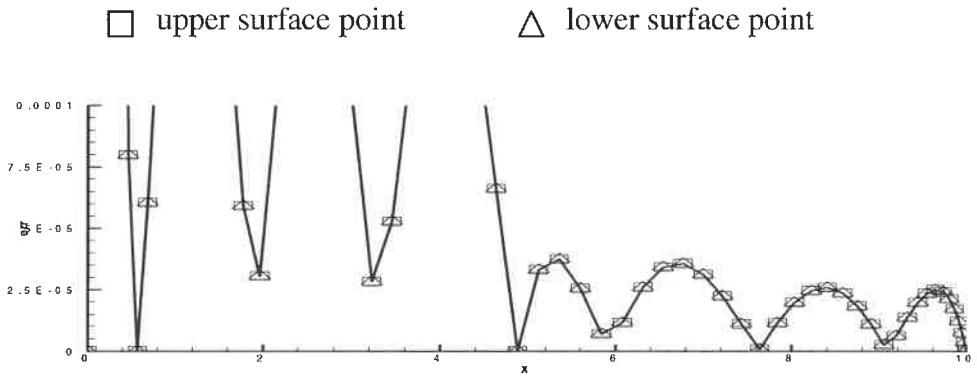

(c) Error distribution without additional nodes added

Figure 2.12 Parametric Airfoil Optimization Results

7 control points for NACA0012 Max. error: $5.1*10^{-5}$

2.3.2 Airfoil parameterization with x locations optimized

The method for fixing control points does not work well for the last several airfoils, NASA SC(2)-0714, NASA NLF(2)-0415, VR12 and S210 in Table 2.1 because the x distribution function is not suitable to them. Thus a genetic algorithm (GA) method is used for optimization of the x locations combined with the gradient method optimization for slopes and curvatures. For the latter three airfoils, one spline node is also automatically added on each curve segment except the ones at the trailing edge. For NASA SC(2)-0714, spline nodes are added only on the two segments near the leading edge. The optimization for x locations is carried out by a micro-GA with 5 members of the population. An acceptable solution can be obtained within 150 generations if the x variation range is appropriately specified, which takes less than one hour on an 800 MHz personnel computer.

From the results illustrated in 2.14, The NASA SC(2)-0714 can be represented with 11 control points and the maximum error 9.1×10^{-5}. The results is acceptable but the errors are a little larger and the error distribution is not uniform because adding spline nodes does not work very well in this case. New techniques for adding spline nodes should be developed to improve the situation.

NASA NLF(2)-0415 airfoil is represented with 13 control points and the maximum error is 7.56×10^{-5}at the location near the trailing edge, which are shown in Figure 2.13 (a) and (b). The error distribution is aerodynamically favourable since the errors at the forepart of the airfoil are smaller and more uniform. Considering that NLF(2)-0415 is a natural laminar airfoil that the geometry is more complex and there are several areas where the curvature variations are large, the result is excellent. The error distribution of this airfoil with 11 control points is also illustrated in Figure 2.13(c). The larger errors appear only at the aft-part of the airfoil and the maximum error is near 1.2×10^{-4}, which demonstrates

that it is possible to represent accurately this airfoil with 11 control points if the concerned treatments are improved further.

For VR12 airfoil shown in Figure 2.14, the maximum error (1.02×10^{-4}) is little larger than the tolerance requirement but it appears near the trailing edge. For S210 airfoil shown in Figure 2.15, the errors are smaller than 5.5×10^{-5} in key aerodynamic range and the larger errors appear at the lower surface and are smaller than the tolerance requirements.

Though the representation precision can be acceptable for VR12 and S210 airfoils, the optimization are not very successful. From the results shown in Figure 2.14 and Figure 2.15 respectively for VR12 and S210 airfoils, the x location distributions of the control points are obviously not very reasonable, which can be confirmed by the non-uniform error distributions. The errors are larger near the leading edge and the trailing edge while they are smaller at the middle part for VR12. There are larger waves in S210 lower surface error distribution. This is due to the following reasons: 1) x location variation range for each control point is not well specified because GA used utilises binary encoding, which greatly limits the flexible definition of variation ranges for control parameters (see 1.2.2.3). 2) optimization solutions may correspond to local minima that are not good enough because they are calculated with the micro GA . Micro GA is much more efficient than general GA but its search range is most likely to be limited. 3) The strategy that the control points are selected from the original airfoil points is not flexible especially for airfoils which have few points or of which the original points are not well distributed. 4) The method for adding additional spline nodes may not be appropriate to these kinds of airfoils. 5) The accurate representation capability of the spline curve may be limited for complex geometries.

○ control point △ original point ——— parametric airfoil

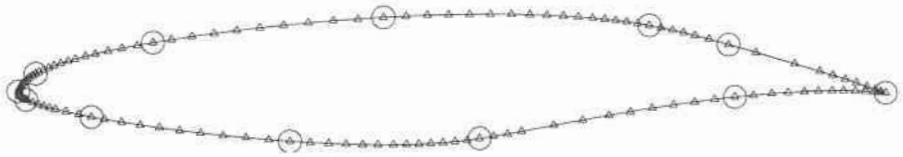

(a) Geometric form comparison between the original airfoil and the parametric one with 13 control points

□ upper surface point △ lower surface point

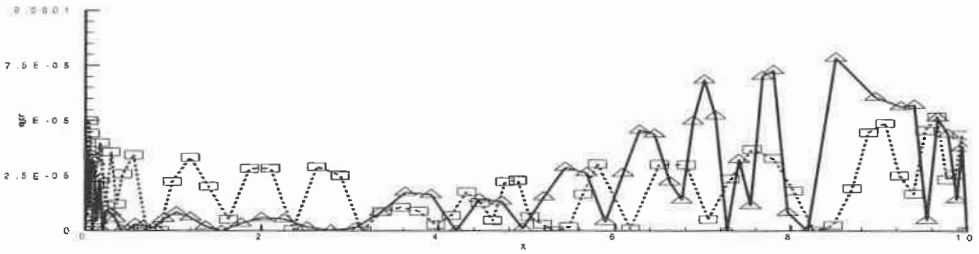

(b) 13 control points; Max. error: $7.6*10^{-5}$

□ upper surface point △ lower surface point

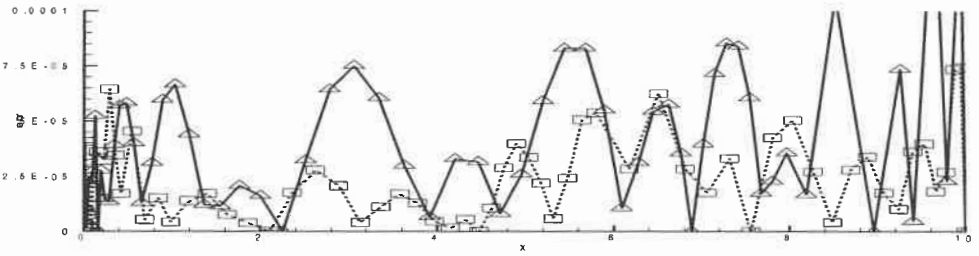

(c) 11 control points; Max. error: $1.2*10^{-4}$

Figure 2.13 Parametric Airfoil Optimization Results

for NASA NLF(2)-0415 with x locations optimized

○ control point △ original point ——— parametric airfoil

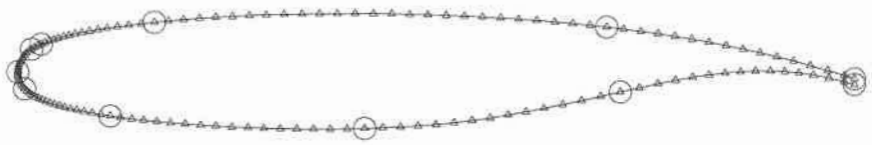

(a) Geometric form comparison between the original airfoil and the parametric one

□ upper surface point △ lower surface point

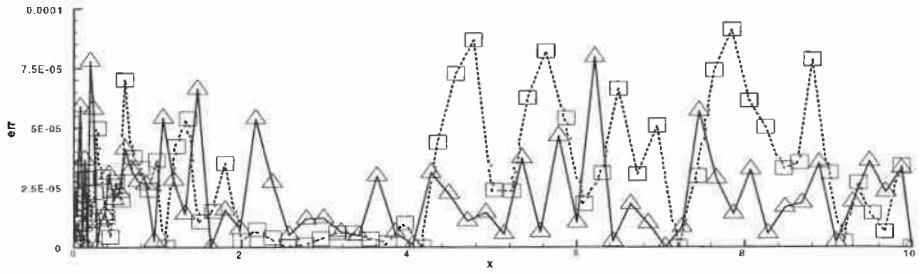

(b) Error distribution with control point x locations optimized

□ upper surface point △ lower surface point

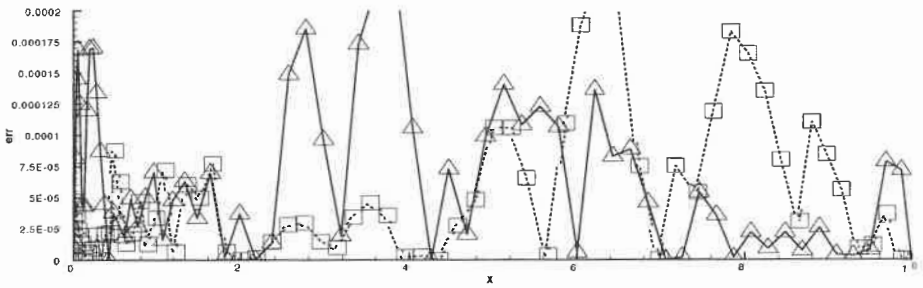

(c) Error distribution without control point x locations optimized

Figure 2.14 Parametric Airfoil Optimization Results

11 control points for NASA SC(2)-0714 Max. error: $9.13*10^{-5}$

○ control point △ original point ____ parametric airfoil

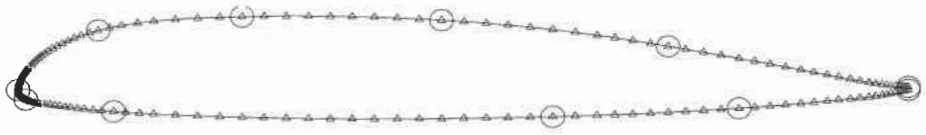

(a) Geometric form comparison between the parametric and original airfoils

□ upper surface point △ lower surface point

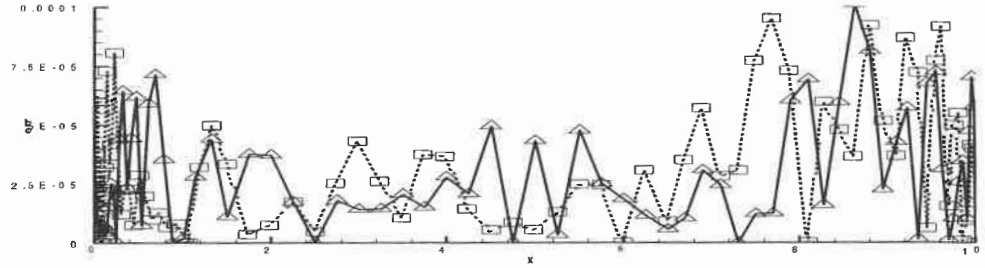

(b) Error distribution with control point x locations optimized

□ upper surface point △ lower surface point

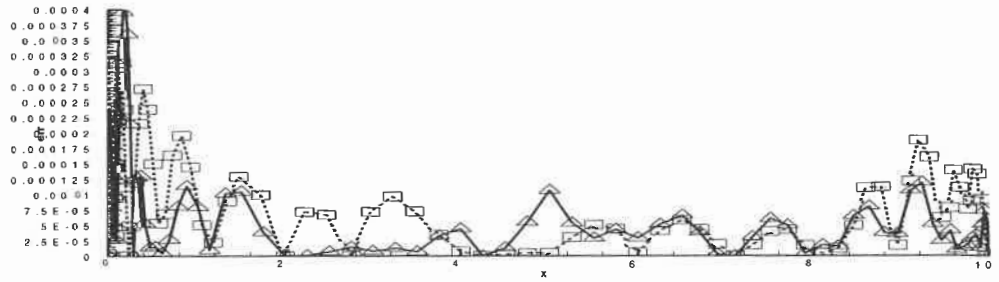

(c) Error distribution without control point x locations optimized

Figure 2.15 Parametric Airfoil Optimization Results

11 control points for VR-12 Max. error: $1.01*10^{-4}$

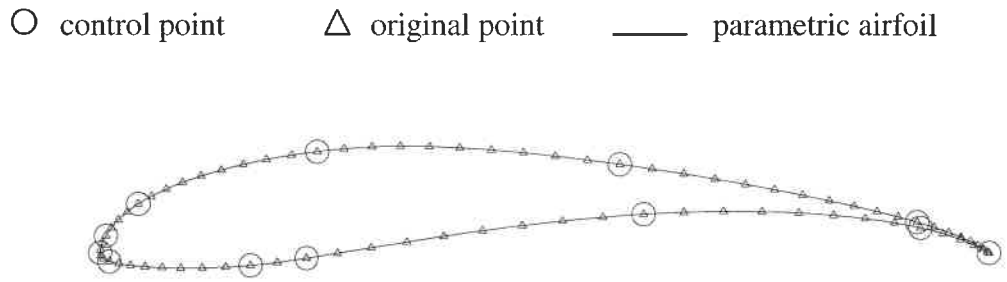

(a) Geometric form comparison between the parametric and original airfoils

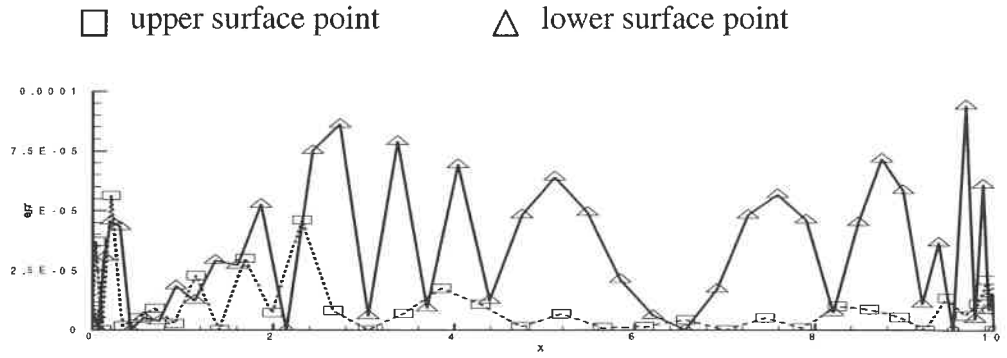

(b) Error distribution with control point x locations optimized

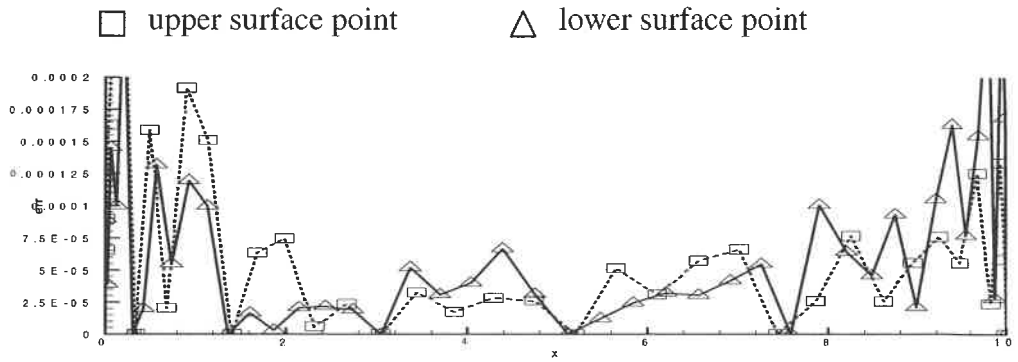

(c) Error distribution without control point x locations optimized

Figure 2.16 Parametric Airfoil Optimization Results

13 control points for S1210 Max. error: $9.7*10^{-5}$

2.3.3 Comparisons with some other results

Comparisons with some results of NURBS method (Trépanier J. -Y., Lépine J. L. and Pépin F) that is most accurate of all the other methods are shown in Table 2.2. The objective of these comparisons is just to get some ideas about the precision of the present method because the two methods are not based on the same comparison conditions.

Table 2.2 Control Point Number and Maximum Error Comparisons

AIRFOIL	CONTROL NUMBER		MAXIMUM ERROR	
	This Method	NURBS	This Method	NURBS
NACA2412	9	9	5.7×10^{-5}	8.0×10^{-5}
NASA64a010	9	11	6.4×10^{-5}	7.8×10^{-5}
RAE2822	11	13	2.5×10^{-5}	7.8×10^{-5}
VR12	11	11	1.0×10^{-4}	8.2×10^{-5}
S1210	13	13	9.7×10^{-5}	7.3×10^{-5}

For the former three cases of fixed control points, the results of the present method are obviously superiors to those of NURBS. For the latter two that need the optimization of control points, NURBS results are a little better. Thus the present method has no advantage over NURBS method for these kinds of geometrically complex airfoils, considering that NURBS needs only three control parameters at each point. The raisons may be: 1) the GA optimization used is not very appropriate and 2) NURBS is more powerful for complex geometric representations. Luckily, VR12 is only designed for rotary-crafts and rarely used. S1210 is a high lift airfoil that is only used in theoretic researches and cannot find practical applications because of its severe structural weaknesses.

CHAPTER 3
ITERATIVE INVERSE
AERODYNAMIC DESIGN METHOD

3.1 Governing Equations

The energy equation or momentum equation with the isentropic relations along a streamline can be written as

$$\frac{\gamma}{\gamma - 1}\left(\frac{p}{\rho}\right) + \frac{V^2}{2} = \frac{\gamma}{\gamma - 1}\left(\frac{p_\infty}{\rho_\infty}\right) + \frac{V_\infty{}^2}{2} \tag{3.1}$$

where p is the pressure, ρ the density, V the velocity, γ is the ratio of specific heat and the subscript ∞ represents free-stream values.

The momentum equation normal to the streamline has the following form:

$$\rho V^2 \kappa = \frac{\partial p}{\partial \eta} \tag{3.2}$$

where κ is the curvature and η is the coordinate normal to airfoil surface.

For a streamline tube very near the airfoil as shown in Figure 3.1, with the first order accuracy for η, the continuity equation can be approximated as

$$\rho V \eta + \frac{1}{2}\frac{\partial \rho V}{\partial \eta}\eta^2 = C \tag{3.3}$$

where C is a constant.

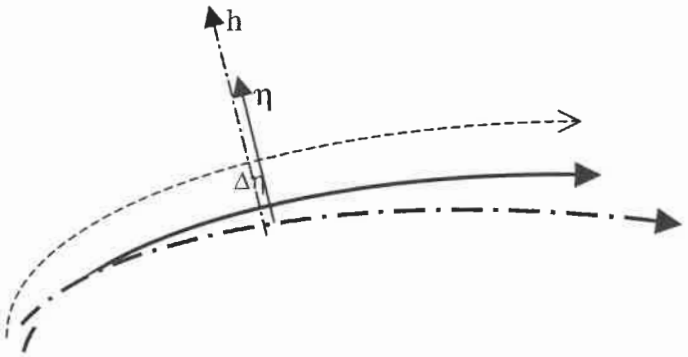

——— Airfoil surface -------- Streamline

—·— Reference coordinate (or curve)

Figure 3.1 Streamline Tube and Its Coordinates near Airfoil

Supposing small differences or perturbation between target and design airfoils, the following equations can be obtained:

$$
\begin{aligned}
&(\rho V)_o = \rho V + \Delta(\rho V) \\
&\eta_o = \eta + \Delta\eta \\
&\left(\frac{\partial \rho V}{\partial \eta}\right)_o = \frac{\partial \rho V}{\partial \eta} + \Delta\left(\frac{\partial \rho V}{\partial \eta}\right)
\end{aligned}
\tag{3.4}
$$

where the subscript o represents object values.

Substitute (3.4) into (3.3):

$$
\begin{aligned}
&(\rho V)_o \Delta\eta + \eta\Delta(\rho V) + \eta\Delta\eta \frac{\partial \rho V}{\partial \eta} + \\
&\frac{1}{2}\eta^2\Delta\left(\frac{\partial \rho V}{\partial \eta}\right) + \eta\Delta\eta\Delta\left(\frac{\partial \rho V}{\partial \eta}\right) = 0
\end{aligned}
\tag{3.5}
$$

The target pressure distribution is generally specified for inverse design and therefore it is convenient to express the variables in (3.5) as functions of pressure coefficients with the above equations and the following state equation (3.6), the sound speed relation (3.7), the isentropic relation (3.8) and the pressure coefficient definition (3.9)

$$P = \rho RT \tag{3.6}$$

$$a^2 = \gamma RT \tag{3.7}$$

$$\left(\frac{p}{\rho}\right)^{\gamma} = \left(\frac{p_\infty}{\rho_\infty}\right)^{\gamma} \tag{3.8}$$

$$C_p = \frac{p - p_\infty}{\frac{1}{2}\rho V_\infty^2} \tag{3.9}$$

where R is the gas constant, a represents the sound speed and C_p the pressure coefficient.

Thus the following dimensionless relations can be obtained:

$$F(C_p, M_\infty) = \frac{\rho V}{\rho_\infty a_\infty} = \sqrt{2}\,\left(1 + \frac{1}{2}\gamma M_\infty^2 C_p\right)^{1/\gamma} A \tag{3.10}$$

where

$$A = \left[\frac{1}{2}M_\infty^2 + \frac{1}{\gamma - 1} - \frac{1}{\gamma - 1}\left(1 + \frac{1}{2}\gamma M_\infty^2 C_p\right)^{1 - 1/\gamma}\right]^{1/2} \tag{3.11}$$

Consequently

$$\frac{1}{\rho_\infty a_\infty}\frac{\partial \rho V}{\partial \eta} = -\frac{\partial F}{\partial C_p}\frac{\partial C_p}{\partial n} = F' f \kappa \tag{3.12}$$

where M is Mach number and f is the function of C_p and M_∞ as following

$$f(C_p, M_\infty) = \frac{4}{M_\infty^2}\left(1 + \frac{1}{2}\gamma M_\infty^2 C_p\right)^{1/\gamma} A^2 \tag{3.13}$$

From equations (3.10) and (3.12), equation (3.5) becomes:

$$\eta F + \frac{1}{2}\eta^2 \kappa F' f = 0 \tag{3.14}$$

Substitute η, F, κ and f in equation (3.14) respectively with $\eta + \Delta\eta$, $F + \Delta F$, $\kappa + \Delta\kappa$ and $f + \Delta f$, ignore the higher order terms of $\Delta\eta$,

$$\left(\frac{1}{2}\eta + \Delta\eta\right)\eta F' f\, \Delta\kappa + \left(F_o + \eta F'_o f_o \kappa\right)\Delta\eta +$$

$$\eta \Delta F + \frac{1}{2}\eta^2 \kappa \Delta(F' f) = 0 \tag{3.15}$$

From (3.4), and Figure 3.1 :

$$\eta_o \approx h_o - h_{os}; \qquad \eta \approx h - h_s$$

As a result

$$\Delta\eta \approx (h_o - h) - (h_{os} - h_s) = \Delta h - \Delta h_s \tag{3.16}$$

where h is the coordinate normal to the reference curve (which can be considered as one of target and designed airfoil surfaces), the subscripts o and s mean objective and surface values respectively.

The streamlines very near the airfoil surface are geometrically similar to the airfoil form itself and there is nearly no difference between streamlines very far away from an airfoil owing to the same free-stream condition; therefore it can be supposed that the difference between a near streamline around the target airfoil and the corresponding one around the design airfoil is proportional to and smaller than that between the two airfoils. That is to say,

$$\Delta \eta = - D \Delta h_s \tag{3.17}$$

where D is a small positive constant and can be made equal to the initial streamline value of the design airfoil without loss of generality

$$D = \eta_0 / c \tag{3.18}$$

where the subscript 0 represents the initial value.

In addition, note that the curvature increment

$$\Delta \kappa = \frac{\partial^2 \Delta h_s}{\partial s^2} \tag{3.19}$$

Therefore from (3.14) through (3.18), the following equation can be deduced:

$$A1 \frac{\partial^2 \Delta h_s}{\partial s^2} + A3 \Delta h_s + B = 0 \tag{3.20}$$

where

$$A1 = (\frac{1}{2}\eta + \Delta \eta)\, \eta\, F' f$$

$$A3 = -(F_o + \eta F'_o f_o \kappa)\frac{\eta_0}{c} \qquad (3.21)$$

$$B = \eta \Delta F + \frac{1}{2}\eta^2 \kappa \Delta (F' f)$$

The above equation cannot be applied directly for the sake of the following fact. The ordinary differential equation (3.20) is very stiff. The first coefficient A1 is of the same order as the other ones only near the leading edge away from which A1 decreases very rapidly. But this term cannot be ignored even if it can be made much smaller by choosing a smaller $\Delta \eta$. Otherwise it is impossible to obtain a reasonable solution near the leading edge due to its larger curvature variations. Furthermore, applying the equation (3.20) to the whole airfoil leads to non-physical solutions. That is because the other ignored terms can be of the same order as the coefficient A1 or even greater than it in the other ranges. Therefore physically it is meaningless to keep using this equation. In addition, the constant D is little arbitrarily determined because exactly it is also an unknown variable. But if the initial point is chosen as the stagnation point or the leading edge with zero value, the geometric variations Δh_s near the leading edge is generally so small that this small arbitrarily determined constant D has nearly no influence to the solution if the full equation is applied only near the leading edge. Therefore for the other part of airfoils, the following algebraic equation is used, which is equation (3.20) with the first term ignored:

$$A3 \Delta h_s + B = 0 \qquad (3.22)$$

For transonic flow, it can be confirmed that $F'(= \partial (\rho V)/ \partial C_p)$ dominating the properties of the first coefficient of equation (3.20) is positive for supersonic flow, negative for subsonic flow and null at sonic point. That is to say, the sonic point is a singular point for equation (3.20). In fact, this singular point does not pose any serious problem to applications because this term is much smaller than the other ones, hence it can be ignored within the supersonic zone and equation (3.22) might be used instead. Moreover, the term B of equation (3.22) dominated by the difference $\Delta F (= \Delta(\rho V))$ also shows

different tendencies for subsonic and supersonic flows, thus with the same pressure difference, the direction of the geometric perturbations for supersonic flows is opposite to that of subsonic ones. In addition, for supersonic flows, the flow influence region is only limited in Mach zones and as a result, equation (3.22) should be adapted and it is more suitable to use the following differential form of equation (3. 15) with the first term ignored treated as initial value problems:

$$A2T\,\Delta\eta' + A3T\Delta\eta + BT = 0 \tag{3.23}$$

where

$$\begin{aligned} A2T &= F_o + \eta F'_o f_o \kappa \\ A3T &= F'_o C_p'_o + \eta' F'_o f_o \kappa \\ BT &= \eta \Delta (F' C_p') + \eta' \Delta F + \eta\eta' \kappa \Delta (f F') \end{aligned} \tag{3.24}$$

However, transonic flows with their small supersonic zones can be greatly different from pure supersonic ones with very far free boundaries. The supersonic variation relation between the geometry and the pressure is not valid everywhere for transonic flow, especially at beginning of the small supersonic zone where the general geometry and pressure variations may still obey the subsonic relations. This phenomenon may be simply explained by reflection of expansion waves from the very near sonic line as shown by Farrari C. or Moulden T. H . These reflected waves are compressive and attend to slow down the flow. Therefore if there is a small concave region even invisible on the airfoil surface, the flow may decelerate instead of accelerating because of the effects of reflected compressive waves and vice versa. Moreover, for transonic flows it is not appropriate to express the geometry similarity assumption of near streamlines to the airfoil surface as in equation (3.17), an additional relation of streamline slopes may be preferred. What is more, the above equations are based on the surface values rather than the whole flow field. Therefore they cannot reflect transonic flow characteristics such as

wave interference. The correction to transonic effects must be taken into account, which is realised by the treatments based on following ideas. Streamline slopes are the same along their isoclines, but only from the surface variables is it impossible to define the isoclines. Consequently, an approximated relation is tried from characteristic lines whose direction is known at the airfoil surface. The angles ϑ of the streamline line relative to Cartesian coordinate x satisfies the following relation (Moulden, T. H. p110) :

$$\vartheta + \omega = \text{constant} \tag{3.25}$$

where ω is Prandtl-Meyer function.

It is supposed that the slope difference of near streamlines between the target and design airfoils is proportional to and smaller than that between the two airfoil forms along the characteristic lines:

$$\Delta h_s' - \Delta h_c' = D \Delta h_s' \tag{3.26}$$

where D represents a small positive constant and the subscript c the value at the characteristic line.

Since the equation will be solved as an initial value problem, the left characteristics are supposed to be dominant according to the analyse about the inflection wave that can directly affect the flow before a research point. Thus from the geometric relations shown in Figure 3.2 and the Mach angle relation:

$$\eta' = h' - h_s' \approx h_c' + \frac{\partial h_c'}{\partial s} \Delta s - h_s'$$

$$\Delta s \approx \eta \operatorname{ctan}(\mu) = (M^2 - 1)^{1/2} \tag{3.27}$$

$$\frac{\partial h_c'}{\partial s} \approx \frac{\partial h_s'}{\partial s} = \kappa$$

where μ is the angle between the characteristic line and the streamline line.

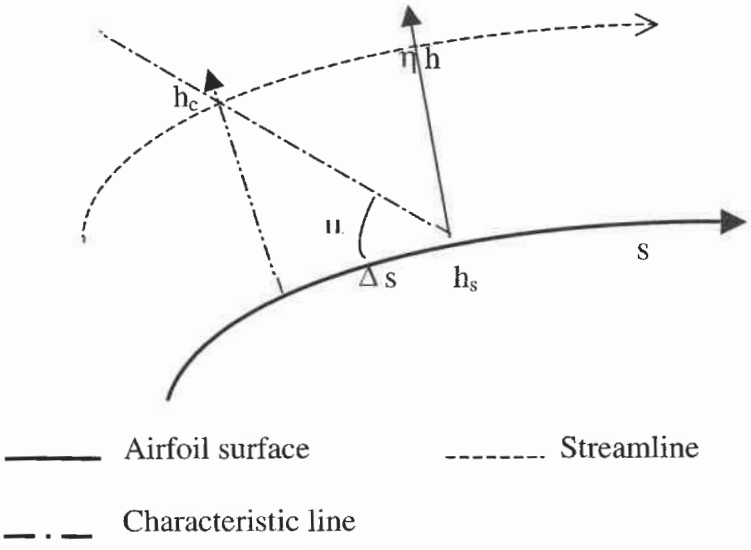

Figure 3.2 Geometric relations among an airfoil surface, a near streamline and a left characteristic line from the airfoil

With similar relations with (3.17) and higher order or supposed higher order terms ignored, the following approximated differential equation for transonic flows can be obtained

$$C \Delta h_s' - \kappa \eta [(M_o^2 - 1)^{1/2} - (M^2 - 1)^{1/2}] - \kappa \Delta \eta (M_o^2 - 1)^{1/2} + \Delta \eta' = 0 \qquad (3.28)$$

The above equations are only applied for correction purposes. And thus they are only required to predict correct tendencies rather than exact values because solutions will be improved in iteration process. Of cause, the approximation precision will exert great influence on convergence speed, that is to say, on the efficiency of the method.

In brief, equations (3.20) and (3.22) are used for subsonic flows and equation (3.23) and (3.28) are suitable for supersonic flows but the second and third terms of equation (3.28) should be ignored while transonic flow calculations are most complicated of these three cases and their numerical calculation process will be explained in detail in the next section as a example.

3.2 Perturbation Calculation, Design Process and Flow solver

3.2.1 Initial conditions

3.2.1.1 Selection of initial points

The geometry similarity assumption of near streamlines to the airfoil surface is not valid near the stagnation point where the geometric shape of even a very near streamline is greatly different from the airfoil shape. But the nearer the streamline line is to the airfoil surface, the smaller this invalid region is. Thus taking the stagnation point as the initial point with zero initial value may solve this problem. However, the errors too near the stagnation points can be too large to be accepted especially during first several iterations if the stagnation point is directly taken as the initial point. Taking a nearer streamline for calculation, that is to say, smaller η_0 value can help solve this problem but not during the first several iterations because the stagnation point of the initial airfoil is not close to or even relatively far away from the target one. In addition, the convergence speed is very slow if the used η_0 is too smaller. That is why smoothing or strained transfer should be used. But these two techniques will probably affect the designed airfoil precision and

thus their applications should be cautious. In order to avoid this kind of problems, it is appropriate to take the two discrete numerical points around the stagnation point of the design airfoil as the initial calculation points instead of this stagnation point directly and then to calculate the perturbation before and after the stagnation point separately. This measure has been found to be effective because with the increase of iteration times the two stagnation locations generally become so close and can be confined between the two initial points that the invalidity of the similarity assumption cannot bring about any serious problem.

The above problems are not unique for this new method; they should exist for the other direct correction methods but there is no concerned discussion published.

3.2.1.2 Initial values

A proper initial value η_0 is generally of 1% airfoil chord length for subsonic flows and 0.1% for supersonic flows for equation (3.14) according to the calculation experiences.

The initial geometric perturbation Δh_s and its first order derivative to airfoil surface $\Delta h_s'$ must be specified to solve equation (3.20). The initial Δh_s is given by interpolation from the stagnation point where Δh_s is always taken as zero. The initial $\Delta h_s'$ is made proportional to the slope difference between the target and design stagnation positions for the time being. The sign of Δh_s depends on the local pressure coefficient difference and that of $\Delta h_s'$ on local pressure gradient difference. Though the above treatments are proved effective, careful studies should be made in the future.

The initial Δh_s can be directly made proportional to the local pressure coefficient difference and the initial $\Delta h_s'$ to local pressure gradient difference but it is difficult to control their magnitudes.

3.2.2 Geometric Perturbation Calculation

For transonic flows, the main process for geometric perturbation calculation is as follows:

1) Calculate F, F′ and f with calculated pressure coefficients by equations (3.10), (3.11) and (3.13).
2) Calculate the near streamline coordinates η with the given initial value η_0 and the calculated coefficients F, F′ and f by equation (3.14).
3) Solve equation (3.20) with Runge-Cutta four-step method or the other methods with the specified initial conditions.
4) When a jump appears in the solution of equation (3.20) or the ratio of its first coefficient and its second one is smaller than a given value (1% is generally used), equation (3.22) is applied instead.
5) From the first sonic point, equations (3.23) and (3.28) are solved as the initial value problem.
6) After the shock position or the last sonic point, equation (3.20) is used once more.
7) Coordinate transfer to make the supersonic solution matched with the subsonic one after the shock and keep it unchanged near the first sonic point during first several iterations.

Step 7) can be looked as a correction measure if the shock on the airfoil in iteration is stronger because transonic flows depend on all the wave interferences and propagations and shocks are envelops of compressive waves. The assumption that the left characteristics are dominant is mainly based on design and calculation experiences and for meeting the need of calculation convergence and it may cause larger errors near strong shocks.

Moreover, equations (3.23) and (3.28) are solved with the second order middle point method and equation (3.20) solved with Runge-Cutta four-step method. Although

theoretically the later method is of fourth order precision, it is difficult to have the initial conditions with higher order precision. Thus the calculation accuracy may not be good enough. But this could slow down the convergence speed rather than cause serious errors to the final solution in iterative correction process.

3.2.3 Design process[1] and convergence criteria

The following is the airfoil design process:

1) Calculate the pressure distribution of the initial airfoil using a flow solver (viscous or non-viscous).
2) Strained coordinate transfer for the target C_p distribution during the first several iterations.
3) Calculate the normal geometric perturbation as shown in the last section.
4) Correct the calculated perturbations and make the strained coordinate transfer for them if needed.
5) Non uniform relaxation for convergence acceleration
6) Add the geometric perturbation normal to the calculation airfoil.
7) Smoothing the new airfoil.
8) Calculate the new leading edge and trailing edge positions, transfer them to original ones or make the trailing edge gap equal to the given one if specified.
9) Repeat the above steps until the convergence criterion is satisfied.

Different convergence criteria are employed in design process. The principal one is that the maximum pressure coefficient difference between the target and the designed is smaller than 0.006. Even this value is not very small but it is still so demanding that this kind of criterion has never been acceptable in any iterative correction method. In fact,

---

[1] The simplified flow chart of the design program is shown in Appendix 6. The concerned explanations about the strained coordinate transfer, airfoil smoothing and non uniform relaxation can be found in section 3.3

the precision of iterative inverse methods (Barger, Campbell and Takanashi) is generally judged from the graphical differences between the target and design pressure or velocity distributions and its exact amplitude like the maximum pressure and geometric difference has been rarely discussed, the only exception may be the E. William's paper in which the maximum pressure difference is given for one of his best results and the precision is still measured by graphical differences for the other results. Moreover, William H. uses the convergence criterion that the lift coefficient difference is less than a given value. But this criterion cannot be applied independently because the lift difference is even zero while the pressure differences can be very larger. Thus in this research, the solution is also accepted at given iteration times if the graphical differences between the target and the designed pressure coefficients are small enough because the convergence criterion for the specified maximum pressure coefficient difference cannot be always satisfied.

3.2.4 Flow solver

The flower solver used is MSES of Mark Drela, MIT, which is a numerical airfoil development system. It includes capabilities to analyse, modify and optimize single and multi-element airfoils for a wide range of Mach and Reynolds numbers. It has its own airfoil design code based on optimization for the least-squire pressure difference. In this research, only its analysis code based on the matched Euler equation and the boundary layer method is used.

The numerical formulation of MSES consists of a finite-volume discretization of the steady Euler equation on an intrinsic streamline grid. Streamline block grids are initiated by a panel method and the farthest grid location can be only of the twice airfoil chord as the flow far field can be represented by high order vortex and doublets located at the airfoil's aerodynamic centre. The boundary layers and trailing wakes are described by a two-equation integral formulation with lagged-dissipation closure. The non-viscous and

viscous regions are fully coupled via the displacement thickness. The solid-body boundary condition is used on the airfoil surface. The artificial viscosity is also used to maintain numerical stability and allow shock capturing. The "envelope method", which is a simplified version of the e^n method, is used for prediction of transition. Instead of tracking the Tollmien-Schlichting (TS) wave amplitudes for many individual frequencies as in the e^n method, the envelope method determines for each surface point the amplitude of whatever frequency happens to be most amplified at that point, which greatly simplifies the calculation process. The overall system is solved using a full Newton method.

3.3 Some Special Treatments

3.3.1 Strained Coordinate Transfer

Pressure differences between the target and calculated airfoils near the leading edge and the shock positions can be so large especially during first several iterations that the calculated geometric perturbation may be greatly deformed because of the large differences between their stagnation points, suction peak positions and the shock locations. Geometry smoothing can help solve the problem. But the strained coordinate transfer may be more efficient.

The concept of employing coordinate straining to remove non uniformities from perturbation solutions of non-linear problems is well established and originally proposed by Lighthill five decades ago and found more applications in 1970s and 1980s by Nixon, Stephen S and others but it has never been applied to geometric treatments of airfoil design. The basic idea of the technique is that a straightforward perturbation solution may possess the right form, but not quite at the appropriate location.

There are two kinds of strained transfer used according to Stephen S.: 1) in "classical" sense, strained transfer is applied to full governing equations and boundary conditions. Thus the differential equations so obtained are generally more complicated than their

original ones, and 2) strained transfer is employed directly to the known non-uniform solution, and then solving algebraic rather differential equations. It is obvious that the second one is more suitable for the method based only on the known airfoil surface variables.

This technique was often used for non-linear interpolation of two similar solutions. The coordinate transfer is carried out generally with the aid of polynomials. The strained range and its vanishing manner should be carefully considered. For inverse design purpose, the requirements for strained coordinate transfer are much more demanding in order to keep the geometric precision of the designed airfoil. Thus in this research the transfer is applied only during the first several iterations for accelerating the convergence and a transfer based on Bézier spline is tried instead of polynomials for the sake of control flexibility.

The critical points of the two solutions like leading edge, trailing edge, stagnation point, suction peak position, sonic point and shock position may be selected as strained points according to different situations. The strained transfer is used for similar solutions while the pressure distribution of the calculated airfoil during first iterations may not be similar at all to the target. For example, one of them has a suction peak near the leading edge and another not. Therefore only some of the above points need to be selected as strained points in this case.

Although the calculation results have already proved that the strained transfer can evidently accelerate the design convergence, there are still some problems to be solved, for example, if the distance between the two corresponding strained points is too large, the program may break down. Moreover some formula used now is not very appropriate to the problems. Furthermore, it is difficult to accurately calculate the stagnation locations because of the following fact. As pressure coefficients are only calculated at discrete points, the stagnation points need to be extrapolated, which may cause larger

errors owing to the steep flow gradient in this area. In fact, the pressure coefficient at the stagnation point can be easily calculated for isentropic flows but it is unknown itself for viscous cases. Though this kind of errors cannot be large relatively, they can be great enough to affect the designed airfoil precision.

3.3.2 Airfoil Smoothing

Geometry smoothing is very important and even essential to some inverse methods for which the airfoil is smoothed per design iteration (William E.). As airfoil smoothing effects need to be meticulously controlled, it is impossible to directly apply the general methods which tend to smooth an airfoil too much or too less. Therefore, special methods suitable for airfoil smoothing must be developed.

One of suitable airfoil smoothing methods is based on rational Chebychev polynomials. In this method the airfoil upper surface and lower surface are fitted separately, leading edge and trailing edge are fixed and the curvature is kept continuous at the leading edge. Moreover, NASA airfoil smoothing method may be also effective. In this research, several other smoothing methods are adapted. The global smoothing method used is the optimized airfoil parameterization method that is described in the above chapters. This method can keep the third order derivatives continuous but its smoothing effects are very local because it is designed for accurately representing the original curves. So in shock region, another smoothing method is added. This method is based on the original idea of Renz W. and modified. Why this method is accepted is based on the following ideas: even if the graphic difference between two curves is invisible, their curvature difference may be evident. As a result, smoothing curvature seems to be more effective. But smoothing second order derivatives is much more convenient mathematically than smoothing curvatures. Thus they are locally smoothed with the least-squares polynomial fitting. The areas where smoothing and non-smoothing are connected are smoothed by the Bézier function. The differences between the smoothed derivatives and the original

ones are integrated back to get the geometry difference. In addition, during the first several iterations, the leading edge is smoothed with the sixth order polynomial fitting if the maximum perturbation is larger than a specified value (about 0.001). The Bézier function is widely used in the leading edge region in design process and it has been fund to be very efficient because the Bézier function can keep the general tendency of the original curve, damp the too high peaks and keep the slope continuous at the two ends. If this kind of smoothing is not used, the calculation convergence is slower because of the oscillations and noises of the geometric perturbation solution near the leading edge which is due to the following factors: (1) the sensitivity of aerodynamic characteristics to the leading edge shapes, (2) the differences of the suction peak and stagnation locations and (3) numerical errors caused by extrapolation of the stagnation locations (in the case of strained transfer used), interpolation of the pressure coefficient at the leading edge and flow calculation owing to the very large gradient in this area, etc.. Some other more detailed discussion about this problem can be found in the section about the initial conditions.

Besides, least-squires fitting for airfoil smoothing is treated by solving the norm equation for the time being instead of using the singular value decomposition though the later is obviously superiors to the former because the norm equation is generally very ill conditioned in most practical applications. The former method is accepted only because it takes much less time for programming.

3.3.3 Non uniform relaxation

In design process, the sub-relaxation is necessary to guarantee the calculation convergence especially during first several iterations because the calculated perturbation may be deformed due to too large pressure differences near the leading edge while the super-relaxation should generally be used for accelerating the convergence. But the relaxation factor cannot be made constant directly because 1) the geometric perturbations

near leading edge tend to be larger owing to large pressure gradients and they oscillate and contain some noises because of the reasons discussed in the last section, 2) geometric perturbations are too large in the supersonic region of transonic flows as the flows are very sensitive to smaller perturbations, and 3) geometric perturbations are generally smaller in the aft part of airfoil upper surface and on the lower surface at high angles of attack. This may be caused by taking the same constant D in equations (3.17) and (3.26) for the entire airfoil. The problem can be solved by treating the D as a function of curvature lengths but it is more convenient to use different relaxation factors.

In this research, three or four constant relaxation factors are used respectively in the leading edge region, the upper surface, and lower surface or supersonic region. Linear or non-linear relaxation factor distribution can also be used but it may deform geometric perturbations. The regions for using different relaxation factors are delimited from 1) sonic point, 2) zero perturbation point and 3) minimum perturbation point that is taken as the coordinate origin for amplifying the perturbations after this point. The relaxation factors used varied between 0.3 and 5, which is adjusted automatically in the program according to the amplitudes of geometric perturbations and the pressure differences. Relaxation factors should be selected in such a way that the convergence speed to the target values should be more uniform at every point of the airfoil. If the pressure differences in one part of the airfoil are already near zero and there are still larger differences in the other part, the convergence is much slower. In addition, a large relaxation factor can sometimes give rise to a serious problem that small perturbation waves are amplified. The amplified waves reduce the convergence speed rather than accelerate it, which is one of reasons why geometry smoothing is necessary.

CHAPTER 4
AIRFOIL INVERSE DESIGN RESULTS[2]

4.1 Airfoil design for high subsonic flows

In order to avoid complicated flows containing shock waves, the first test design is selected for $M_\infty = 0.60$, $Re = 1.00\times10^7$ and $\alpha = 1.50$ d. The target airfoil is RAE2822 and the initial airfoil is NACA0012. The large difference between the two airfoils is suitable for testing the capability of the method. The strained coordinate transfer is used during the first ten iterations. The strained points are the leading edge, the trailing edge, the pressure peak location and the stagnation point during the first 5 iterations and the same points are selected except the pressure peak location for the next 5 iterations.

The design results are presented in Figure 4.1 with the pressure distribution and the airfoil shape comparisons among the initial, target and design airfoils. The convergence is very fast, the differences between the target and design are very small even in 5 design iterations, for example, and the lift coefficient difference is smaller than 1%, which is appropriate for initial design problems. In 15 iterations, the maximum pressure coefficient difference, which appears near the leading edge, is 0.006 while the geometric difference is smaller than 5.0×10^{-5} in the key aerodynamic range. The precision is surprisingly good.

The curves illustrated in Figure 4.2 shows that the convergence is not monotonous and there are some jumps, which are mainly caused by leading edge smoothing. In the program, the leading edge smoothing is carried out if the maximum perturbation is large than 0.001. The smoothing method based on the least-squires fitting of a 6^{th} order general

[2] All the airfoils used in this chapter, target and initial, are represented by their parametric ones using the method of this thesis with NC = 11 and NPOINT = 3 in appendices 7 and 8.

------ Initial (NACA0012) ——— Target (RAE2822) –·–·– 5 Iterations

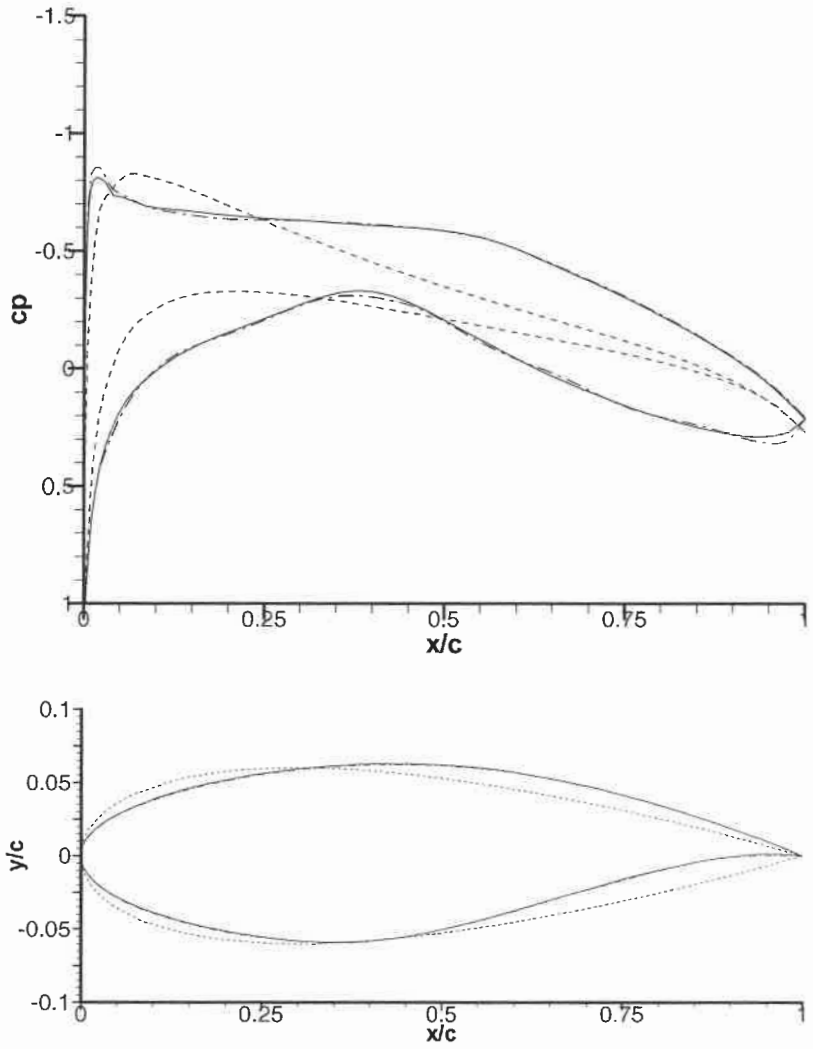

(a)

Figure 4.1 Inverse Airfoil Design Results

Airfoils and Pressure Distribution Comparisons

$M_\infty = 0.6$, $Re = 1\times10^7$ and $\alpha = 1.50$ d.

------Initial (NACA0012) ——— Target (RAE2822) –·–·– 15 Iterations

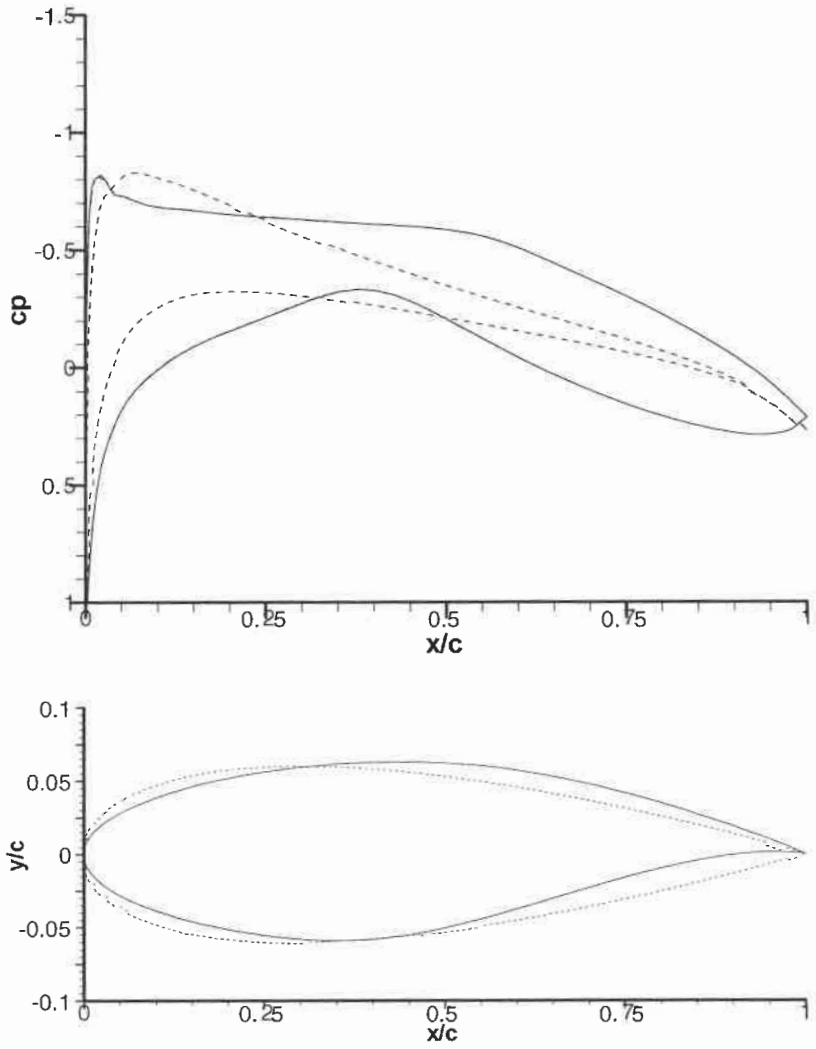

(b)

Figure 4.1 Inverse Airfoil Design Results

Airfoils and Pressure Distribution Comparisons

$M_\infty = 0.6$, $Re = 1\times10^7$ and $\alpha = 1.50$ d.

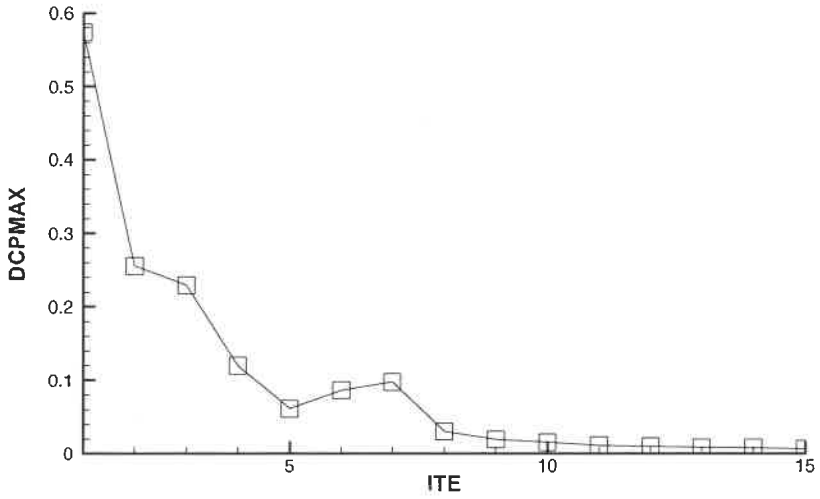

(a) $M_\infty = 0.600$, $Re = 1\times10^7$ and $\alpha = 1.50$ d.

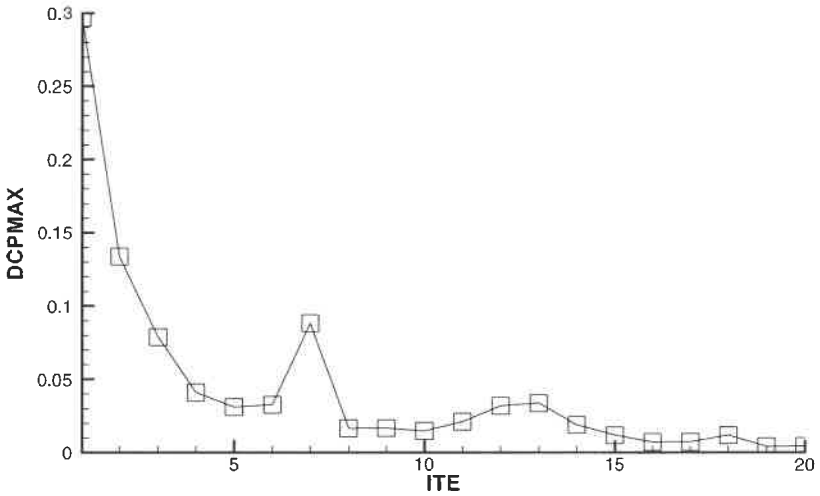

(b) $M_\infty = 0.725$, $Re = 1\times10^7$ and $\alpha = 0.00$ d.

Figure 4.2 Convergence Curves

Maximum Error Variations via Iterations

Initial Airfoil: NACA0012; Target Airfoil RAE2822

polynomial (described in the last chapter) always tends to smooth the leading edge too much. Therefore, when the maximum perturbation is larger than this specified and then the smoothing is made, a jump appears. But after the jump, the convergence may be accelerated. If the smoothing is stopped after the given iteration, the calculation results shows that the general convergence tendency is monotonous but the convergence speed can be slower. Thus, the best way to solve this problem may be to develop a more appropriate smoothing method.

Another design case shown in Figure 4.3 is for $M_\infty = 0.725$, $Re = 1.00\times10^7$ and $\alpha = 0.0$ d. The target airfoil and the initial one are also RAE2822 and NACA0012 respectively. This case is selected for the sake of comparisons with the results (corresponding to the same flow conditions but for non-viscous flow) of William E.. But the strained coordinate transfer is not applied because of the larger difference of the suction peak locations between the target and the initial pressure distributions. In addition, the stagnation point locations are too close to the leading edge to be calculated with enough accuracy just from the pressure distributions at given x positions.

The convergence is not as good as the above case because a supersonic region appears on the upper surface of the initial airfoil during the first several iterations and the strained coordinate transfer is not used. But it is still fast enough, in 20 design iterations the pressure coefficient differences are smaller than 0.0045 in the leading edge region and 0.007 in the remaining part. In contrast, the results of William E. is obtained after 50 iterations and the precision is not given but the pressure and the geometry differences are visible even from the much smaller figure. Consequently it is certain that the present method is much more rapid and accurate in this case. And it is not surprised that William's method is mainly developed for low speed flows.

------Initial (NACA0012) ——Target (RAE2822) –·–·– 10 Iterations

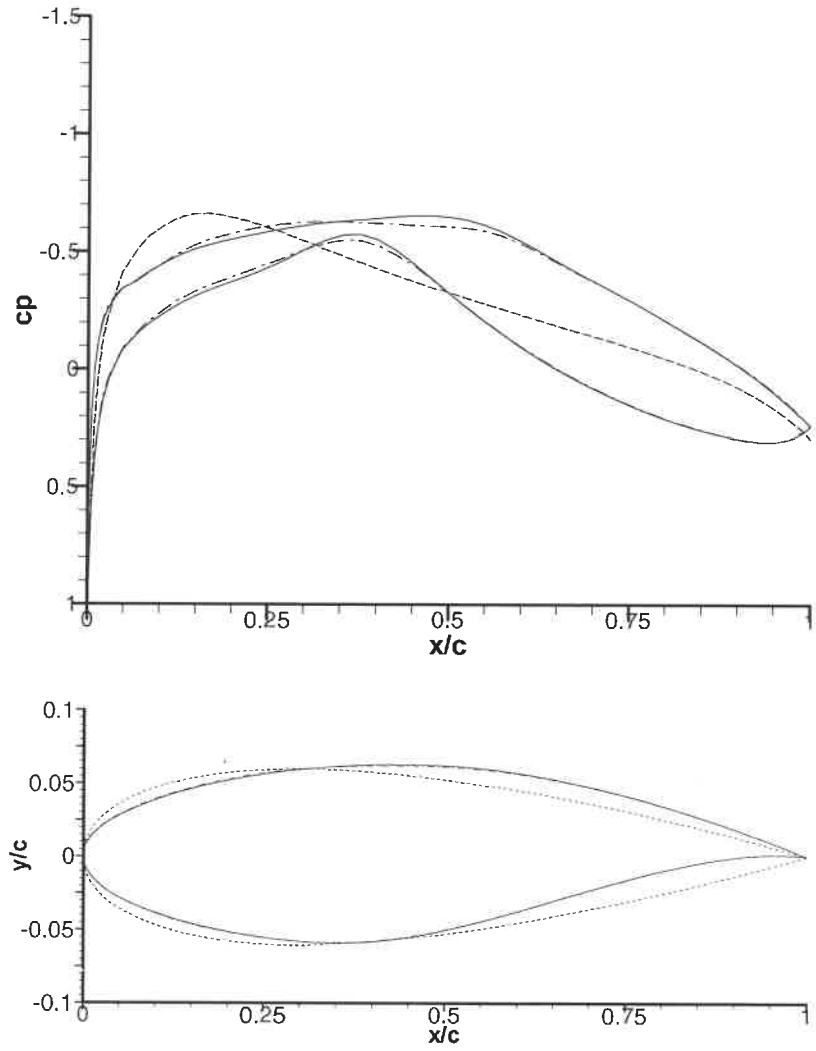

(a)

Figure 4.3 Inverse Airfoil Design Results

Airfoils and Pressure Distribution Comparisons

$M_\infty = 0.725$, $Re = 1\times10^7$ and $\alpha = 0.00$ d.

------ Initial (NACA0012) ——— Target (RAE2822) –·–·– 20 Iterations

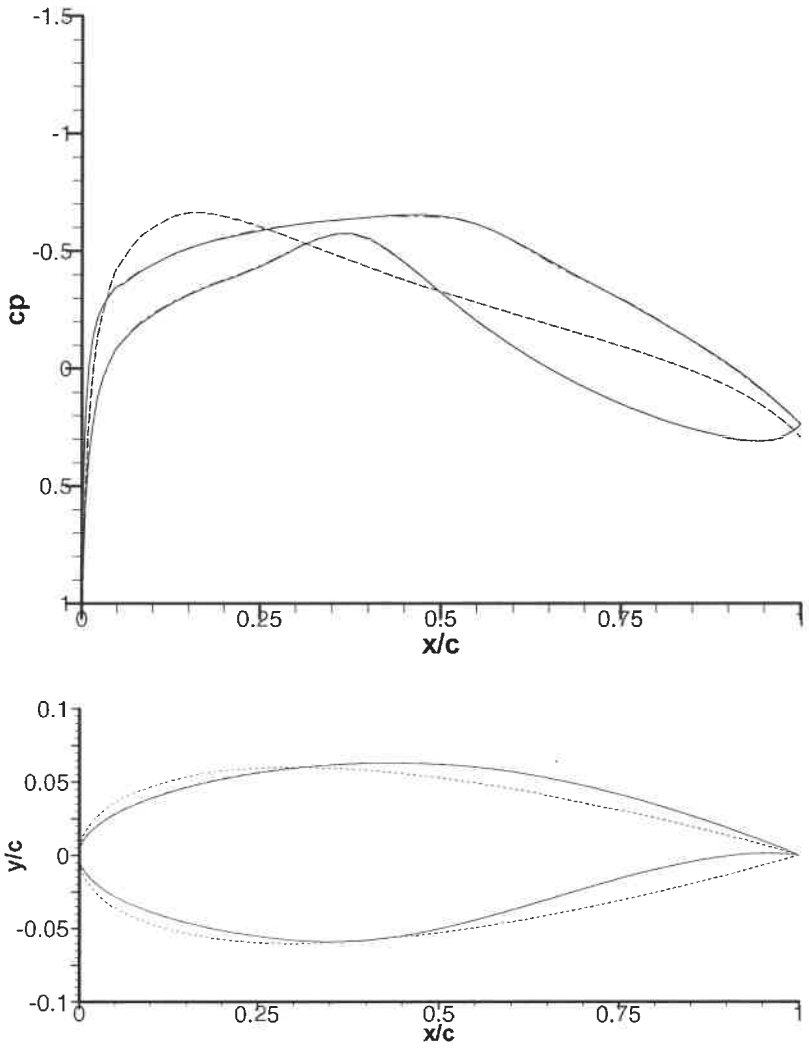

(b)

Figure 4.3 Inverse Airfoil Design Results

Airfoils and Pressure Distribution Comparisons

$M_\infty = 0.725$, $Re = 1\times10^7$ and $\alpha = 0.00$ d.

4.2 Airfoil design for low speed flows

The first low speed design case is selected for $M_\infty = 0.3$, $Re = 1.00\times10^7$ and $\alpha = 4.0$ d. The target airfoil is RAE5212 and the initial airfoil is NACA0012. The strained transfer is also used during the first ten iterations.

From the results illustrated in Figure 4.4(a) and (b), the convergence is very fast. In 5 iterations, the geometry and pressure differences between the target and design are small and the lift coefficient difference is smaller than 3%. There is nearly no visible difference in 15 iterations, the lift coefficient difference is smaller than 0.001, the precision is good enough from the practical point of view. Compared with William's results which are his best results and obtained in 25 iterations, the present method is much more efficient but less accurate. The difference may be caused by the following fact. The pressure is calculated in William's design only by a panel method and there is no convergence problem while in this thesis the flow is simulated by the coupled Euler and boundary layer method. The boundary layer transition is fixed near the suction peak location. Thus the suction peak is more sensitive to geometric perturbations. In addition, the solutions are not fully converged.

The second low speed design is effectuated for $M_\infty = 0.3$, $Re = 1.00\times10^7$ and $\alpha = 5.0$ d. The target airfoil is NACA2412 and the initial airfoil is NACA0012. The strained transfer is also used for the first ten iterations.

The pressure distribution and geometry comparisons presented in Figure 4.5 (a) to (c) show that the method provides the accurate results once more in 20 design iterations. There is nearly no visible difference between the target and design pressure distributions in this case. The lift coefficient differences are about 3% and 0.1% respectively for 5 iterations and 15 iterations. In 20 iterations, the pressure coefficient differences are smaller than 0.005 everywhere except near the leading edge where the maximum value is

------ Initial (NACA0012) ——— Target (RAE5212) –·–·– 5 Iterations

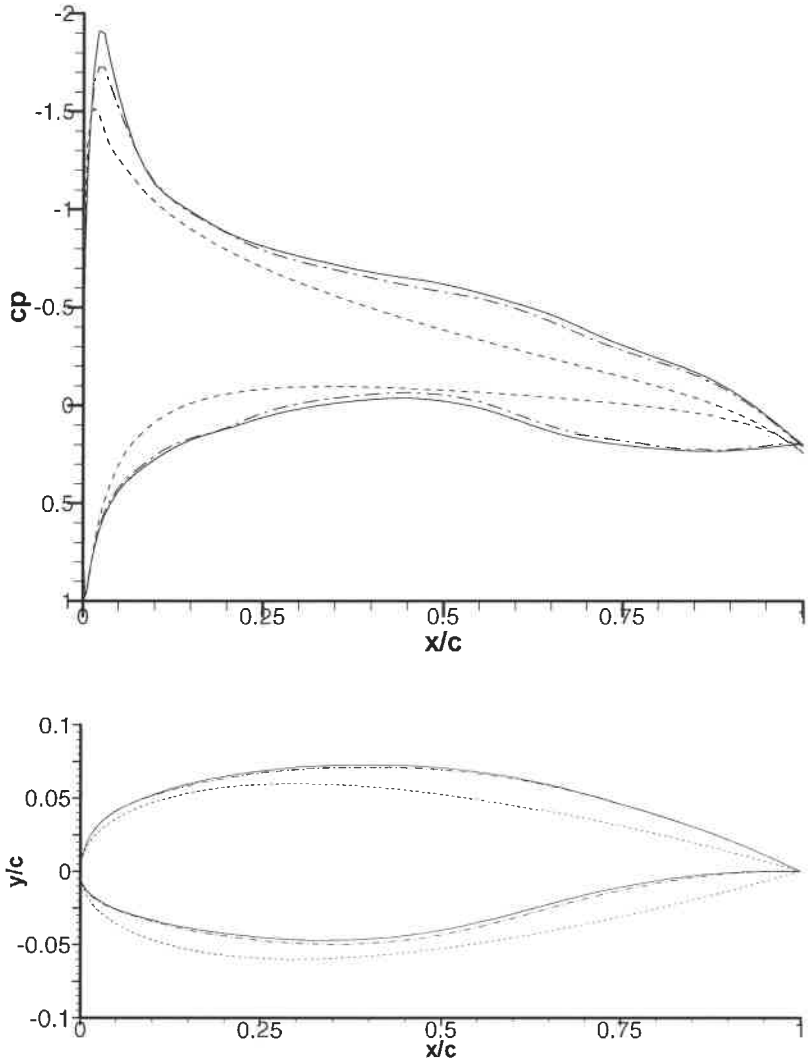

(a)

Figure 4.4 Inverse Airfoil Design Results

Airfoils and Pressure Distribution Comparisons

$M_\infty = 0.30$, $Re = 1\times10^7$ and $\alpha = 4.00$ d.

------ Initial (NACA0012) ——— Target (RAE5212) –·–·– 15 Iterations

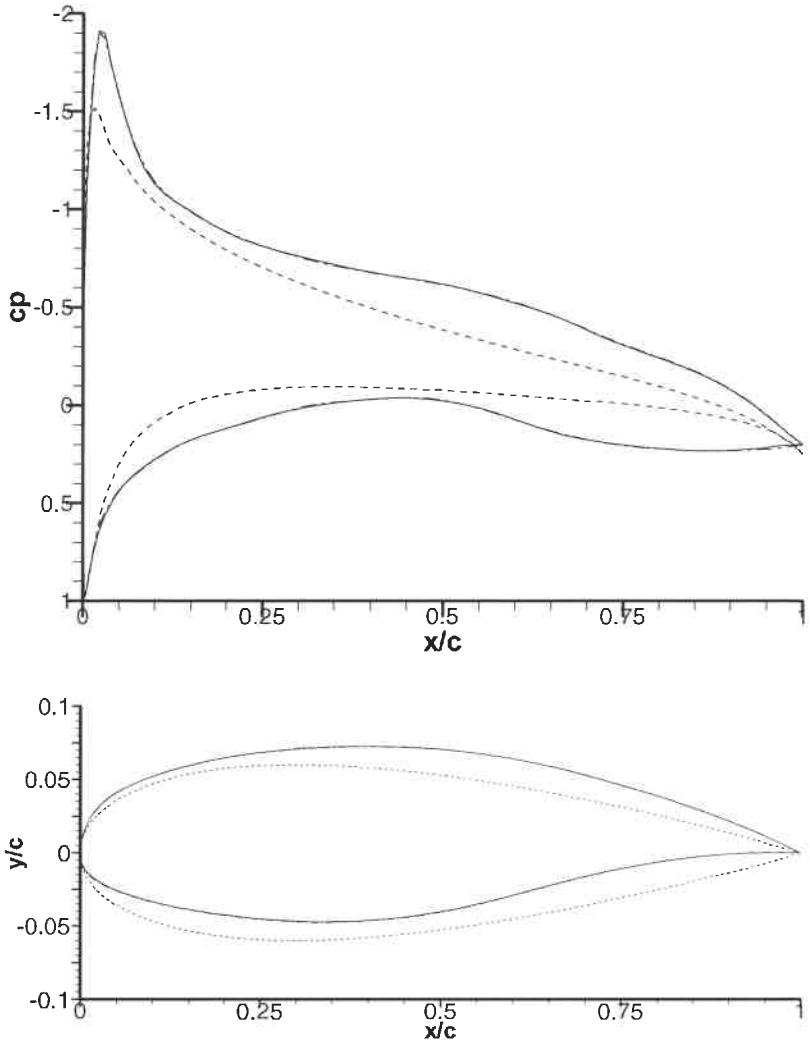

(b)

Figure 4.4 Inverse Airfoil Design Results

Airfoils and Pressure Distribution Comparisons

$M_\infty = 0.30$, $Re = 1\times10^7$ and $\alpha = 4.00$ d.

------ Initial (NACA0012) ——— Target (NACA2412) -·-·- 5 Iterations

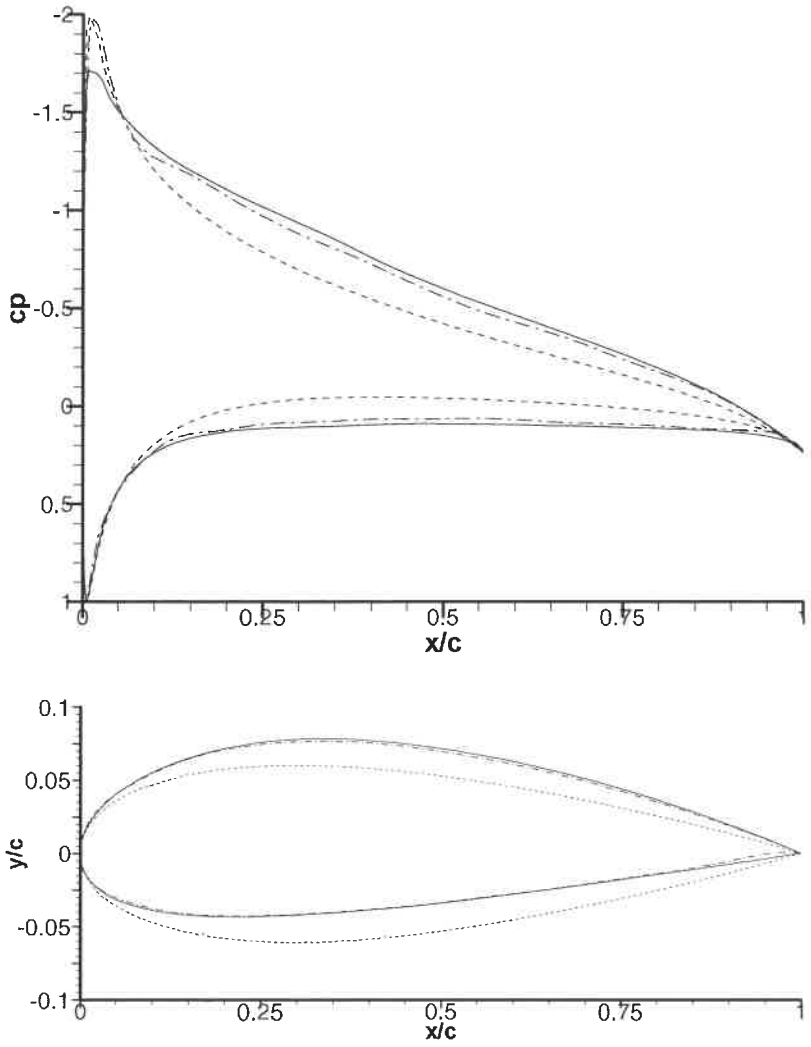

(a)

Figure 4.5 Inverse Airfoil Design Results

Airfoils and Pressure Distribution Comparisons

$M_\infty = 0.30$, $Re = 1\times10^7$ and $\alpha = 5.00$ d.

------ Initial (NACA0012) ——— Target (NACA2412) -·-·- 15 Iterations

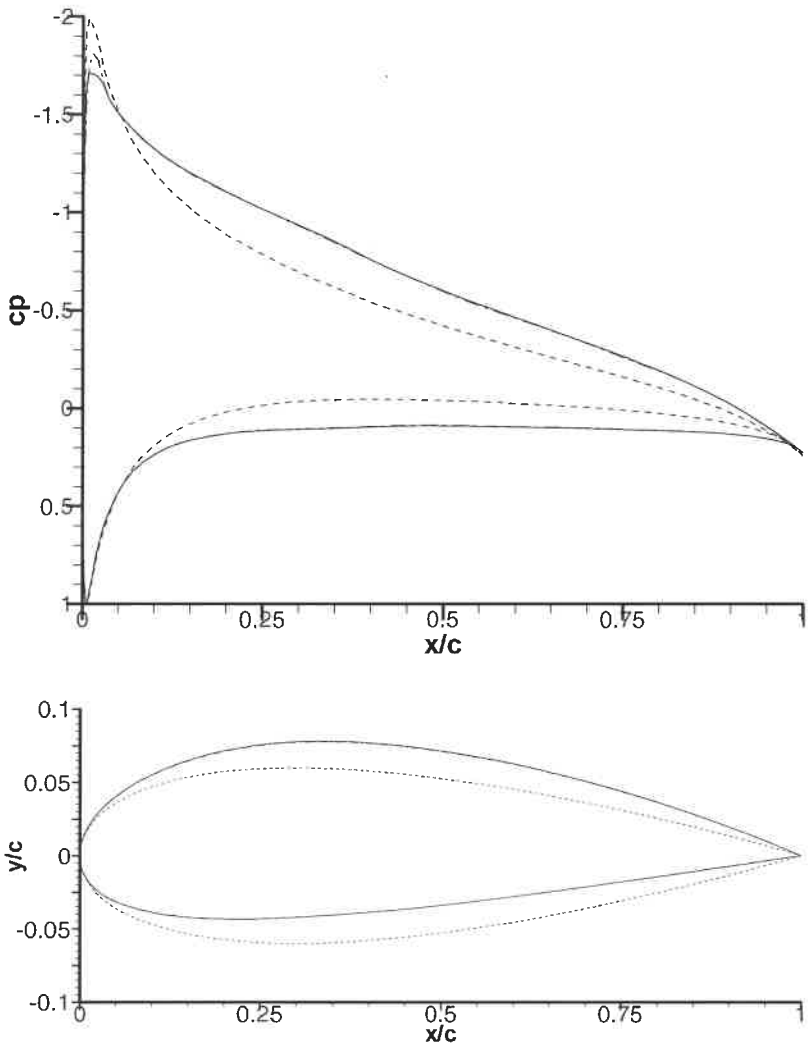

(b)

Figure 4.5 Inverse Airfoil Design Results

Airfoils and Pressure Distribution Comparisons

$M_\infty = 0.30$, $Re = 1\times10^7$ and $\alpha = 5.00$ d.

------ Initial (NACA0012) ——— Target (NACA2412) –·–·– 20 Iterations

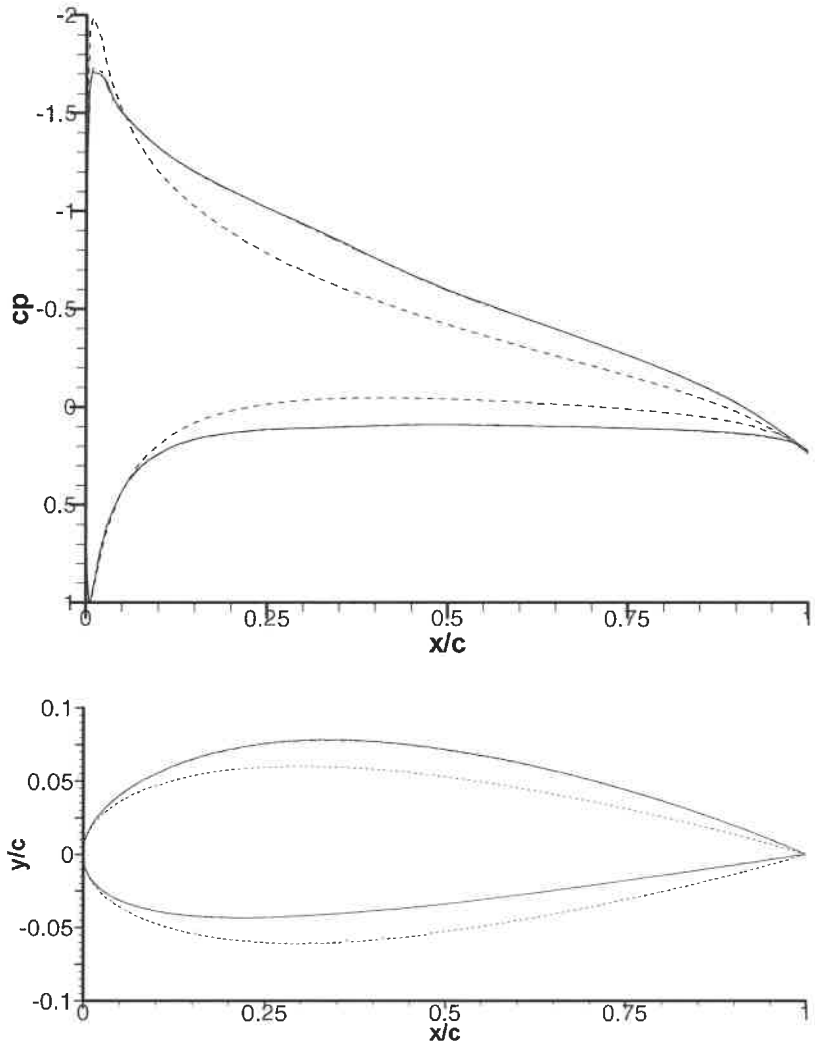

(c)

Figure 4.5 Inverse Airfoil Design Results

Airfoils and Pressure Distribution Comparisons

$M_\infty = 0.30$, $Re = 1\times10^7$ and $\alpha = 5.00$ d.

still a little large (0.035) . This difference is not visible from Figure 4.5(c) because of the large pressure gradient in this region. Considering that 1) the maximum geometric differences are smaller than 7.0×10^{-5} near the leading edge, which are excellent, 2) the flow solution is not fully converged at these conditions, and 3) the pressure differences are smaller enough in the other part of the airfoil, thus the larger pressure differences near the leading edge are mainly caused by the amplification of flow solver errors and the other interpolation errors (discussed in 3.3.1 and 3.3.2) to the geometric differences. In comparison with William's results of the similar conditions, gained in 25 iterations, the present method is more efficient and accurate in this case.

4.3 Transonic airfoil design

The design conditions are $M_\infty = 0.715$, $Re = 1.00\times10^7$ and $\alpha = 2.3$ d. The target airfoil is RAE2822 and the initial airfoil is NACA0012. The strained transfer is also used for the first 20 iterations.

From the results presented in Figure 4.6(a) to (c), the convergence is also rapid. In 5 design iterations, the geometric differences (shown in Figure 4.5(a)) between the target airfoil and the design are small but the pressure distribution differences are still large owing to the sensitivity of transonic flows to small perturbations. From the pressure distribution of the design airfoil, two shocks appear during the first several design iterations, which makes the flow complicated and the convergence much slower. The first shock is caused by the invisible non-monotonous variations of the curvature in this region. It is possible to solve this problem by appropriately smoothing. As is talked in 3.3.2, smoothing second derivatives is used in this research but the smoothing is still based on the least-squires fit of a general 6^{th} order polynomial that is not very appropriate for airfoil smoothing. Thus more effective smoothing methods must be developed in order to improve design results furthermore.

------ Initial (NACA0012) ——— Target (RAE2822) -.-.- 5 Iterations

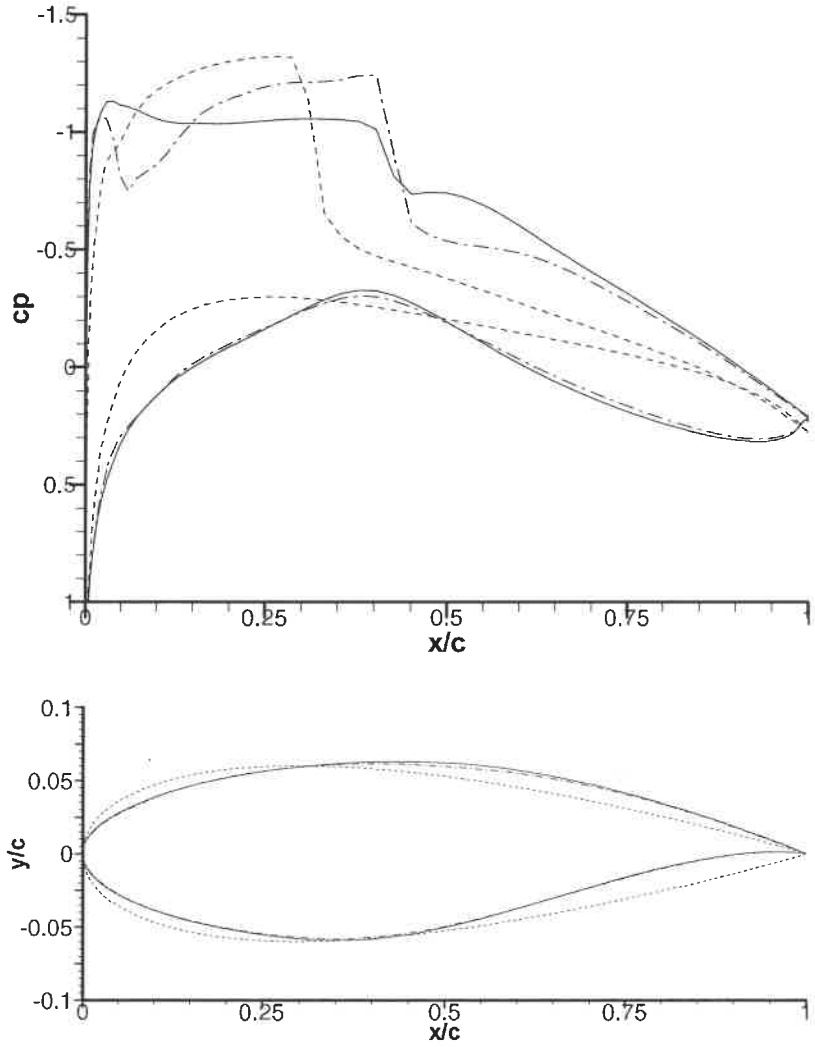

(a)

Figure 4.6 Inverse Airfoil Design Results

Airfoils and Pressure Distribution Comparisons

$M_\infty = 0.715$, $Re = 1\times10^7$ and $\alpha = 2.30$ d.

------ Initial (NACA0012) ——— Target (RAE2822) –·–·– 15 Iterations

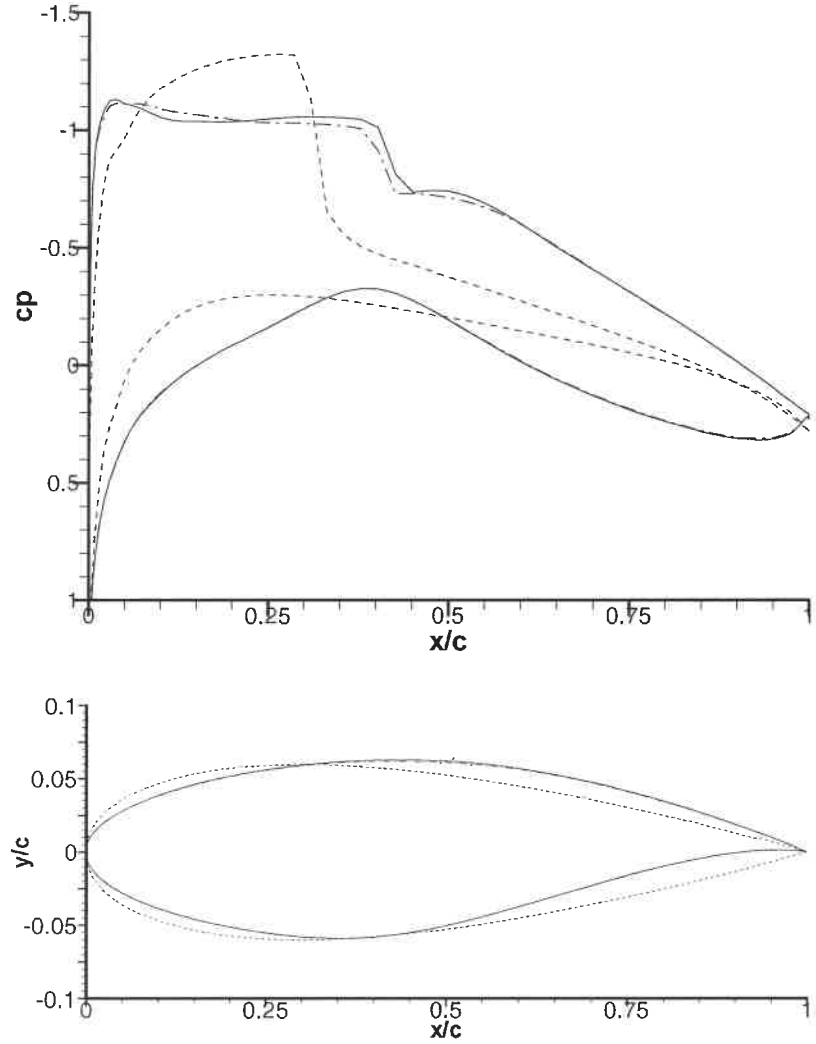

(b)

Figure 4.6 Inverse Airfoil Design Results

Airfoils and Pressure Distribution Comparisons

$M_\infty = 0.715$, $Re = 1\times10^7$ and $\alpha = 2.30$ d.

------ Initial (NACA0012) —— Target (RAE2822) –·–·– 25 Iterations

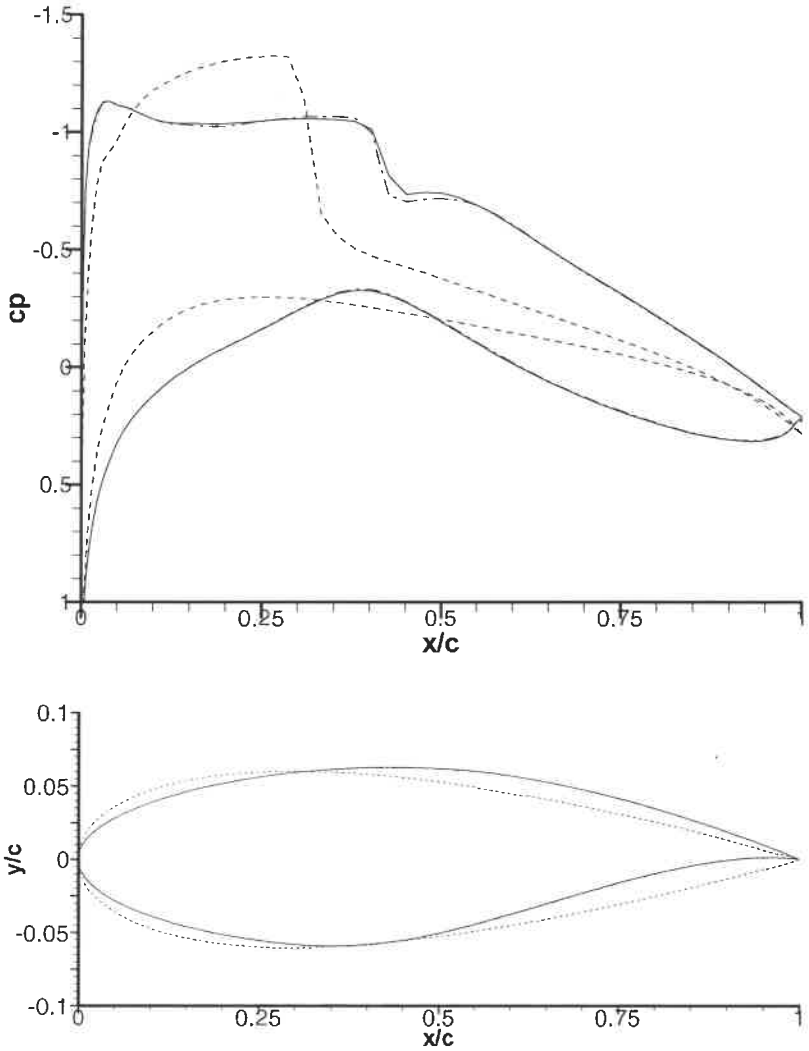

(c)

Figure 4.6 Inverse Airfoil Design Results

Airfoils and Pressure Distribution Comparisons

$M_\infty = 0.715$, $Re = 1\times10^7$ and $\alpha = 2.30$ d.

The comparison results (Figure 4.6(b)) in 15 design iterations demonstrate that the pressure distribution of the design airfoil is favourable, the lift coefficient difference between the target and the design is smaller than 2% and the shock strength is little smaller than that of the target. From the comparison results shown in Figure 4.5(c) after 25 design iterations, the pressure distribution of the design airfoil around the suction peak coincides with that of the target, which means that the calculation for the leading edge region is accurate. The results are very satisfactory from the practical point of view and comparisons with the transonic results (Barger, Campbell, Takanashi and Yu N.) of the other iterative methods, although there are visible pressure differences near the shock locations, which is caused by the following factors. As a pressure jump appears owing to the shock wave at the same location, there is also a jump in calculated geometric perturbations. Furthermore, calculated geometric perturbations are greatly deformed near the shock locations of the target and design airfoils. Smoothing is generally used for solving this problem. But it is hard to make the two shocks coincide together because it is very difficult to accurately control the smoothing effects. The author has tried to solve the problem by the strained coordinate transfer and some other new ways but there are still some problems to be solved.

CONCLUSION

5.1 Optimized airfoil parameterization

- The new method can accurately represent nearly any airfoil with few than 13 control points, e.g., NACA airfoils by 7 to 9 points and supercritical airfoils by 11 points. Moreover, the method is also very efficient. In most cases, optimized results converge within only 10 seconds on an 800 MHz personnel computer. Therefore, this method compensates for the deficiencies of the existed methods and possesses a great potential to improve the efficiency of airfoil or wing designs.

- As the control points for this method are directly located on the representative airfoil, it is much easier to calculate geometric characteristics (curvature and higher order derivatives), to add constrains such as thickness requirements and for use in local airfoil modifications than the other methods. In addition, designer's experiences can be directly carried on.

- The technique of automatically adding additional spline nodes can greatly improve the airfoil representation precision.

- The selection of objective function has a great influence to optimization results. The least-squires fit is also appropriate to the parametric airfoil approximation and the objective function that consists of the average error and the maximum errors for each curve segment is obviously superior to the commonly used objective function composed only by the average error and the unique maximum error of the entire airfoil.

- The distribution function of fixing control points may not be suitable to all kinds of airfoils. Future works include: (a) applying different distribution functions for different types of airfoils, (b) finding appropriate relations between control points and airfoil curvature distributions and (c) automatically adapting control points according to calculated error distributions and fixing the control points by iteration process. If the above works are finished, the optimization of control points will not be necessary in any case.

- In order to improve the efficiency and the accuracy of the method furthermore for the special cases that control points need to be optimized, the more appropriate optimization method should be adapted.

5.2 Iterative inverse aerodynamic design

- The new method is not only very efficient but also accurate enough for both compressible and low speed flows, especially the leading edge shape can be precisely calculated, which is impossible for nearly all the other methods.

- The efficiency and the accuracy of the method depend more on the techniques such as the strained coordinate transfer, geometry smoothing and non-uniform relaxation for accelerating the convergence than on the method itself.

- The transonic correction based on the assumption for the effects of waves reflected from the free boundary (sonic line) is effective but detailed studies regarding its potential to improve transonic solutions should be conducted.

- Geometry smoothing is essential to design efficiency, but smoothing effects are hard to control. In order to improve the design efficiency furthermore, more suitable smoothing methods should be studied.

- The strained coordinate transfer is an effective way to accelerate the convergence but further research on its ability to accurately reflect the geometric variations should be made.

- For the treatment of geometric discontinuity caused by shock waves, new techniques must be exploited to replace the commonly used techniques like airfoil smoothing in order to meet higher precision requirements in transonic flows.

REFERENCES

ASHOK D. BELEGUNDU and TIRUPATHI R. CHANDRUPATLA (1998). Optimization Concepts and Applications in Engineering. PRENTICE HALL, Upper Saddle River, NJ 07458.

BARGER, R. L. and BROOKS, C. W. JR. (1974). A Streamline Curvature Method for Design of Supercritical and Subcritical Airfoils. NASA TN D-7770, Sept.

BERNARD, E., SCHMITZ, A. BOSCHER, E. GARCIA, N., CEBECI, T. (1998). Two-Dimensional Aircraft High-Lift System Design and Optimization. AIAA paper 98-0123, Jan.

BURGREEN, G. and BYSAL, O. (1994). Aerodynamic Shape optimization Preconditioned Conjugate Gradient Methods. AIAA Journal, Vol. 32, No. 11, Nov., pp 2145-2152.

CAMPBELL, R. L. (1998). Efficient Viscous Design of Realistic Aircraft Configurations. AIAA Paper 98-2539, June.

DAVID L. CARROLL (2001). http://cuaerospace.com/carroll/ga.html.

FERRARI, C. and TRICOMI F. G. (1968). Transonic Aerodynamics, THE JOHNS HOPKINGS UNIVERSITY, SILVER SPRING, MARYLAND.

FUHIO YAMAGUCHI (1988). Curves and Surfaces in Computer Aided Geometric Design, Springer-Verlag.

GERALD FARIN (1993). Curves and Surfaces for Computer Aided Geometric Design, Third Edition, ACADEMIC PRESS, INC.

HARTWICH, P. M., AND AGRAWAL, S. (1996). Orthonormal Functions for Airfoil and Wing parameterization. 14th Applied Aerodynamics Conference, AIAA paper 96-2419, June, pp. 359-369.

LIGHTHILL M. J. (1949). A technique for rendering Approximate Solutions to Physical Problem Uniformly Valid. Philosophy magazine, Vol. 40, pp. 1197-1201.

MARK DRELA (2000). http://raphael.mit.edu/projects&research.html.

MITSUO GEN, RUNWEI CHENG (2000). Genetic Algorithms & Engineering Optimization. Wiley Series in Engineering Design and Automation, Hamid R. Parsaei, Series Editor.

MOULDEN T. H. (1984). Fundamentals of Transonic Flow. A Wiley-Interscience Publication, JOHN WILEY & SONS.

NIXON D. (1978). Perturbation of a Discontinuous Transonic Flow. AIAA Journal, Vol. 16, Jan., pp. 47-52.

NIXON D. (1978). Perturbation in Two and Three-Dimensional Transonic Flows. AIAA Journal, Vol. 16, July, pp. 669-709.

RENZ W. (1982). Interactive Smoothing of Digitized Point Data. Computer Aided Design, 14(5): 267-269.

STEPHEN S. STAHARA (1982). Rapid Approximate Determination of Nonlinear Solutions: Application to Aerodynamic Flows and Design/Optimization Problems. Transonic Aerodynamics, Progress in Astronautics and Aeronautics, Volume 81, pp. 637.

TAKANASHI S. (1985). Iterative Three-Dimensional Transonic Wing Design Using Integral Equations. Journal of Aircraft, Vol. 22, No. 8, August.

TRÉPANIER J. -Y., LÉPINE J. L. and PÉPIN F. (2000). An Optimized Geometric Representation for Wing Profiles Using NURBS. Canadian Aeronautics and Space Journal, Vol. 46, No. 1, March.

VENKATARAMAN, P.(1995). A new procedure for airfoil definition. AIAA Applied Aerodynamics Conference, 13th, San Diego, CA, June 19-22, Technical Papers. Pt. 2.

VENKATARAMAN, P. (1996). Optimal airfoil design. AIAA Applied Aerodynamics Conference, 14th, New Orleans, LA, June 17-20, Technical Papers. Pt. 1.

WILLIAM E. MILHOLEN II(2001). Efficient Inverse Aerodynamic Design Method for Subsonic Flows. Journal of Aircraft, Vol. 38, No. 5, September-October.

WILLIAM H. PRESS, SAUL A. TEUKOLSKY, WILLIAM T. VETTERLING and BRIAN P. FLANNERY. Numerical Recipes in Fortran, The Art of Scientific Computing, Second Edition, Cambridge University Press.

YU, N. J., and CAMPBELL, R. L. (1992). Transonic Airfoil and Wing Design Using Navier-Stokes Codes. AIAA Paper 96-2651, June.

APPENDIX 1

SIXTH ORDER HERMITE INTERPOLATION FUNCTION

$$H_{0,0} = -6t^5 + 15t^4 - 10t^3 + 1$$

$$H_{0,1} = 6t^5 - 15t^4 + 10t^3$$

$$H_{1,0} = -3t^5 + 8t^4 - 6t^3 + t$$

$$H_{1,1} = -6t^5 + 7t^4 - 4t^3$$

$$H_{2,0} = -\frac{1}{2}t^5 + \frac{3}{2}t^4 - \frac{3}{2}t^3 + \frac{1}{2}t^2$$

$$H_{2,1} = \frac{1}{2}t^5 - t^4 + \frac{1}{2}t^3$$

APPENDIX 2

INTRODUCTION TO PROGRAM AIRY

Program Airy is developed in Fortran by the author and is divided into two main parts respectively for airfoil parameterization and airfoil inverse aerodynamic design of which the principles and methods are described in this thesis. It consists of the following files: airj73d.f, rj73.f, OPT.H, OUT.H, REVERS.H and XYCC.H.

The source file airj73d.f is applied for airfoil parameterization and contains the program of about 4500 lines in Fortran, of which the flow chart and the main functions of subroutines are illustrated in Appendix 3. The detailed parameter descriptions can be found in the concerned subroutine. The program has been used for nearly six months and proves being very robust, especially for optimization with x location fixed. The only exception is: the optimization diverges if there are some non-smooth points near the trailing edge of an original airfoil. In the case of optimization for x locations, if satisfactory results cannot be obtained within nearly two hours, the variation range of control points should be specified once more. This part will be improved in the future.

The source file rj73.f is for airfoil inverse design and has 4000 lines in Fortran. Its simplified flow chart is demonstrated in appendix 6. The program cannot be used independently and a flow solver must be needed to provide pressure coefficients on the airfoil. The program works well in all the research cases but it should be developed further for commercial applications.

Files OPT.H, OUT.H, REVERS.H and XYCC.H contain array definitions and parameters required for optimization, output, inverse design and airfoil parameterization respectively. The detailed illustration can be found in the concerned subroutines and functions.

For genetic algorithm optimization, the original program is from D.L. Carroll and includes the following files: GAga170.f, ga.inp, ga2.inp, ga.out, ga.restart, params.f and ReadMe. The program and user manual can be downloaded freely from the web site (see reference list) for research purposes.

APPENDIX 3

FLOW CHART OF MAIN PROGRAM AIRY

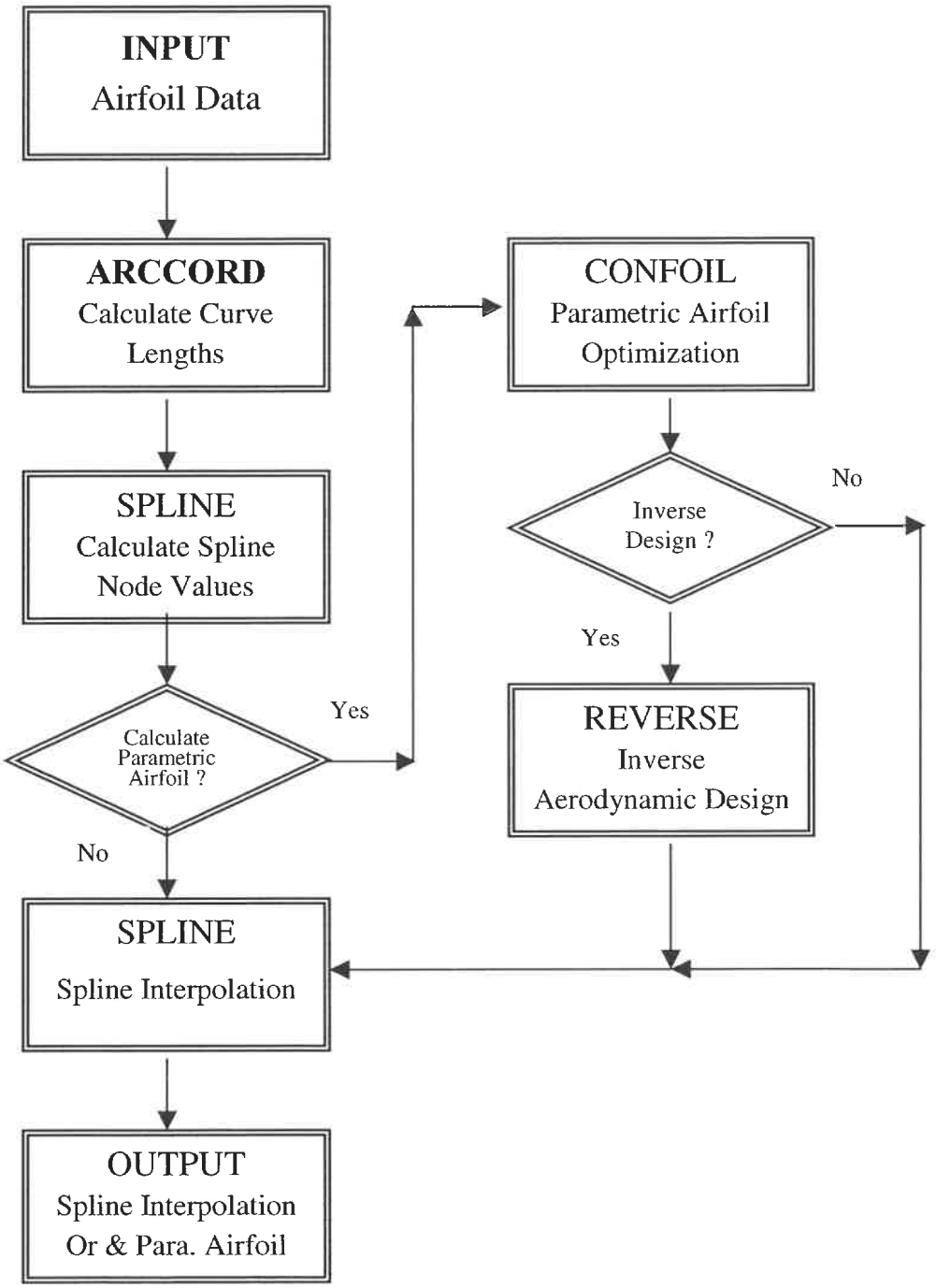

APPENDIX 4

FLOW CHART OF SUBROUTINE SPLINE

FOR SPLINE INTERPOLATION

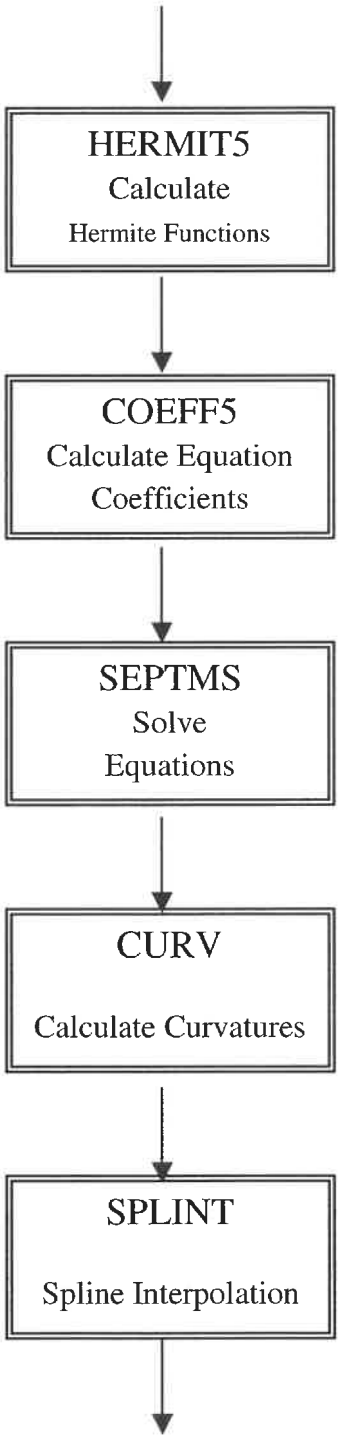

APPENDIX 5
SIMPLIFIED FLOW CHART OF SUBROUTINE CONFOIL FOR PARAMETRIC AIRFOIL OPTIMIZATION

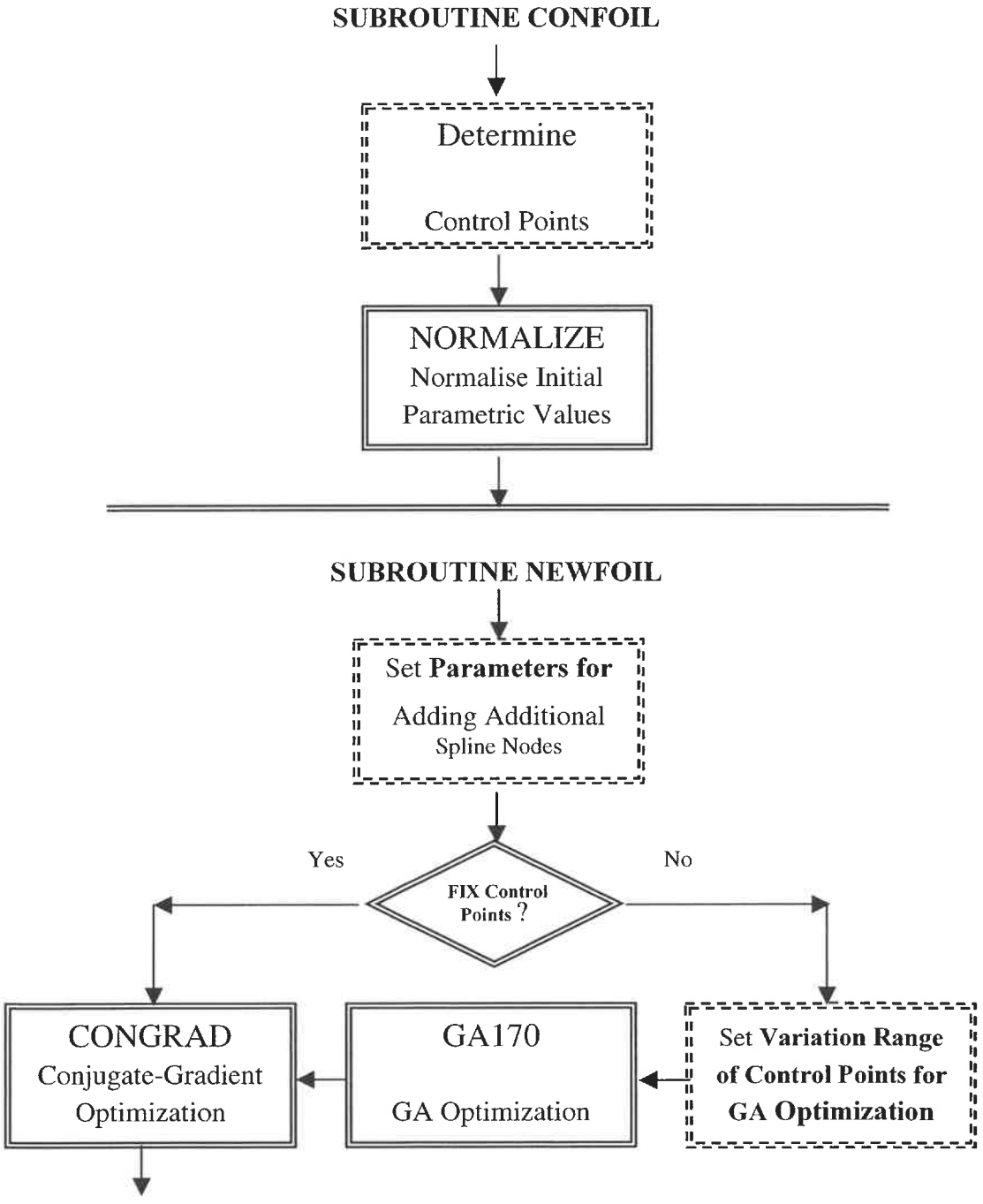

APPENDIX 6

SIMPLIFIED FLOW CHART OF SUBROUTINE REVERSE FOR ITERATIVE INVERSE AERODYNAMIC DESIGN

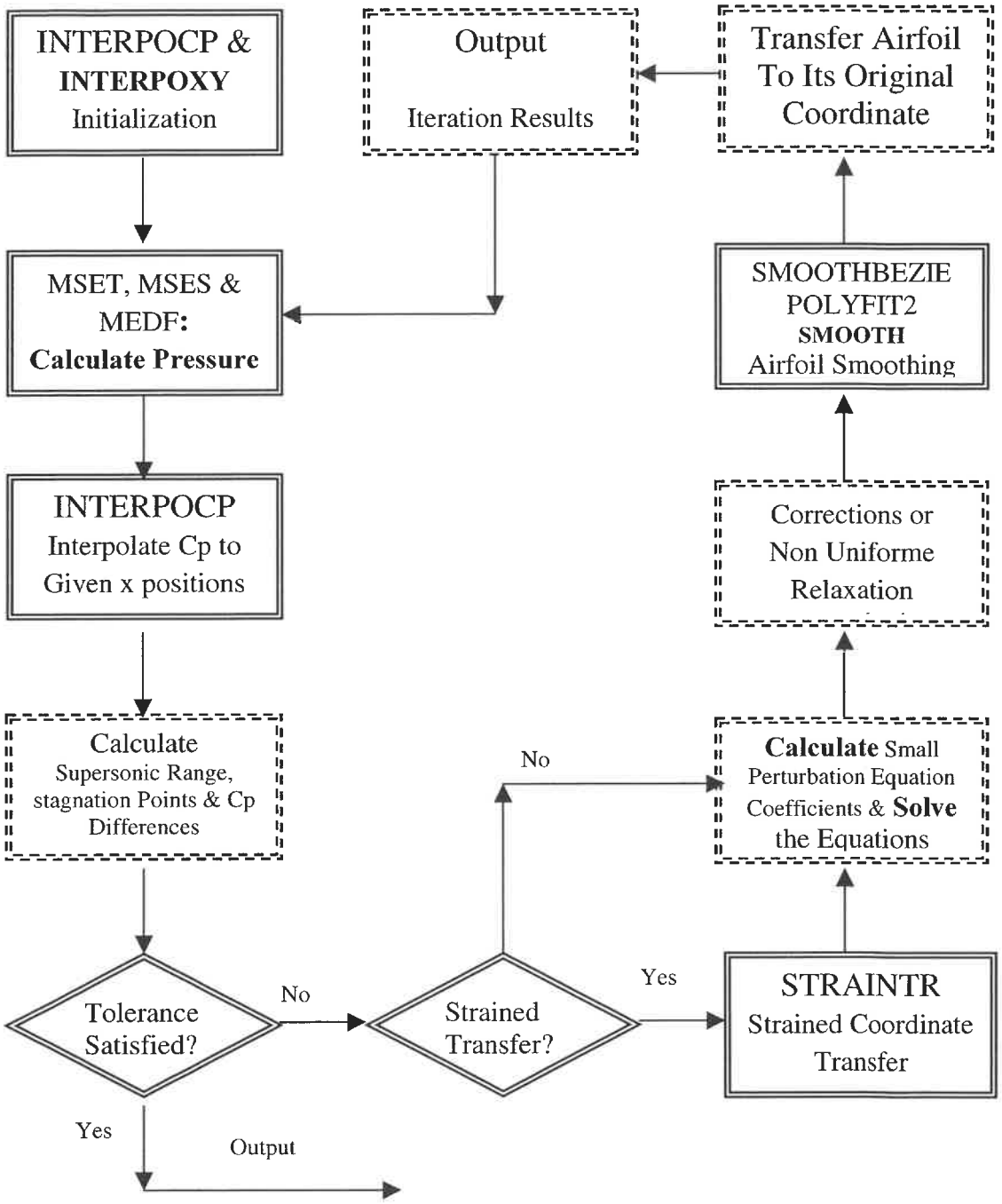

APPENDIX 7
INPUT DATA DISCRIPTIONS
FOR PROGRAM AIRY

Input control file is named as aircontrol.dat of which the format example is given in Appendix 7 and the control parameters are descried as following:

```
      SUBROUTINE INPUT
C  ======================================================================
C  INPUT ALL THE DATA & CONTROL PARAMETERS
C  ======================================================================
C  CONTROL PARAMETERS FOR INPUT & GEOMETRIC TREATMENTS
C  ----------------------------------------------------------------------
C  IFOR   :  airfoil input format
C            =1  DATA INPUT FROM LOWER SUR. TRAILING EDGE TO UPPER SUR. T.E.
C            =2  INPUT DIRECTION  OPPOSITE TO 1
C            =3  FIRST UPPER SUR. THEN LOWER SUR. & BOTH FROM L.E.
C            =4  PARAMETRIC AIRFOIL INPUT
C            =5
C  KYES   :  =1
C            =2  PARAMETRIC AIRFOIL INPUT AS INITIAL GUESS FOR GA OPTIMIAZATION
C  KDER   :  =1  DERIVATIVES INPUT  ONLY EFFECTIVE WHEN KYES = 1
C  KUL    :  =1  UPPER & LOWER SURFACE TO BE TREATED SEPARATELY
C  ----------------------------------------------------------------------
C  CONTROL PARAMETERS FOR PARAMETRIC AIRFOIL & OPTIMIZATION
C  ----------------------------------------------------------------------
C  NC     :  NUMBER OF CONTROL POINTS FOR PARAMETRIC AIRFOIL
C  NPOINT:  CONTROL PARAMETER FOR OPTION OF ADDING POINTS
C            EVEN NUMBER : TWO POINTS ADDED NEAR L.E. BETWEEN TWO CONTROL P.
C            ODD NUMBER  : ONE POINT NEAR L. E.
C            = 1,2   : ONLY ADDE POINTS NEAR L.E.
C            = 3,4   : FOR ALL BUT WITHOUT ADDED POINT NEAR T.E.
C            = 5,6   : ADDE POINS BETWEEN ALL THE CONTROL POINTS
```

```
C              = 7     : SAME WITH 5 FOR TIME BEING
C              = 8     : FOR ALL WITH ONE POINT ADDED BUT TWO NEAR L.T.
C              = 9,10  : ADDE POINTS ONLY FOR FORWEED HALF AIRFOIL
C              = 11,12: WITHOUT ADDING POINTS FOR T.E. OF LOWER SURFACE
C   KOPT  : CONTROL PARAMETER  FOR OPTIMIZATION
C              =1  DEFAUT WITHOUT OPTIMIZING X POSITIONS
C              =2  SPECIAL OPTIMIZATION FOR MINI. MAX. ERR.  (WEIGHTED)
C              =3  GENETIC ALGORITHMS USED FOR OPTIMIZING X LOCATIONS.
C              OTHER NUMBER    NO OPTIMIZATION
C   KRO    :  CONTROL PARAMETER FOR REOPTIMIZATION IF  THERE  ARE SOME
C              BAD POINTS
C              =1   YES    OTHERS   NO
C   KGA   :   FOR GA OPTIMIZATION OF INVERSE CALCULATION
C              =1   ONLY Y DERIV. YCP TAKEN  AS OPTIMIZATION PARAMETERS
C              =2   ADDE TWO THICKNESS FACTORS FOR UPPER & LOWER SUR. &
C             THE OTHERS SAME WITH CAS 1
C              =3   SAME WITH CAS 1 BUT  L.E.  CURVATURE FACTOR IS ALSO
C             TAKEN AS OPT. PARAM.
C             BEST OPTION OF ALL THE TESTED CASES (2001.10.11)
C             =4   YCP & CURVATURES CC AS OPT. PARAMETERS
C             =5   YCP, CC & Y POSITIONS AS OPT. PARAM.
C             FOR  CAS 1 & 2,  Ys  ARE  CALCULATED  ACCORDING  TO  3TH
C             CONTINUTY AT NODES
C             * * USELESS FOR THIS VERSION
C  ------------------------------------------------------------------
C   CONTROL PARAMETERS FOR INVERSE DESIGN
C  ------------------------------------------------------------------
C   KREV  :
C              =1     INVERSE CALCULATION TO BE CARRIED OUT
C             OTHERS  NO INVERSE DESIGN
C   INRE  :  CP INPUT CONTROL
C              =1     IN FORMAT OF MSES OUTPUT
C              =2     IN FORMAT OF EULER2D
C   AM     : UPSTREAM MUCH NUMBER
C   TETH  : TRAILING EDGE THICKNESS
```

```
C  ------------------------------------------------------------------
C  ------------------------------------------------------------------
C   CONTROL PARAMETERS FOR OUTPUT
C  ------------------------------------------------------------------
C   KOUT :  OUTPUT OPTION FOR GRAPHIC SOFTWARE
C               =1  TECPLOT
C               =2  GNUPLOT
C  ------------------------------------------------------------------
C
```

Airfoil input file name is input in the first line of the control file aircontrol.dat. Moreover, some control parameters for inverse design are directly input from the keyboard, of which the input descriptions are shown on the screen.

APPENDIX 8
INPUT CONTROL FILE
aircontrol.dat
FORMAT EXAMPLE

```
==========================================================================
RAE2822.dat  :  File name of input airfoil data
----------- CONTROL PARAMETERS FOR INPUT & GEOMETRIC TREATMENTS ----------
3        :  IFOR      ----- input format (see descriptions in subroutine INPUT)
3        :  KYES      ----- =1  parametric airfoil
2        :  KDER      ----- =1  derivatives input only effective when KYES = 1
2        :  KUL       ----- =1  upper & lower surface to be treated separately
----------- CONTROL PARAMETERS FOR PARAMETRIC AIRFOIL & OPTIMIZATION ------------
11       :  NC        ----- number of control points for the parametric airfoil
3        :  NPOINT    ----- control option for adding points(see detail in INPUT)
1        :  KOPT      ----- control parameter for optimization (see detail in INPUT)
0        :  KRO       ----- re-optimization if =1
5        :  KGA       ----- for GA optimization of inverse design (in INPUT) useless for this version
----------- CONTROL PARAMETERS FOR INVERSE DESIGN ------------------------------------------
0        :  KREV      ----- =1  inverse calculation                 others:  no
1        :  INRE      ----- =1  Cp input in format of MSES      =2  EULER2D format
0.6      :  AM        ----- upstream  MACH number
0.0      :  TETH      ----- trailing edge thickness
----------- CONTROL PARAMETERS FOR OUTPUT ------------------------------------------------------
1        :  KOUT ----- =1  TECPLOT    =2 GNUPLOT
==========================================================
```

APPENDIX 9
OUTPUT FILES DISCRIPTIONS

Output control is set in the input file aircontrol.dat. The main output files:

1. Parametric airfoil

Spline5out.dat : the complete output includes 1) the airfoil with more points interpolated from the original by the spline, 2) the original airfoil, 3) the parametric airfoil and 4) the interpolated airfoil from the parametric to the original x positions.
Six output variables x, y, xp, yp, xpp, ypp correspond to Cartesian coordinates, their curvilinear derivatives of the first order and second order respectively.

Error.dat : output errors between the original and parametric airfoils.
Output variables i, err, x, y are point number index, error and the Cartesian coordinates of the original airfoil.

2. Inverse design

Iteration.dat : output error information for each iteration. Output variables:
ITE: iteration time.
ICPMLE, ICPMU, ICPML: point number index respectively corresponding to maximum errors on the leading edge, upper surface and lower surface.
DCPMLE, DCPMU, DCPML: maximum errors respectively on the above three points
DHMMO: maximum geometric perturbation value on the leading edge.

Xycptec.dat : output geometric and pressure information every 5 iteration and the best solution.
The fist part is for the original airfoil and the second for the designed.

x, y : Cartesian airfoil coordinates

xs: strained x coordinate

cpt, cps or cpr, cprs : pressure coefficient and its derivative to x for the target airfoil or designed.